nature cell biology

Article

https://doi.org/10.1038/s41556-024-01522-8

Caspase-2 is a condensate-mediated deubiquitinase in protein quality control

Received: 6 September 2023

Accepted: 9 September 2024

Published online: 31 October 2024

Check for updates

Yingwei Ge[1,9], Lijie Zhou[1,2,9], Yesheng Fu[1,9], Lijuan He[1], Yi Chen[1,3], Dingchang Li[4], Yuping Xie[1], Jun Yang[5,6], Haitao Wu[5,6], Hongmiao Dai[1], Zhiqiang Peng[1,2], Yong Zhang[1,2,7], Shaoqiong Yi[1], Bo Wu[1], Xin Zhang[1], Yangjun Zhang[1], Wantao Ying[1], Chun-Ping Cui[1], Cui Hua Liu[7,8] ✉ & Lingqiang Zhang[1] ✉

Protein ubiquitination plays a critical role in protein quality control in response to cellular stress. The excessive accumulation of ubiquitinated conjugates can be detrimental to cells and is recognized as a hallmark of multiple neurodegenerative diseases. However, an in-depth understanding of how the excessive ubiquitin chains are removed to maintain ubiquitin homeostasis post stress remains largely unclear. Here we found that caspase-2 (CASP2) accumulates in a ubiquitin and proteasome-positive biomolecular condensate, which we named ubstressome, following stress and functions as a deubiquitinase to remove overloaded ubiquitin chains on proteins prone to misfolding. Mechanistically, CASP2 binds to the poly-ubiquitinated conjugates through its allosteric ubiquitin-interacting motif-like region and decreases overloaded ubiquitin chains in a protease-dependent manner to promote substrate degradation. CASP2 deficiency in mice results in excessive accumulation of poly-ubiquitinated TAR DNA-binding protein 43, leading to motor defects. Our findings uncover a stress-evoked deubiquitinating activity of CASP2 in the maintenance of cellular ubiquitin homeostasis, which differs from the well-known roles of caspase in apoptosis and inflammation. These data also reveal unrecognized protein quality control functions of condensates in the removal of stress-induced ubiquitin chains.

Numerous recent discoveries have shown that several biomolecules assemble into a single or multiple phases of condensates (mainly assembled by liquid–liquid phase separation) in the cellular matrix when encountering changes in the internal and external environment such as heat shock (HS), oxidative stress and osmotic stress[1–4]. More importantly, defective disassembly of these biomolecule condensates post stress is recognized as a major contributor to ageing and neurodegenerative diseases[2,5–7]. The ubiquitin-proteasome system (UPS), a basic and conservative protein quality control (PQC) network under stress, is associated with these biomolecular condensates and is responsible for the degradation of misfolded proteins and disassembly of condensate[4,8]. Defects in the UPS result in inefficient degradation capability due to excessive ubiquitination (also referred to as overloaded ubiquitination here) and promote the liquid–solid phase transition of biomolecular condensates[9–11].

Excessive accumulation of ubiquitinated conjugates could be detrimental to cells[12] and is recognized as a hallmark of multiple neurodegenerative diseases[13–16]. However, the mechanisms underlying the removal of these excessively accumulated ubiquitin chains (also called overloaded ubiquitin chains) remain largely elusive. Although caspase-2 (CASP2) is a member of the family of cysteine proteases reported to be associated with cell death, the primary function of

A full list of affiliations appears at the end of the paper. ✉e-mail: liucuihua@im.ac.cn; zhanglq@nic.bmi.ac.cn

CASP2 besides cell-death control remains unclear[17]. Here we show that CASP2 is recruited into a ubiquitin and proteasome-positive biomolecular condensate and is required for the proper removal of overloaded ubiquitin chains under stress, defects of which result in the accumulation of pathological TAR DNA-binding protein 43 (TDP-43) aggregates and motor defects in vivo.

Results

CASP2 maintains ubiquitin homeostasis post stress

To understand the spatial dynamic regulation of ubiquitination homeostasis following cellular stress, we sequentially separated three HeLa cell fractions (Soluble I, Soluble II and Pellet) to detect the accumulation of ubiquitination after diverse stresses (Fig. 1a). We detected elevated ubiquitination in the Soluble II and Pellet fractions following HS or treatment with bortezomib (BTZ) but not other stresses (Fig. 1b). To further identify the potential factors involved in the overloaded ubiquitination, we performed liquid chromatography with tandem mass spectrometry (LC–MS/MS) on the Pellet fraction of samples following HS or BTZ treatment. After filtration we obtained 204 commonly detected candidates in the HS and BTZ treatment groups (Fig. 1c, Extended Data Fig. 1a,b and Supplementary Table 1). Proteins involved in essential biological processes and the previously reported HS-induced insoluble proteins[18,19] were specifically enriched in the Pellet fractions of the HS and BTZ treatment groups (Fig. 1d and Extended Data Fig. 1b,c), which is consistent with the previous finding that specific cellular activities are restricted under stress[18]. Moreover, DAXX, TRIM11, SQSTM1 and UBXN1, which have been recognized as PQC-related proteins[20–23], were also enriched (Extended Data Fig. 1d,e), hinting that proteins responsible for proper proteostasis regulation were enriched in the Pellet fraction.

In addition to previously reported proteostasis-related candidates—such as ubiquitin ligases, deubiquitinases (DUBs), proteasome subunits and autophagy regulators—CASP2 was notable as an unexpected protease accumulated in the Pellet fraction (Extended Data Fig. 1a). As the second caspase discovered in mammalian cells, CASP2 has always been recognized as an orphan caspase with no certain functions and substrates[17,24–26]. Interestingly, we confirmed that CASP2 accumulated in the Soluble II and Pellet fractions after HS or BTZ treatment (Fig. 1d,e and Extended Data Fig. 1f), suggesting a potential role of CASP2 in stress-induced overloaded ubiquitination. Further analysis confirmed that CASP2 accumulated in the Soluble II and Pellet fractions following stress, which was consistent with the change of ubiquitination (Extended Data Fig. 2a,b). Similarly, in the recovery stage after HS, the accumulated ubiquitinated conjugates and CASP2 were synchronously decreased in the Soluble II and Pellet fractions (Extended Data Fig. 2c), suggesting that the accumulation of CASP2 is reversible. Moreover, compared with the classical apoptotic caspases, only caspase-9, which has the highest sequence similarity to CASP2, accumulated in the Soluble II and Pellet fractions after proteome stress (Extended Data Fig. 2d). Apart from exotic stress, overexpression of proteotoxicity proteins, such as the heterologous protein firefly luciferase and yeast Ubc9 harbouring temperature-sensitive mutant (Ubc9ts), also disrupts proteostasis[27–29]. We found that green fluorescent protein (GFP)–luciferase or mCherry–Ubc9ts overexpression led to the accumulation of CASP2 in the Pellet fraction, whereas GFP and mCherry had no such effect (Extended Data Fig. 2e,f), further verifying that CASP2 is involved in ubiquitin homeostasis. Importantly, CASP2 accumulated in the Soluble II and Pellet fractions post HS and BTZ treatment was not a splicing form (an activated CASP2 resulted from autohydrolysis of the CASP2 proenzyme), indicating that the traditional proteolytic activation might not be required for its function in ubiquitin homeostasis (Extended Data Fig. 2g).

To verify whether CASP2 is required to regulate the overloaded ubiquitination, we constructed a *CASP2*-knockout (*CASP2*-KO) HEK293T cell line and found that CASP2 deletion caused an accumulation of poly-ubiquitinated conjugates in the Soluble II and Pellet fractions during the recovery stage after HS (Fig. 1f). Furthermore, Ubc9ts exhibited a distinct increase in ubiquitination after HS and gradually returned to normal levels during the recovery, whereas the loss of CASP2 decreased the turnover of ubiquitinated Ubc9ts (Fig. 1g). Consistent with these data, the ubiquitin-positive puncta, especially Lys48-linked ubiquitin (Lys48-Ub), were mostly cleared away in control cells after recovery for 2 h, whereas the *CASP2*-KO cells still had a certain number of puncta that remained unremoved (Fig. 1h–j). Together, CASP2 is recruited into the insoluble fraction under proteome stress and CASP2 deficiency leads to the accumulation of protected stress-induced ubiquitinated conjugates.

CASP2 deficiency is detrimental to cells post stress

We then performed tandem ubiquitin-binding entity (TUBE)-based ubiquitinome analysis to detect the ubiquitinated conjugates accumulated in *CASP2*-KO cells after HS. After discarding the Soluble I fraction, the remaining fractions from the HS and recovery groups were lysed and incubated with immobilized TUBE beads (Fig. 2a), and the TUBE-captured proteins were analysed using quantitative MS (Supplementary Table 2). The ratio of proteins recovered after HS was calculated by comparing the intensity of these TUBE-captured proteins in the recovery groups to that in the HS groups (ratio = intensity_{R2h} / intensity_{HS}); more than 80% of the proteins in *CASP2*-KO cells had a higher ratio compared with the control cells (Fig. 2b), indicating that these proteins were excessively ubiquitinated in the *CASP2*-KO groups. Next, we sorted out 116 different proteins for further enrichment analysis (Extended Data Fig. 3a). Remarkably, eleven proteins were highly relevant to amyotrophic lateral sclerosis (ALS; Fig. 2c and Extended Data Fig. 3b)—a progressive neurodegenerative disease affecting nerve cells in the brain and spinal cord—including TDP-43 (encoded by *TARDBP*) and TANK-binding kinase 1 (TBK1; Fig. 2d). Consistent with the observed phenotypes of the heterologous protein Ubc9ts (Extended Data Fig. 2f), overexpression of TDP-43 also disrupted the function of the UPS and induced the accumulation of ubiquitinated conjugates and CASP2 in the Pellet fraction, whereas another protein, von Hippel–Lindau tumour suppressor (VHL), which is prone to forming misfolded mutants and did not induce overloaded ubiquitination, had no such effect (Extended Data Fig. 3c). It has been reported that overloaded ubiquitination and hyperphosphorylation of TDP-43 and TBK1 are pathological features of ALS[30–32]. A pull-down assay showed that TDP-43 in *CASP2*-KO cells had higher levels of ubiquination and decreased turnover compared with control cells (Extended Data Fig. 3d). Moreover, CASP2 co-localized with phosphorylated TDP-43 (pTDP-43) in cells subjected to HS or BTZ treatment (Fig. 2e and Extended Data Fig. 3e) and *CASP2*-KO cells accumulated more pTDP-43 puncta after HS compared with control cells (Extended Data Fig. 3f,g). Furthermore, endogenous TDP-43 and TBK1 as well as their phosphorylated forms accumulated at higher levels in the Soluble II and Pellet fractions of *CASP2*-KO cells during recovery compared with control cells (Fig. 2f and Extended Data Fig. 3h), suggesting that CASP2 is required to decrease the ubiquitination level and subsequent aggregate formation of these toxic proteins after HS.

The formation of aggregates of toxic proteins such as TDP-43 ultimately elicits cell death[33]. We found that *CASP2*-KO cells had reduced colony-forming efficiency after HS (Fig. 2g,h). Moreover, the *CASP2*-KO cells were more susceptible to BTZ treatment and had elevated cell death rates (Fig. 2i,j and Extended Data Fig. 3i,j). These data indicate that CASP2 knockout causes aberrant proteostasis and pathological protein aggregation in cells.

CASP2-deficient mice display motor defects

Considering that aberrant proteostasis and pathological protein aggregation (especially the ubiquitin-positive inclusion body) are recognized as a hallmark of ageing and neurodegenerative disease[34,35], we subsequently analysed whether *Casp2*-KO mice had related phenotypes. Previous studies have reported that *Casp2*-null mice are viable and exhibit

https://doi.org/10.1038/s41556-024-01522-8

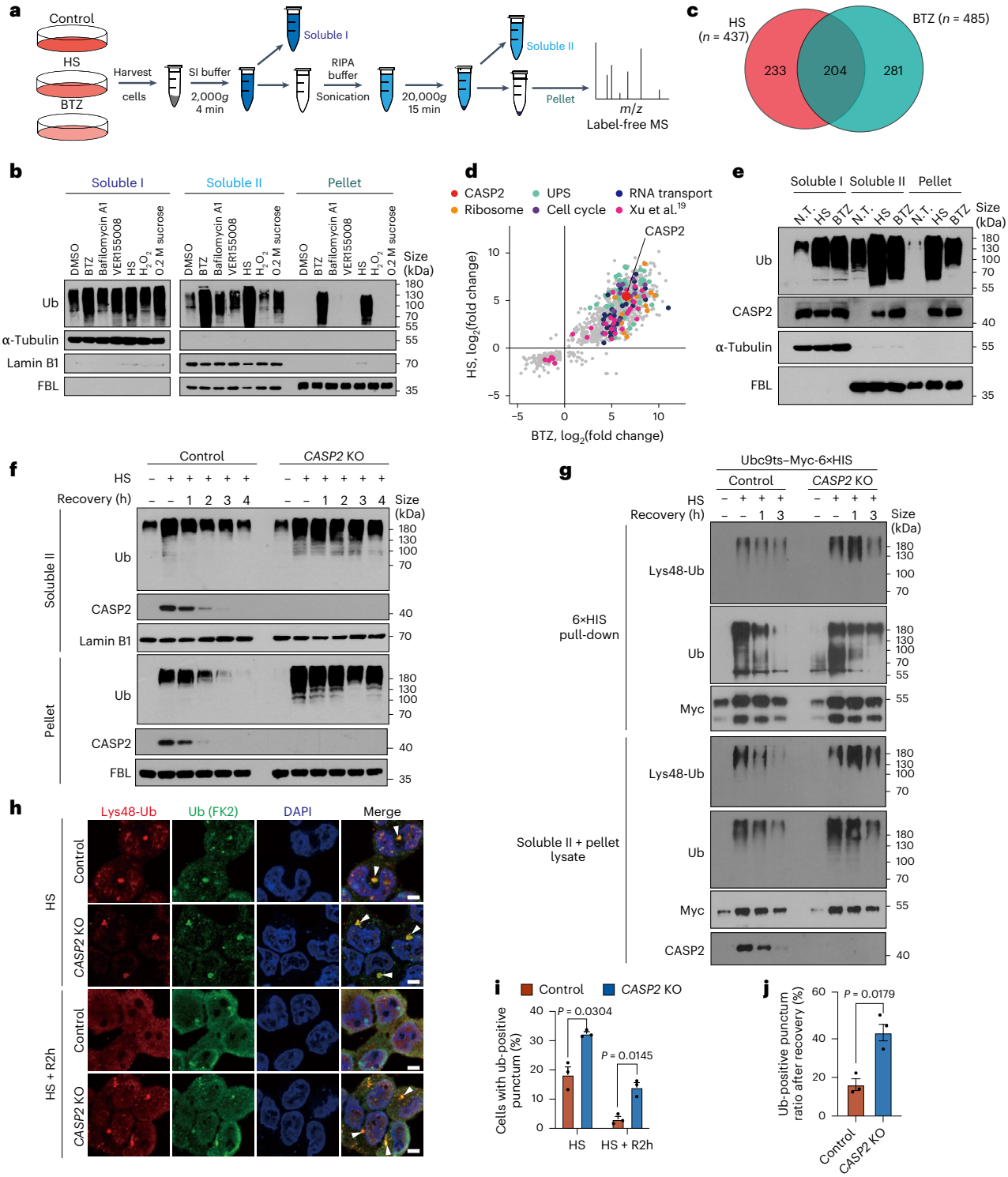

Fig. 1 | CASP2 is required to regulate the overloaded ubiquitin chains under proteome stress. a, Schematic of the process of cell fraction separation and MS analysis of the Pellet fraction. **b**, Immunoblot analysis of ubiquitination in HeLa cell fractions following exposure to different stressors. DMSO, dimethylsulfoxide. **c**, Number of significantly different proteins in the Pellet fractions of HS- and BTZ-treated cells. **d**, Two-dimensional dot plot of the significantly enriched proteins identified in HS- and BTZ-treated cells. **e**, Immunoblot analysis of CASP2 and ubiquitination in cell fractions of SH-SY5Y cells. N.T., not treated. **f**, Immunoblot analysis of ubiquitination in the Soluble II and Pellet fractions of HEK293T cells exposed to HS (42 °C, 2 h) and recovery (37 °C) at the indicated time points. **g**, Immunoblot analysis of Ubc9ts ubiquitination HEK293T cells expressing Myc-6×histidine (His)-tagged mCherry–Ubc9ts following HS (42 °C, 2 h) and recovery (37 °C) at the indicated time points. **h**, Representative immunofluorescence images of control and *CASP2*-KO HEK293T cells exposed to HS (42 °C, 2 h) or recovery (37 °C, 2 h) after HS (HS + R2h). The arrowheads point to ubiquitination-positive puncta. Scale bars, 5 µm. DAPI, 4′,6-diamidino-2-phenylindole. **i**, Percentage of cells in **h** with ubiquitination-positive puncta. **j**, Ratio of ubiquitination-positive puncta ratio after recovery, calculated by dividing the percentage of the R2h group by the percentage of the HS group in **i**. **h**–**j**, $n = 3$ independent experiments per group. **i**,**j**, Two-tailed paired Student's *t*-test. Data are shown as the mean ± s.e.m. All data are representative of three independent experiments. Ub, ubiquitination; FBL, Fibrillarin.

https://doi.org/10.1038/s41556-024-01522-8

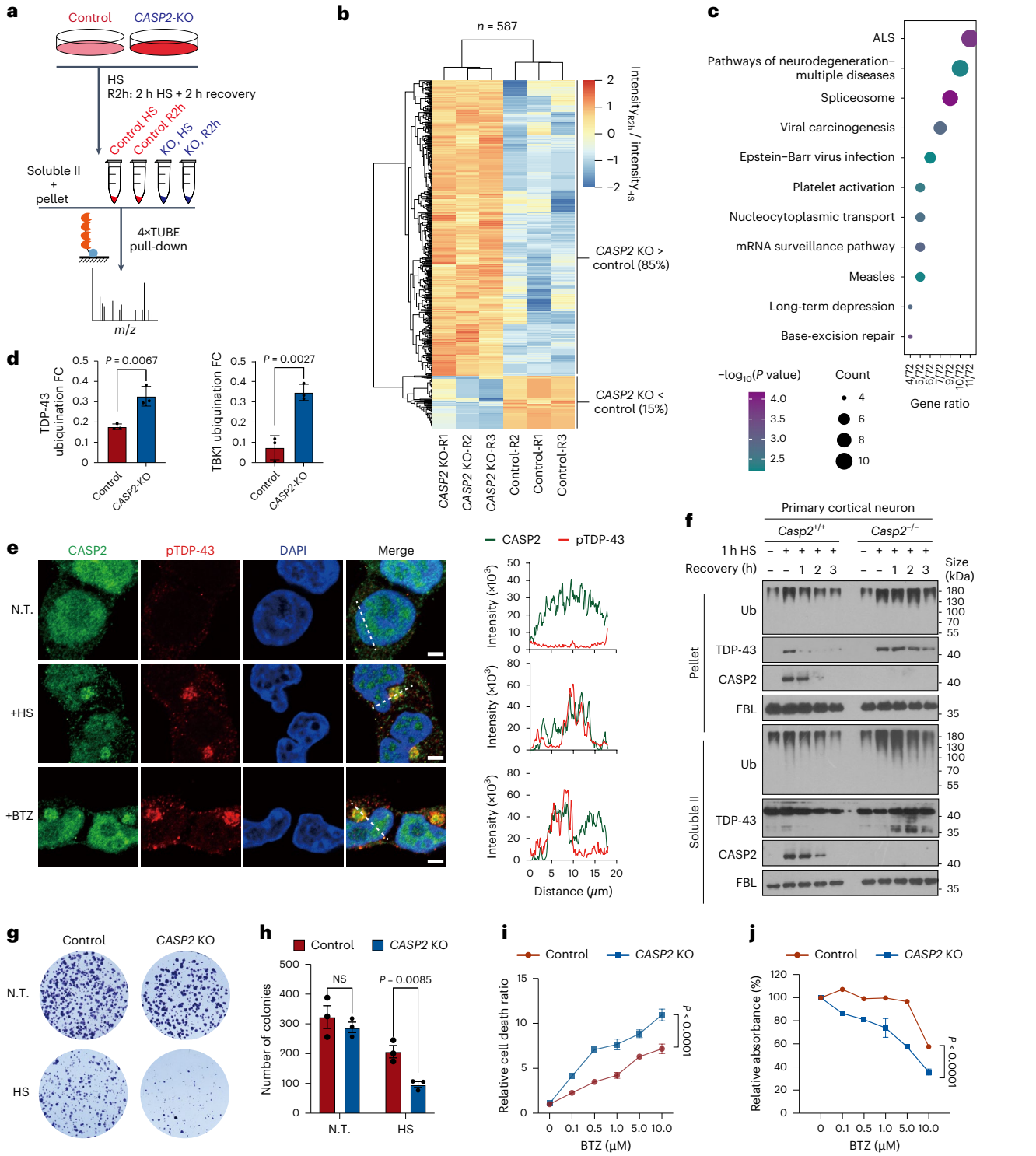

Fig. 2 | CASP2 deficiency is detrimental to cell homeostasis following proteome stress. a, Schematic illustrating the TUBE-captured ubiquitinated proteins in the Soluble II and Pellet fractions of control and *CASP2*-KO cells exposed to HS (42 °C, 2 h) and recovery (37 °C, 2 h). **b**, Relative abundance of ubiquination, determined as the ratio of proteins recovered after recovery to those recovered after HS, in fractions of control and *CASP2*-KO cells. R1–3, replicates 1–3. **c**, Kyoto Encyclopedia of Genes and Genomes pathway analysis of proteins that were significantly changed in *CASP2*-KO cells compared with control cells. **d**, Fold change (FC) in TDP-43 and TBK1 ubiquitination, determined using MS, in control and *CASP2*-KO HEK293T cells. Two-tailed unpaired Student's *t*-test; $n = 3$ independent replicates per group. **e**, Representative images of immunofluorescent staining of CASP2 and pTDP-43 in HEK293T cells following HS (42 °C, 2 h) and BTZ (1 μM, 8 h) treatment (left). The fluorescence intensities along the dashed line were plotted (right). Scale bars, 5 μm. **f**, Immunoblot analysis of ubiquitination and CASP2 in the Soluble II and Pellet fractions of primary cortical neurons exposed to HS (42 °C, 1 h) and recovery (37 °C) at the indicated time points. **g**, Colony formation assay of control and *CASP2*-KO HEK293T cells treated with or without two rounds of HS. **h**, Quantification of the colonies in **g**. Two-tailed unpaired *t*-test; NS, not significant ($P > 0.05$); $n = 3$ independent replicates per group. **i**,**j**, Cell death (**i**) and survival (**j**) of control and *CASP2*-KO HEK293T cells exposed to different concentrations of BTZ for 36 h. Two-way analysis of variance. **i**, The cell death ratio was evaluated by detecting the release of adenylate kinase (AK) from damaged cells; $n = 4$ independent replicates per group. **j**, Cell survival was measured using a cell counting kit-8 assay; $n = 3$ independent replicates per group. All data are shown as the mean ± s.e.m. Data are representative of three independent experiments.

limited phenotypes, such as ageing-related traits and inflammation of organs[36,37]. Here we found that the *Casp2*-KO mice (10–14 months old) exhibited overt hindlimb-clasping disorder compared with control mice (Fig. 3a and Extended Data Fig. 4a). Consistent with these data, a rotarod test and grip force assay revealed impaired motor function in *Casp2*-KO mice (Fig. 3b,c). In a gait analysis we observed shortened stride lengths (Extended Data Fig. 4b,c) and decreased movement speed (Extended Data Fig. 4d–f) in *Casp2*-KO mice. Furthermore, electromyography was performed to measure the innervation between nerves and muscles in those mice. The myogenic motor-evoked potential was lower in *Casp2*-KO mice compared with controls (Fig. 3d) and resting electromyographic recordings revealed spontaneous fibrillation in the gastrocnemius of *Casp2*-KO mice (Fig. 3e), indicating defects in the connectivity between the upper and lower motor neurons. *Casp2*-KO mice indeed had increased numbers of fragmented neuromuscular junctions (NMJs) in the tibialis anterior (Fig. 3f,g). Moreover, the number of choline acetyltransferase-positive neurons was decreased in the ventral horn of the spinal cord of *Casp2*-KO mice (Extended Data Fig. 4g,h). These data collectively confirmed neuromuscular denervation in *Casp2*-KO mice, which is a common phenotype observed in motor neuron diseases[38].

Next, the relationship between phenotypes of *Casp2*-KO mice and pathological protein TDP-43 aggregation was analysed. Immunofluorescence assays showed that CASP2 co-localized with the ubiquitin-positive and pTDP-43-positive puncta in the primary motor cortex and spinal cord of control mice (Extended Data Fig. 4i,j). Furthermore, Lys48-Ub-positive puncta in the primary motor cortex of the *Casp2*-KO mouse brains were more prominent, both in size and quantity, and these puncta co-localized with the accumulated pTDP-43 (Fig. 3h–j), suggesting that ubiquitination and pathological aggregation of TDP-43 is associated with the neuromuscular denervation phenotypes of *Casp2*-KO mice.

To further verify the in vivo role of CASP2 in the progression of TDP-43 proteinopathies, neonatal mice were intracerebroventricularly (i.c.v.) injected with adeno-associated virus (AAV)-PhP.eB vectors containing GFP or GFP–TDP-43 (AAV–GFP and AAV–TDP-43, respectively) on postnatal day 1 (Fig. 3k). Interestingly, the intensity of GFP–TDP-43 in the primary motor cortex of AAV–TDP-43-injected *Casp2*-KO mice was higher than the control AAV–TDP-43-injected mice, whereas no differences in intensity were observed between the AAV–GFP groups (Fig. 3l,m). The brains of *Casp2*-KO mice accumulated more GFP–TDP-43 in the insoluble pellet compared with other groups (Fig. 3n). Similarly, GFP–TDP-43 was more prominent in the spinal cord and brainstem of AAV–TDP-43-injected *Casp2*-KO mice (Extended Data Fig. 5a–d). Motor behavioural experiments confirmed that motor impairments were more severe for *Casp2*-KO mice injected with AAV–TDP-43 (Fig. 3o, Extended Data Fig. 5e–h and Supplementary Video 1). As expected, resting electromyographic recordings of *Casp2*-KO mice i.c.v. injected with AAV–TDP-43 displayed more prominent high-frequency spontaneous firings of the motor units compared with the other groups (Extended Data Fig. 5i). Neuromuscular denervation pathology in *Casp2*-KO mice i.c.v. injected with AAV–TDP-43 was verified by NMJ staining and counting of choline acetyltransferase-positive neurons (Extended Data Fig. 5j–o). Moreover, the primary motor cortex of AAV–TDP-43-injected *Casp2*-KO mice possessed more pTDP-43 and Lys48-Ub-positive puncta than control mice following i.c.v. injection with AAV–TDP-43 (Fig. 3p). These data suggested that overexpression of TDP-43 in vivo greatly promoted disease progression compared with the natural process of ageing and *Casp2* KO accelerated these phenotypes, further confirming that CASP2 is required to decrease the accumulation of the pathological protein TDP-43, which avoids the proteostasis function disruption and neuromuscular denervation in mice.

CASP2 is integrated into a ubiquitin-positive condensate

To further explore the ubiquitination-associated regulatory role of CASP2 in living cells, the dynamic cellular distribution of CASP2 was analysed using monomeric GFP (mGFP)-tagged CASP2 stably expressed in HEK293T cells. Based on the observation that overexpression of wild-type CASP2 caused cytotoxicity[26], we used the inactivated C320A mutant (CASP2-CA) for stable expression. We found that CASP2 gradually concentrated and formed a visible punctum after 1 h of HS treatment (Fig. 4a and Supplementary Video 2). Similarly, CASP2 formed a punctum following BTZ treatment for 6 h (Fig. 4a and Supplementary Video 3), which was consistent with the immunoblotting results (Extended Data Fig. 2a,b). Furthermore, among all caspases, only CASP2 formed apparent puncta with HS or BTZ treatment (Extended Data Fig. 6a). Similarly, when cells were transfected with Ubc9ts–mCherry, CASP2 accumulated together with Ubc9ts to form a large punctum (Fig. 4b). Notably, we observed that CASP2-involved puncta had liquid-like properties and recovered after photobleaching (Fig. 4c), suggesting that the puncta were biomolecular condensates formed via liquid–liquid phase separation. Moreover, the CASP2-containing condensate had clear co-localization with ubiquitinated conjugates in cells (Fig. 4d,e), whereas other DUBs identified in the Pellet fraction (Extended Data Fig. 1a) did not co-localize with ubiquitin (Extended Data Fig. 6b).

We found that incubation of the fluorescently labelled CASP2 full-length (FL)-CA protein with GFP–8Ub (linear ubiquitin chains containing 8 ubiquitins) formed obvious spherical condensates in vitro (Fig. 4f). Fusion of small condensates (containing CASP2 and ubiquitin) into a larger condensate was observed (Fig. 4g). Moreover, 1 M NaCl, 1,6-hexanediol and 1,2-propylene glycol[39], but not 2,5-hexanediol, were capable of disrupting the in vitro-formed condensate (Fig. 4h). Interestingly, CASP2 could not form condensates with GFP–mono-ubiquitin (monoUb; Fig. 4f), probably due to the need of a multivalent interaction for condensates formation[9]. These data suggest that CASP2 forms liquid-like condensates with poly-ubiquitin chains.

Fig. 3 | CASP2-deficient mice exhibit motor defects. a, Representative images (left) and quantification of the hindlimb-clasping phenotype (right) of *Casp2*$^{+/+}$ and *Casp2*$^{-/-}$ mice; $n = 22$ and 21 mice, respectively. **b**, Rotarod test of *Casp2*$^{+/+}$ and *Casp2*$^{-/-}$ mice; $n = 20$ and 22 mice, respectively. **c**, Grip force of *Casp2*$^{+/+}$ and *Casp2*$^{-/-}$ mice; $n = 22$ and 25 mice, respectively. **d**, Quantitative analysis (up) and representative images (bottom) of myogenic motor-evoked potential (MMEP) in gastrocnemius muscles of *Casp2*$^{+/+}$ and *Casp2*$^{-/-}$ mice; $n = 4$ mice per group. **e**, Resting electromyographic of gastrocnemius muscles of *Casp2*$^{+/+}$ and *Casp2*$^{-/-}$ mice. **f**,**g**, Representative images (**f**) and quantification (**g**) of NMJs in the tibialis anterior of *Casp2*$^{+/+}$ and *Casp2*$^{-/-}$ mice; $n = 3$ mice per group. **f**, The arrow indicates the denervated or partially innervated endplate. NF/Syn, neurofilament/synapsin; α-BTX, α-bungarotoxin. **h**, Size of Lys48-Ub puncta in *Casp2*$^{+/+}$ and *Casp2*$^{-/-}$ mouse brains; $n = 41$ and 155 puncta, respectively. **i**, Number of Lys48-Ub in *Casp2*$^{+/+}$ and *Casp2*$^{-/-}$ mouse brains; $n = 4$ mice per group. **j**, Representative immunofluorescence images of Lys48-Ub and pTDP-43 in the primary motor cortex of *Casp2*$^{+/+}$ and *Casp2*$^{-/-}$ mice. Arrowheads indicate the Lys48-Ub and pTDP-43-positive puncta. **k**, Mice were injected (i.c.v.) with AAV–GFP and AAV–TDP-43 into each ventricle on postnatal day 1 (P1). **l**,**m**, Representative images (**l**) and quantification (**m**) in the primary motor cortex of *Casp2*$^{+/+}$ and *Casp2*$^{-/-}$ mice injected with AAV–TDP-43; $n = 3$ mice per group. **f**,**j**,**l**, Magnified views of the regions in the white boxes are presented (bottom in **f**; right in **j** and **l**). **n**, Immunoblot analysis of GFP and GFP–TDP-43 in AAV-injected *Casp2*$^{+/+}$ and *Casp2*$^{-/-}$ mouse brains. **o**, Grip force of *Casp2*$^{+/+}$ and *Casp2*$^{-/-}$ AAV-injected mice; $n = 12$ (*Casp2*$^{+/+}$ AAV–GFP), 9 (*Casp2*$^{-/-}$ AAV–GFP), 14 (*Casp2*$^{+/+}$ AAV–TDP-43) and 11 (*Casp2*$^{-/-}$ AAV–TDP-43) mice. **p**, Representative images of Lys48-Ub and pTDP-43 co-localization with GFP–TDP-43 in the primary motor cortex of *Casp2*$^{+/+}$ and *Casp2*$^{-/-}$ AAV-injected mice. Arrows indicate the GFP-TDP-43, Lys48-Ub and pTDP-43-positive puncta. **a**–**d**,**g**,**i**, Two-tailed unpaired Student's *t*-test. **h**, Mann–Whitney *U*-test. **m**,**o**, Two-way ANOVA with Tukey's multiple comparisons test. NS, not significant ($P > 0.05$). All data are shown as the mean ± s.e.m. Data are representative of three independent experiments. Scale bars, 25 μm (**f**), 10 μm (**j**), 100 μm (**l**) and 50 μm (**p**).

https://doi.org/10.1038/s41556-024-01522-8

CASP2 has been reported to formed a large complex in incubated cell lysate[40], but the components and functions of this large complex remain unexplored. Using size-filtration chromatography of the Soluble II fraction, we found that CASP2 was also involved in a large complex (molecular weight of nearly 2,000 kDa) in the Soluble II fraction after HS (Fig. 5a). To investigate this CASP2-associated complex further, exogenous FLAG-tagged CASP2 was used to co-immunoprecipitate the components of this large complex from the Soluble II fraction,

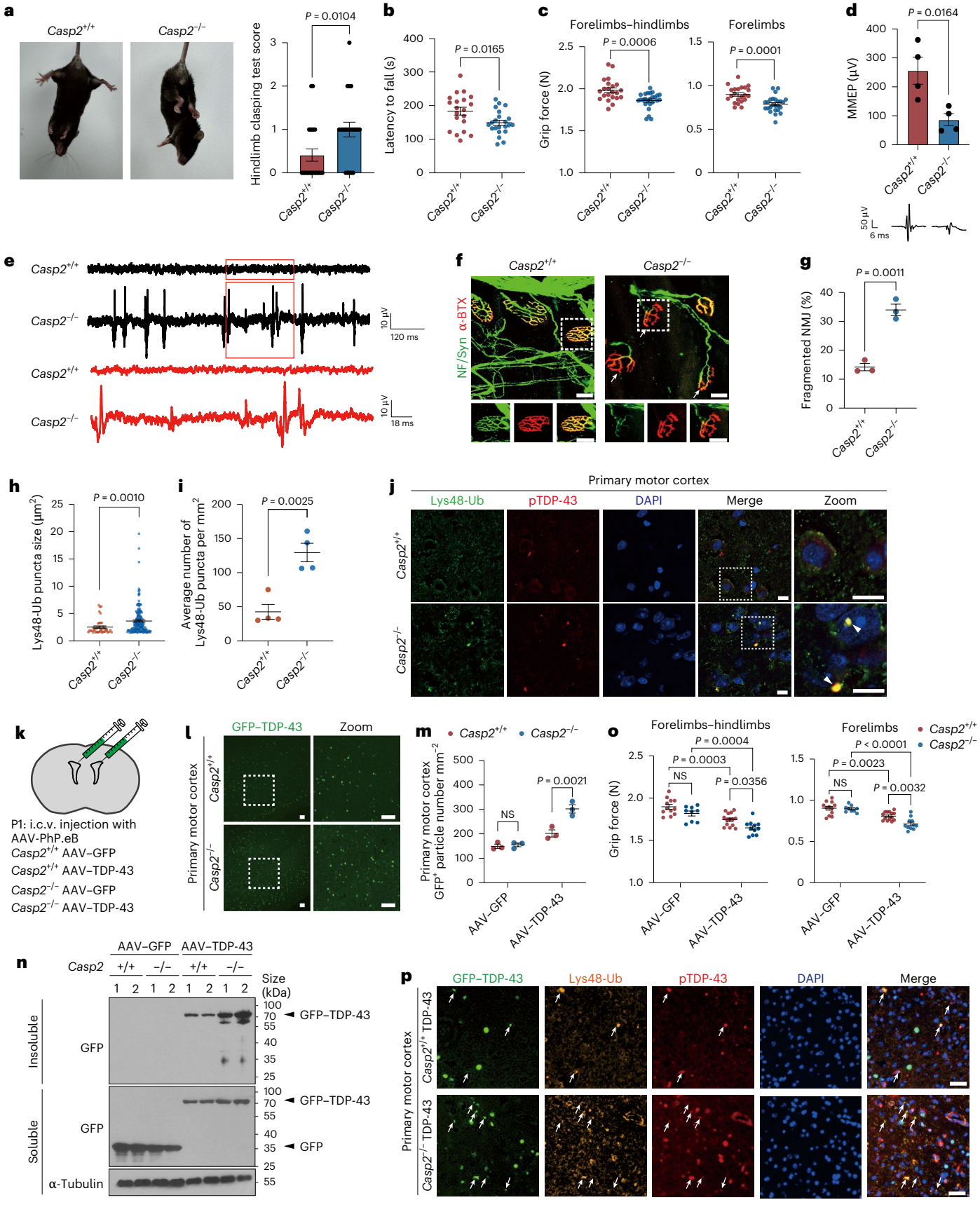

https://doi.org/10.1038/s41556-024-01522-8

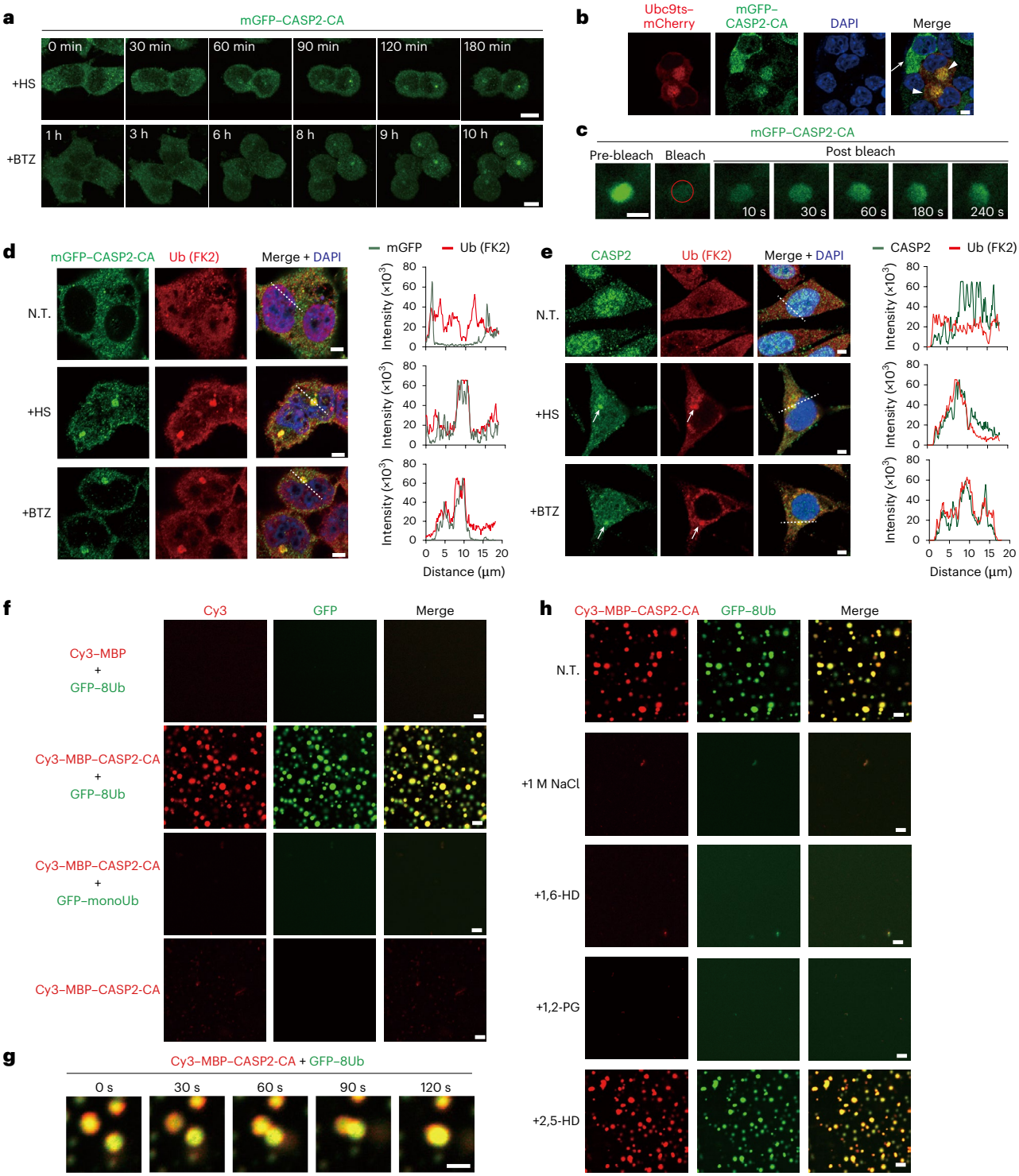

Fig. 4 | CASP2 is integrated into a ubiquitin-positive condensate. **a**, Representative images of live-cell fluorescence imaging during HS or BTZ treatment of HEK293T cells stably expressing mGFP–CASP2-CA. **b**, Representative fluorescence images of CASP2 and Ubc9ts in HEK293T cells stably expressing mGFP–CASP2-CA and transfected with mCherry-tagged Ubc9ts. The arrowheads indicate co-localization of CASP2 and Ubc9ts in a large punctum and the arrow points to diffusely distributed CASP2 without Ubc9ts overexpression. **c**, Fluorescence recovery after photobleaching (red outline) of an mGFP–CASP2-CA punctum in HEK293T cells. Time-lapse images of bleached cells. **d**, Representative fluorescence images of poly-ubiquitin (FK2) in HEK293T cells stably expressing mGFP–CASP2-CA after HS (42 °C, 2 h) and BTZ (1 μM, 8 h) treatment (left). The fluorescence intensities along the dashed line were plotted (right). **e**, Representative images of immunofluorescence staining of endogenous CASP2 and poly-ubiquitin (FK2) in SH-SY5Y cells after HS (42 °C, 2 h) and BTZ (1 μM, 8 h) treatment (left). Arrows indicate the ubiquitin-positive puncta. The fluorescence intensities along the dashed line were plotted (right). **f**, Representative images of phase separation by mixing Cy3-labelled maltose-binding protein (MBP)–CASP2-FL-CA protein (20 μM) with GFP–8Ub or GFP–monoUb (20 μM). **g**, Liquid-droplet fusion of Cy3–MBP–CASP2-FL-CA and GFP–8Ub proteins. **h**, Liquid droplets of Cy3–MBP–CASP2-FL-CA and GFP–8Ub proteins were treated with 1 M NaCl, 1,6-hexanediol (1,6-HD), propylene glycol (1,2-PG) or 2,5-hexanediol (2,5-HD). Scale bars, 10 μm (**a**), 5 μm (**b**,**d**–**f**,**h**), 2 μm (**c**,**g**). Data are representative of three independent experiments.

https://doi.org/10.1038/s41556-024-01522-8

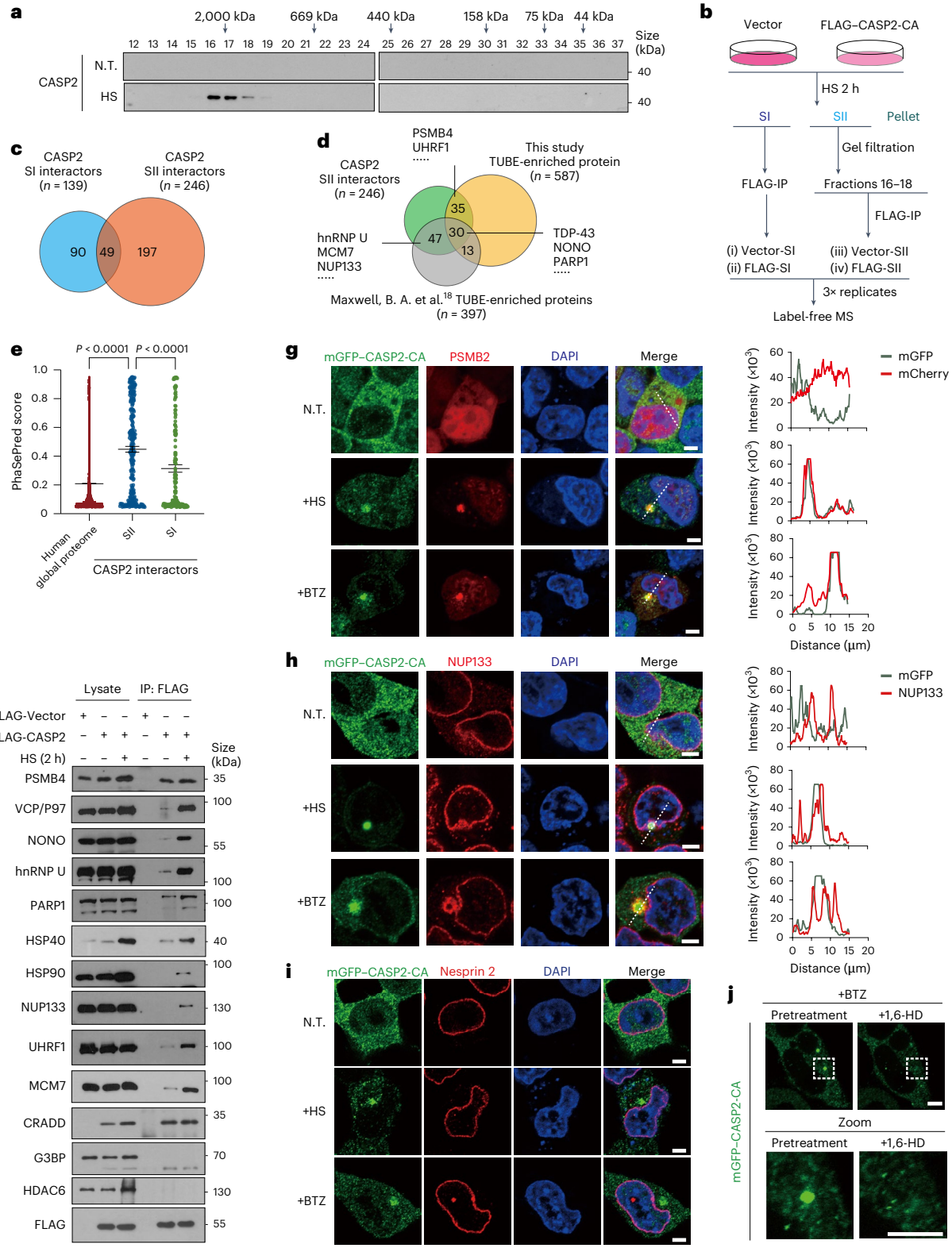

Fig. 5 | CASP2-containing condensate is highly related to overloaded ubiquitination. a, Immunoblot analysis of CASP2 in Soluble II fractions separated using gel filtration chromatography. **b**, Schematic of the experiment using immunoprecipitation with MS (IP–MS) for identification of the interactors of CASP2 in Soluble I and II fractions exposed to HS (42 °C, 2 h). **c**, Number of filtered potential interactors of CASP2 in the Soluble I and II fractions. **d**, Number of CASP2 interactors that are shared between Soluble II fractions and TUBE-enriched proteins. **e**, PhaSePred scores of proteins from the indicated groups. One-way ANOVA with Dunnett's multiple comparisons test. **f**, Immunoblot analysis of the interactors of CASP2 in Soluble II fractions of HEK293T cells with or without HS (42 °C, 2 h). **g**–**i**, Representative images of PSMB2–mCherry (**g**), NUP133 (**h**) and nesprin 2 (**i**) in HEK293T cells stably expressing mGFP–CASP2-CA treated with HS (42 °C, 2 h) and BTZ (1 μM, 8 h). Scale bars, 5 μm. **g**,**h**, The fluorescence intensities along the dashed line were plotted (right). **j**, Representative fluorescence images of mGFP–CASP2-CA in HEK293T cells following treatment with BTZ for 6 h and 5% 1,6-hexanediol (1,6-HD). Magnified views of the regions in the white boxes are provided (bottom). Scale bars, 5 μm. All data are shown as the mean ± s.e.m. Data are representative of three independent experiments. SI, Soluble I; SII, Soluble II; IP, immunoprecipitation.

which was compared with the co-immunoprecipitated compound from the Soluble I fraction (Fig. 5b and Supplementary Tables 3 and 4). Quantitative proteomics identified a total of 336 interactors in these two fractions and 49 interactors were detected in both fractions (Fig. 5c). We noticed that the previously identified interactors of CASP2—that is, TRAF1, TRAF2 and BIRC2—were mostly enriched in the Soluble I fraction (Extended Data Fig. 7a,b). In contrast, analysis of CASP2 interactors in the Soluble II fraction showed that these proteins were greatly enriched in the ubiquitinated substrates, which are sensitive to HS, as nearly half of the potential interactors were identified in our TUBE-captured proteins and other ubiquitinomics data[18], further confirming that CASP2 in the Soluble II fraction was related to the HS-related overloaded ubiquitination (Fig. 5d and Extended Data Fig. 7c,d). Using PhaSePred[41] to predict the phase-separation property of the interactors, we found that the potential interactors of the Soluble II fraction had more possibilities to undergo phase separation (Fig. 5e). The co-immunoprecipitation assay further suggested that the proteasome subunit proteins, chaperonins and proteins sensitive to HS were enriched as the Soluble II interactors (Fig. 5f). Consistent with these data, the CASP2-containing condensate had clear co-localization with the proteasome subunit PSMB2 (Fig. 5g). Hence, CASP2 is integrated into a large biomolecular condensate that may contain proteasome and ubiquitinated proteins.

Multiple membraneless biomolecular condensates are involved in PQC[42,43]. However, minimal co-localization of CASP2 with the marker proteins of those reported condensates—such as nuclear stress bodies (HSF1) and stress granules (G3BP and USP10) was observed (Extended Data Fig. 7e–g). Furthermore, the CASP2-containing condensate was surrounded by the nuclear pore protein NUP133 (Fig. 5h). Nonetheless, fluorescent staining of outer nuclear envelope markers (nesprin 2) showed that the CASP2-containing condensate was not surrounded by the skeleton of the outer nuclear membrane (Fig. 5i) and this condensate in cells was completely dissolved following treatment with 1,6-hexanediol (Fig. 5j), suggesting that the NUP133-surrounded CASP2-containing condensate is a membraneless compartment. Aggresome has been reported as a stress-induced aggregation in mammalian cells[44]. We found that histone deacetylase 6 (HDAC6), an aggresome marker protein[45], did not co-localize with the CASP2-containing condensate after treatment with HS for 2 h and BTZ for 6 h (Extended Data Fig. 7h). Interestingly, prolonged BTZ treatment forced the CASP2-containing condensate into a larger and irregular aggregate containing HDAC6 (Extended Data Fig. 7h). Therefore, we named this proteome stress-induced and CASP2-containing condensate an ubstressome to emphasise its correlation with stress-induced ubiquitination and the distinct property compared with aggregation.

CASP2 binds overloaded ubiquitin chains via its UIML region

The correlation between CASP2 and ubstressome captured our interest. CASP2 contains a conservative caspase activation and recruitment domain (CARD), a large p19 subunit and a small p12 subunit[46]. Previous findings indicate that the CARD domain is required for nuclear distribution[47]. In our assays the CARD domain of CASP2 (CASP2-CARD) was sufficient to form a punctum, whereas deletion of CARD domain (CASP2–ΔCARD) failed (Fig. 6a). Consistent with these data, only the CASP2 CARD domain formed condensate with ubiquitin in vitro (Extended Data Fig. 8a). Here we compared the CARD domain with the classical ubiquitin-binding domain and recognized that a conservative Phe 102–Thr 109 region (FCEALRET) in the CASP2 CARD domain resembled the ubiquitin-interacting motif (UIM, Fig. 6b and Extended Data Fig. 8b). The UIM adopts a single short α-helix to bind the hydrophobic groove of ubiquitin, comprising a Φ-x-x-Ala-Φ-x-x-Ser sequence (Φ denotes a large hydrophobic residue)[48]. Similarly, the ubiquitin-interacting motif-like (UIML) region of CASP2 docked to the Ile 44 patch (Ile 44, Leu 8, His 68 and Val 70) of ubiquitin in all five top-ranked models predicted by AlphaFold-Multimer[49] via multiple hydrophobics (Fig. 6c). However, these residues of the UIML region (α-helix 5) of CARD in the AlphaFold2-predicted structure were buried in a cluster of helices (Extended Data Fig. 8c). We reasoned that the UIML region of CARD requires further allosteric effects to bind ubiquitin and HS might open the protein conformation. Heat shock indeed greatly promoted CARD to bind ubiquitin chains from cell lysates, and mutants of UIML residues (CARD-3A and CARD-3E) failed to do so (Fig. 6d). Furthermore, CASP2-CARD was capable of binding in vitro-assembled Lys48 poly-ubiquitin chains (Extended Data Fig. 8d,e) and the branched chains (Extended Data Fig. 8f–h), whereas the truncated CARD domain without α5 and α6 and mutants of UIML residues lost this ability (Extended Data Fig. 8e). It is worth noting that the conjunct ubiquitin chains had a molecular weight of >50 kDa (Extended Data Fig. 8d–h), hinting that the UIML of CARD had a higher affinity for longer poly-ubiquitin chains similar to the classical UIM[50]. Interestingly, among all human caspases and the nematode caspase CED-3, only CED-3 had homogeneous UIML residues with CASP2 and pull-down assays confirmed that CASP2 and CED-3 both bound to ubiquitin chains in vitro (Extended Data Fig. 8i), further confirming the binding affinity of UIML residues to ubiquitin chains. Consistent with these data, the mGFP-tagged wild-type CARD (CARD-WT) domain formed condensates in cells, whereas GFP-tagged CARD-3A and CARD-3E remained diffusely distributed (Fig. 6e). Importantly, cells that were pretreated with ubiquitin-activating enzyme (E1) inhibitor (TAK-243) blocked the overloaded ubiquitination, resulting in failure of CASP2 to form detectable puncta after HS or BTZ treatment (Fig. 6f–h), indicating that the recruitment of CASP2 to the ubstressome is dependent on the formation of overloaded ubiquitin chains. Together, these data demonstrate that CASP2 harbours an UIML region in the CARD domain to bind the overloaded ubiquitin chains, which is crucial for the recruitment of CASP2 into the ubstressome.

CASP2 is a DUB towards overloaded ubiquitination

Next, we sought to investigate the mechanisms of the CASP2-containing ubstressome in the removal of overloaded ubiquitination. Unexpectedly, the active forms of CASP2—CASP2 full length (CASP2-FL) and CASP2-ΔCARD reduced the ectopically expressed ubiquitin chains in cells (Extended Data Fig. 9a,b). Overexpression of ubiquitin alone, considered as a form of ubiquitin-associated stress, can dramatically alter the ubiquitin pool[51,52] and induced mGFP–CASP2 to form puncta (Extended Data Fig. 9c). In addition, among the tested mammalian caspases, CASP2 resulted in the highest decrease in the level of exogenous ubiquitin chains (Extended Data Fig. 9d). It is well-known that caspases are proteases that specifically cleave after aspartate[46]. However, the levels of ubiquitin mutants with all five Asp residues replaced by either Glu or Ala were still decreased by CASP2 (Fig. 7a), thereby excluding the possibility of a canonical cleavage mode of CASP2 towards the ubiquitin. Given that overexpression of DUBs directly downregulated the cellular ubiquitination, we speculated that CASP2 might have a DUB-like activity. The decreased effect of CASP2 towards the ubiquitin was indeed similar to the effects of many DUBs (Extended Data Fig. 9e). Moreover, overexpression of USP21 decreased the entire pool of ubiquitin chains in cells, whereas CASP2 only decreased the excessive ubiquitin chains (Extended Data Fig. 9f), indicating that the DUB-like activity of CASP2 only responds to overloaded ubiquitination. Consistent with these data, the overexpressed ubiquitination levels were also enhanced in the Soluble II and Pellet fractions of *CASP2*-KO cells (Fig. 7b). Similar results were observed in HS- or BTZ-treated Pellet fractions (Extended Data Fig. 9g,h), further confirming the cleavage effect of CASP2 towards the overloaded ubiquitination. Furthermore, prokaryotic-expressed CASP2 catalysis core ($CASP2^{cat}$) cleaved ubiquitin chains from both native and boiled cell lysates (Fig. 7c), and using TDP-43 as a substrate, we further demonstrated that CASP2 also cleaved its conjugated ubiquitin chains (Fig. 7d), confirming that CASP2 is capable of cleaving the ubiquitin chains directly.

https://doi.org/10.1038/s41556-024-01522-8

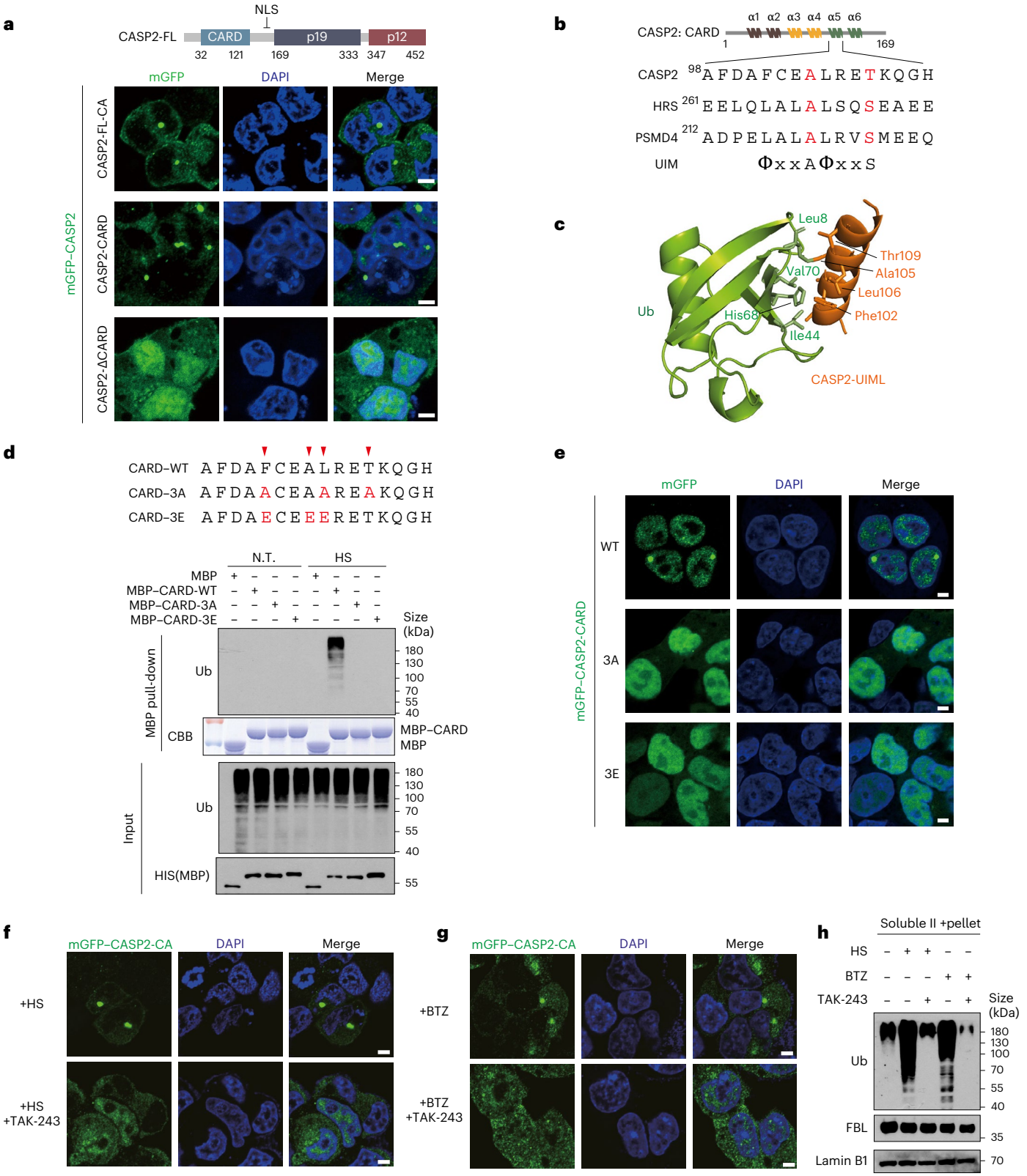

Fig. 6 | CASP2 binds overloaded ubiquitin chains via its UIML region. **a**, Representative fluorescence images of mGFP-tagged CASP2-FL-CA, CASP2-CARD and CASP2-ΔCARD stably expressed in HEK293T cells treated with HS (42 °C, 2 h). NLS, nuclear localization signal. **b**, Sequence alignment of CASP2 helix α5 and other ubiquitin-interacting motifs (UIMs). **c**, Structure model of the CASP2 UIML region bound to ubiquitin. **d**, MBP pull-down assay, followed by immunoblot analysis of the interaction between MBP-tagged CARD-WT, CARD-3A and CARD-3E with ubiquitin chains in whole-cell lysates. CBB, Coomassie brilliant blue staining. **e**, Representative fluorescence images of HEK293T cells stably expressing CARD-WT, CARD-3A or CARD-3E. **f**,**g**, Representative fluorescence images of CASP2 distribution in HEK293T cells stably expressing mGFP–CASP2 and treated with or without TAK-243 (2 μM) following HS (42 °C, 2 h; **f**) or BTZ (1 μM, 8 h; **g**) treatment. **a**,**e**–**g**, Scale bars, 5 μm. **h**, Immunoblots showing the inhibitory effect induced by TAK-243. Data are representative of three independent experiments.

https://doi.org/10.1038/s41556-024-01522-8

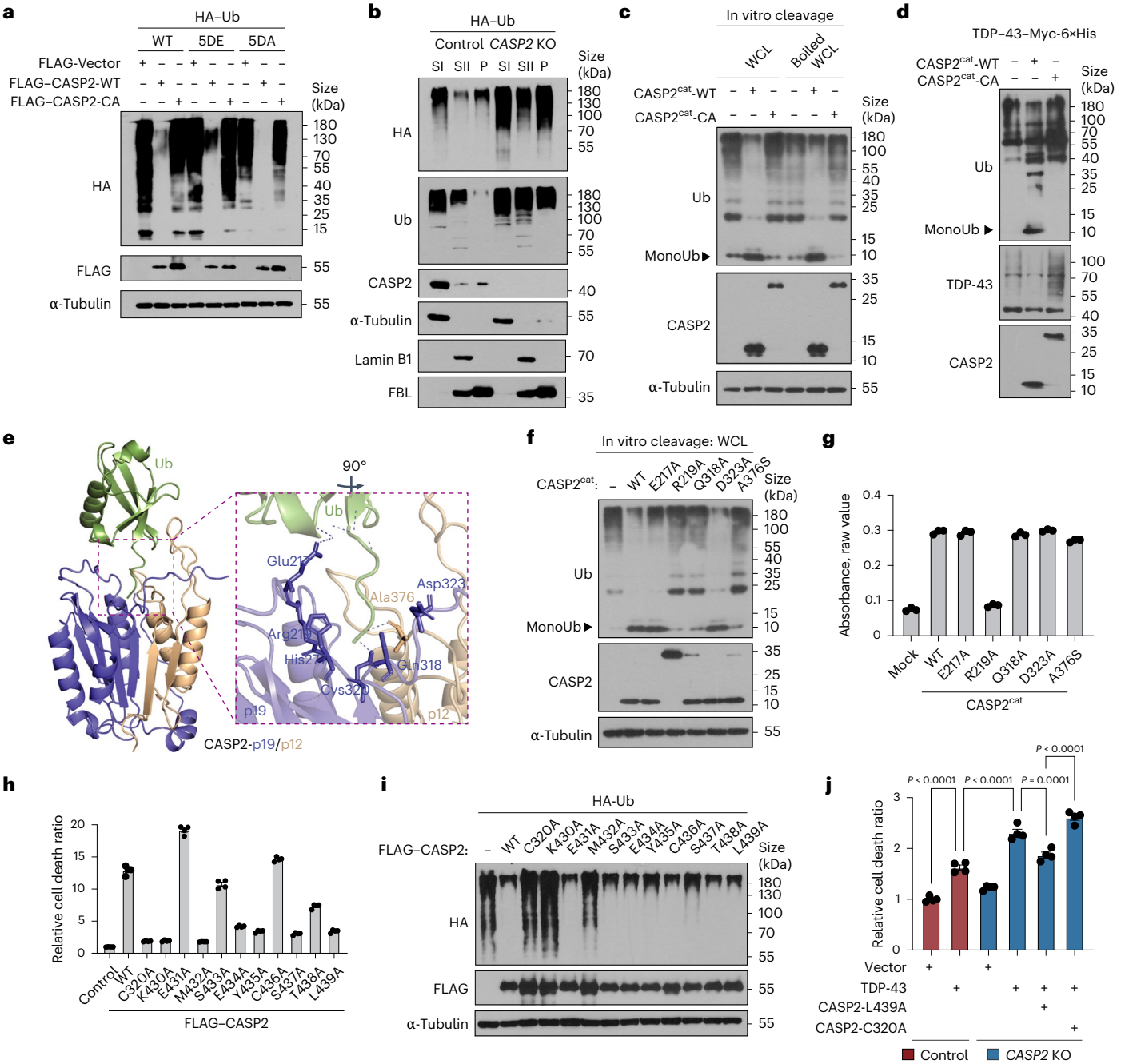

Fig. 7 | CASP2 is a DUB targeting the overloaded ubiquitin chains. **a**, Immunoblot analysis of the indicated proteins in HEK293T cells transfected with haemagglutinin (HA)-tagged ubiquitin (wild-type (WT) and the 5DE and 5DA mutants) and CASP2. **b**, Immunoblot analysis of the indicated proteins in isolated fractions of control and *CASP2*-KO HEK293T cells. SI, Soluble I; SII, Soluble II; P, pellet. **c**, Immunoblot analysis of in vitro cleavage of ubiquitin chains in native or boiled whole-cell lysate (WCL) by CASP2^{cat}. **d**, Immunoblot analysis of in vitro on-bead CASP2^{cat} cleavage of ubiquitinated TDP-43 purified from HEK293T cells. **e**, Structure model of CASP2 recognition of the ubiquitin carboxy (C) terminus. The binding interface is highlighted by a pink dashed box, which has been magnified (right). **f**, Immunoblot analysis of in vitro cleavage of ubiquitin chains in boiled WCL by CASP2^{cat} WT and the indicated mutants. **g**, Activity levels of CASP2^{cat} and its mutants towards the tetrapeptide substrate Ac-Val-Asp-Val-Ala-Asp-pNA, a colorimetric substrate for CASP2, which was used as an in vitro cleavage substrate. Absorbance was detected at 405 nm; $n = 3$ independent replicates per group. **h**, Cell death of HEK293T cells overexpressing CASP2-WT or its mutants. **i**, Immunoblot analysis of the indicated proteins in HEK293T cells transfected with HA-tagged ubiquitin and CASP2-WT or its mutants. **j**, Cell death of control and *CASP2*-KO HEK293T cells overexpressing TDP-43 with or without the CASP2 mutants. One-way ANOVA with Tukey's multiple comparisons test. **h**,**j**, The cell death ratio was evaluated by detecting the release of AK from damaged cells; $n = 4$ independent replicates per group. Data are shown as the mean ± s.e.m. Data are representative of three independent experiments.

The substrate-catalytic pocket of CASP2 is surrounded by several unstructured loops in a classical 12-stranded-β-sheet catalytic core[53]. Docking simulation of CASP2 and ubiquitin using AlphaFold-Multimer[49] showed an optimal conformation where the Arg 72-Leu-Arg-Gly-Gly 76 terminal residues of ubiquitin were inserted into the CASP2 substrate-catalytic groove (Fig. 7e and Extended Data Fig. 10a). Further analysis screened out five residues (Glu 217, Arg 219, Gln 318, Asp 323 and Ala 376) in the CASP2 catalytic pocket, which might be responsible for the recognition and cleavage of ubiquitin. Subsequent protein cleaving assays showed that mutations of the

https://doi.org/10.1038/s41556-024-01522-8

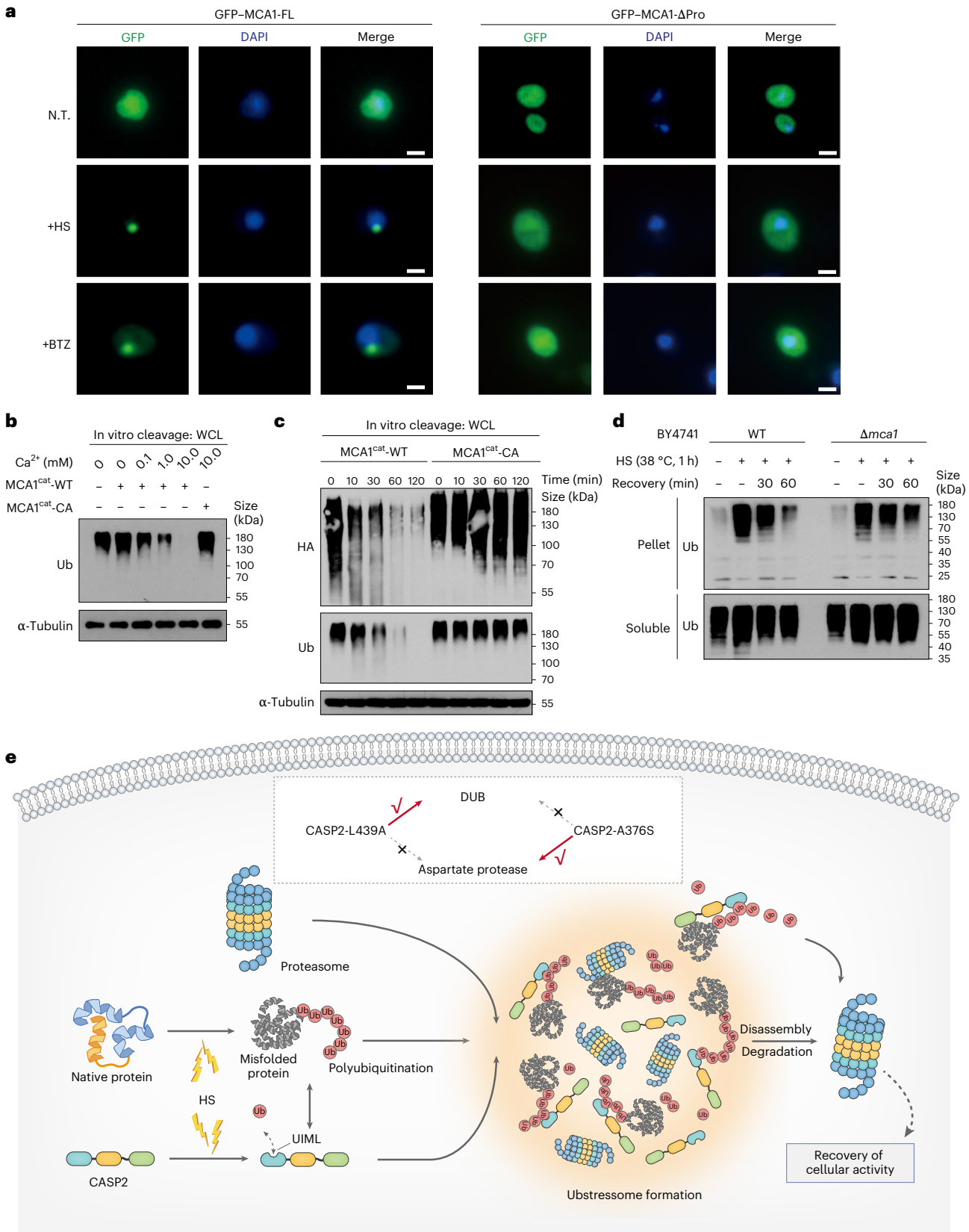

Fig. 8 | Yeast MCA1 decreases overloaded ubiquitin chains to regulate PQC. **a**, Representative fluorescence images of BY4741 yeast cells stably expressing GFP–MCA1-FL and GFP–MCA1-ΔPro after treatment with HS (38 °C, 2 h) or BTZ (2 μM, 12 h). Scale bars, 5 μm. **b**, Immunoblot analysis of the cleavage of ubiquitin chains in boiled whole-cell lysate (WCL) by MCA1^{cat} in the indicated Ca^{2+} concentrations. **c**, Immunoblot analysis of the cleavage of ubiquitin chains over time in boiled WCL by MCA1^{cat}. The reaction mixture contained 10 mM Ca^{2+} to active MCA1. **d**, Immunoblot analysis of ubiquitination in the Soluble and Pellet fractions of MCA1-wild-type and MCA1-deficient (Δ*mca1*) BY4741 yeast cells exposed to HS (38 °C, 1 h) or recovery at the indicated time points. **e**, Model for CASP2 recognizing and decreasing overloaded ubiquitin chains to regulate PQC. Data are representative of three independent experiments.

Arg 219, Gln 318 and Ala 376 residues blocked the cleavage of ubiquitin chains by CASP2 (Fig. 7f). Two mutants (Q318A and A376S) still maintained the ability to hydrolyze the canonical aspartate residues (acetyl) Ac-Val-Asp-Val-Ala-Asp-p-nitroaniline (pNA) and Ac-Val-Asp-Gln-Gln-Asp-pNA; Fig. 7g and Extended Data Fig. 10b) and promote apoptosis when expressed in cells (Extended Data Fig. 10c,d), except for an Arg-Ala mutation at position 219 (R219A). As the expression of the Q318A mutant also showed 30% decreased apoptosis compared with CASP2-WT, we recognized that the Ala 376 residue was the potential site for ubiquitin recognition in the catalytic pocket of CASP2, which is responsible for the non-classical cleavage of ubiquitin chains. Next, we sought to identify the mutant that lacked pro-apoptotic function but still retained the deubiquitinate activity. Considering that ubiquitin recognition was independent of the CASP2 heterodimerization based on the predicted model (Extended Data Fig. 10a), we screened the mutants in the β6-sheet of small subunits (KEMSEYCSTL, amino acid residues 430–439) for the pro-apoptosis property. We found that the expression of L439A mutants resulted in dramatically decreased apoptosis but still cleaved the exogenous ubiquitin chain (Fig. 7h,i and Extended Data Fig. 10e). Meanwhile, expression of the L439A mutant prompted the turnover of the HS-induced ubiquitinated conjugates as well as the pTDP-43 in *CASP2*-KO cells (Extended Data Fig. 10f). More importantly, CASP2-L439A reduced the TDP-43-induced cell toxicity, as revealed by re-overexpressing CASP2-L439A in *CASP2*-KO cells, this result indicates that the DUB activity of CASP2 protected cells from the damage of proteome stress. (Fig. 7j). Collectively, our data identify that CASP2 has previously unrecognized deubiquitinating activity directly targeting the overloaded ubiquitin chains.

Apart from the caspases identified in mammalian species, the caspase homologue metacaspase-1 (MCA1) in yeast is reported to be essential for the clearance of insoluble protein aggregates during proteome stress[54,55]. Similar to CASP2, full-length MCA1 (MCA1-FL) formed a condensate in yeast cells treated with HS or BTZ, whereas deletion of its pro domain led to a diffused distribution under proteome stress (Fig. 8a). Moreover, the MCA1 catalytic core ($MCA1^{cat}$) was capable of cleaving the ubiquitin chains in vitro (Fig. 8b,c) and MCA1-deficient (Δ*mca1*) yeast cells had decreased turnover of poly-ubiquitinated conjugates in the Pellet fraction (Fig. 8d). Thus, the ability of the yeast MCA1 to cleave ubiquitin chains might represent an evolutionally conservative function of caspases in maintaining ubiquitin homeostasis under stress.

Discussion

The removal of stress-induced overloaded ubiquitinated conjugates to maintain homeostasis remains largely undefined. Here we reveal that CASP2 is a crucial protease responsible for the recovery of ubiquitination homeostasis in response to proteome stress. We discover that stress-induced overloaded ubiquitinated conjugates, along with the proteasome, form a biomolecular condensate, which we named an ubstressome, and CASP2 is recruited into the ubstressome through its ubiquitin-binding UIML region. Furthermore, CASP2 functions as a DUB targeting the overloaded ubiquitination, promoting the degradation of these substrates and relieving the toxic state of these proteins (Fig. 8e).

It is generally accepted that caspases prefer to cleave substrates with a specific tetrapeptide sequence consisting of aspartate at the P1 position[46]. However, this dogma is mainly based on in vitro assays without considering substrate interactions and the cellular environment. For example, caspase-4 and caspase-1 cleave gasdermin D via substrate-binding exo-sites instead of a tetrapeptide sequence[56]. Our results uncover a unique cleavage pattern of CASP2 that targets poly-ubiquitin chains, which deepens the knowledge of caspase cleavage preference and specificity. Previous studies indicated dual roles for CASP2 in promoting apoptosis and survival[37], and a recent study showed its protective role in ferroptosis and that loss of CASP2 affects stress pathway gene expression[57,58]. Here we find that CASP2 plays a protective role in cell fitness via an undefined mechanism by decreasing the accumulation of the pathological protein TDP-43. CASP2 is the most evolutionarily conserved caspase among mammalian caspases. However, its function remains largely unclear, leading to the idea that it may be a vestigial remnant[59]. Our data show that CASP2 and MCA1 have evolutionally conservative functions and they act as stress-associated caspases in maintaining ubiquitin homeostasis. Together, we propose that the family of caspases could be subclassed into at least three categories including apoptotic caspases (caspase-8, -9, -3, -6 and -7), inflammatory caspases (caspase-1, -4 and -5) and stress caspases (mammalian CASP2 and yeast MCA1).

Several ubiquitin-related molecules are associated with biomolecular condensates via liquid–liquid phase separation but the composition and assembly of the stress-induced ubiquitination-associated condensates are not fully understood[11,15]. Here we show that HS and proteasome inhibition induce apparent overloaded ubiquitinated conjugates and these conjugates form a biomolecular condensate—the ubstressome. We propose that the formation of the ubstressome can be induced by three factors: (1) excessive de novo ubiquitin synthesis and formation of poly-ubiquitin chains, (2) impaired protein degradation and (3) accumulation of misfolding proteins. We further reveal that the ubstressome represents a biomolecular condensate that may be associated with diverse chaperonins and proteasomes that transiently sequester overloaded ubiquitinated proteins under proteome stress. The overloaded ubiquitin chains provide multivalent binding platforms, which promote the recruitment of other proteins[60]. During the recovery phase following stress, CASP2 along with the proteasome and other cofactors potentially work together to degrade or refold ubiquitinated proteins. Thus, we propose that the ubstressome-mediated deubiquitinating activity of CASP2 helps relieve the damage induced by tangly misfolded proteins.

The accumulation of pathological aggregates, which causes aberrant proteostasis, is a hallmark of ALS. Although activation of autophagy to restore cellular homeostasis has been a promising strategy for the treatment of neurodegenerative disease[61], the elimination of these aggregates in ALS remains elusive. We identify a CASP2-mediated protein aggregate elimination pathway that targets TDP-43 and TBK1. Interestingly, CASP2 also regulated synaptic plasticity and mice lacking CASP2 displayed deficits in the dendritic spine and elevated levels of anxiety[62]. In this study we revealed that *Casp2*-KO mice exhibit neuromuscular denervation, a common phenotype observed in motor neuron diseases, which suggests a role of CASP2 in ALS. Thus, promoting the activation of CASP2 could be an innovative way to recover the protein degrading ability of proteasomes and perhaps provide a potential treatment for ALS.

Online content

Any methods, additional references, Nature Portfolio reporting summaries, source data, extended data, supplementary information, acknowledgements, peer review information; details of author contributions and competing interests; and statements of data and code availability are available at https://doi.org/10.1038/s41556-024-01522-8.

References

1. Banani, S. F., Lee, H. O., Hyman, A. A. & Rosen, M. K. Biomolecular condensates: organizers of cellular biochemistry. *Nat. Rev. Mol. Cell Biol.* **18**, 285–298 (2017).
2. Alberti, S. & Hyman, A. A. Biomolecular condensates at the nexus of cellular stress, protein aggregation disease and ageing. *Nat. Rev. Mol. Cell Biol.* **22**, 196–213 (2021).
3. Frottin, F. et al. The nucleolus functions as a phase-separated protein quality control compartment. *Science* **365**, 342–347 (2019).
4. Yasuda, S. et al. Stress- and ubiquitylation-dependent phase separation of the proteasome. *Nature* **578**, 296–300 (2020).

5. Aguzzi, A. & Altmeyer, M. Phase separation: linking cellular compartmentalization to disease. *Trends Cell Biol.* **26**, 547–558 (2016).
6. Patel, A. et al. A liquid-to-solid phase transition of the ALS protein FUS accelerated by disease mutation. *Cell* **162**, 1066–1077 (2015).
7. Mathieu, C., Pappu, R. V. & Taylor, J. P. Beyond aggregation: pathological phase transitions in neurodegenerative disease. *Science* **370**, 56–60 (2020).
8. Fu, A., Cohen-Kaplan, V., Avni, N., Livneh, I. & Ciechanover, A. p62-Containing, proteolytically active nuclear condensates, increase the efficiency of the ubiquitin-proteasome system. *Proc. Natl Acad. Sci. USA* **118**, e2107321118 (2021).
9. Sun, D., Wu, R., Zheng, J., Li, P. & Yu, L. Polyubiquitin chain-induced p62 phase separation drives autophagic cargo segregation. *Cell Res.* **28**, 405–415 (2018).
10. Johnson, J. O. et al. Exome sequencing reveals VCP mutations as a cause of familial ALS. *Neuron* **68**, 857–864 (2010).
11. Deng, H.-X. et al. Mutations in UBQLN2 cause dominant X-linked juvenile and adult-onset ALS and ALS/dementia. *Nature* **477**, 211–215 (2011).
12. Hallengren, J., Chen, P.-C. & Wilson, S. M. Neuronal ubiquitin homeostasis. *Cell Biochem. Biophys.* **67**, 67–73 (2013).
13. Neumann, M. et al. Ubiquitinated TDP-43 in frontotemporal lobar degeneration and amyotrophic lateral sclerosis. *Science* **314**, 130–133 (2006).
14. Mori, H., Kondo, J. & Ihara, Y. Ubiquitin is a component of paired helical filaments in Alzheimer's disease. *Science* **235**, 1641–1644 (1987).
15. Bennett, E. J. et al. Global changes to the ubiquitin system in Huntington's disease. *Nature* **448**, 704–708 (2007).
16. Shimura, H. et al. Ubiquitination of a new form of α-synuclein by parkin from human brain: implications for Parkinson's disease. *Science* **293**, 263–269 (2001).
17. Bouchier-Hayes, L. & Green, D. R. Caspase-2: the orphan caspase. *Cell Death Differ.* **19**, 51–57 (2012).
18. Maxwell, B. A. et al. Ubiquitination is essential for recovery of cellular activities after heat shock. *Science* **372**, eabc3593 (2021).
19. Xu, G. et al. Vulnerability of newly synthesized proteins to proteostasis stress. *J. Cell Sci.* https://doi.org/10.1242/jcs.176479 (2016).
20. Huang, L. et al. DAXX represents a new type of protein-folding enabler. *Nature* **597**, 132–137 (2021).
21. Zhang, Z.-Y. et al. TRIM11 protects against tauopathies and is down-regulated in Alzheimer's disease. *Science* **381**, eadd6696 (2023).
22. Mukkavalli, S., Klickstein, J. A., Ortiz, B., Juo, P. & Raman, M. The p97–UBXN1 complex regulates aggresome formation. *J. Cell Sci.* **134**, jcs254201 (2021).
23. Bjørkøy, G. et al. p62/SQSTM1 forms protein aggregates degraded by autophagy and has a protective effect on huntingtin-induced cell death. *J. Cell Biol.* **171**, 603–614 (2005).
24. Vakifahmetoglu-Norberg, H. & Zhivotovsky, B. The unpredictable caspase-2: what can it do? *Trends Cell Biol.* **20**, 150–159 (2010).
25. Forsberg, J., Zhivotovsky, B. & Olsson, M. Caspase-2: an orphan enzyme out of the shadows. *Oncogene* **36**, 5441–5444 (2017).
26. Wang, L., Miura, M., Bergeron, L., Zhu, H. & Yuan, J. Ich-1, an Ice/ced-3-related gene, encodes both positive and negative regulators of programmed cell death. *Cell* **78**, 739–750 (1994).
27. Bence, N. F. Impairment of the ubiquitin-proteasome system by protein aggregation. *Science* **292**, 1552–1555 (2001).
28. Gupta, R. et al. Firefly luciferase mutants as sensors of proteome stress. *Nat. Methods* **8**, 879–884 (2011).
29. Betting, J. & Seufert, W. A yeast Ubc9 mutant protein with temperature-sensitive in vivo function is subject to conditional proteolysis by a ubiquitin- and proteasome-dependent pathway. *J. Biol. Chem.* **271**, 25790–25796 (1996).
30. Hasegawa, M. et al. Phosphorylated TDP-43 in frontotemporal lobar degeneration and amyotrophic lateral sclerosis. *Ann. Neurol.* **64**, 60–70 (2008).
31. Neumann, M. et al. Phosphorylation of S409/410 of TDP-43 is a consistent feature in all sporadic and familial forms of TDP-43 proteinopathies. *Acta Neuropathol.* **117**, 137–149 (2009).
32. Shao, W. et al. Two FTD-ALS genes converge on the endosomal pathway to induce TDP-43 pathology and degeneration. *Science* **378**, 94–99 (2022).
33. Zhang, Y.-J. et al. Aberrant cleavage of TDP-43 enhances aggregation and cellular toxicity. *Proc. Natl Acad. Sci. USA* **106**, 7607–7612 (2009).
34. López-Otín, C., Blasco, M. A., Partridge, L., Serrano, M. & Kroemer, G. Hallmarks of aging: an expanding universe. *Cell* **186**, 243–278 (2023).
35. Wilson, D. M. et al. Hallmarks of neurodegenerative diseases. *Cell* **186**, 693–714 (2023).
36. Wilson, C. H. et al. Age-related proteostasis and metabolic alterations in *Caspase-2*-deficient mice. *Cell Death Dis.* **6**, e1615 (2015).
37. Bergeron, L. et al. Defects in regulation of apoptosis in caspase-2-deficient mice. *Genes Dev.* **12**, 1304–1314 (1998).
38. Verber, N. S. et al. Biomarkers in motor neuron disease: a state of the art review. *Front. Neurol.* **10**, 291 (2019).
39. Geiger, F. et al. Liquid–liquid phase separation underpins the formation of replication factories in rotaviruses. *EMBO J.* **40**, e107711 (2021).
40. Read, S. H., Baliga, B. C., Ekert, P. G., Vaux, D. L. & Kumar, S. A novel Apaf-1-independent putative caspase-2 activation complex. *J. Cell Biol.* **159**, 739–745 (2002).
41. Chen, Z. et al. Screening membraneless organelle participants with machine-learning models that integrate multimodal features. *Proc. Natl Acad. Sci. USA* **119**, e2115369119 (2022).
42. Gwon, Y. et al. Ubiquitination of G3BP1 mediates stress granule disassembly in a context-specific manner. *Science* **372**, eabf6548 (2021).
43. Zhang, H. et al. Reversible phase separation of HSF1 is required for an acute transcriptional response during heat shock. *Nat. Cell Biol.* **24**, 340–352 (2022).
44. Johnston, J. A., Ward, C. L. & Kopito, R. R. Aggresomes: a cellular response to misfolded proteins. *J. Cell Biol.* **143**, 1883–1898 (1998).
45. Kawaguchi, Y. et al. The deacetylase HDAC6 regulates aggresome formation and cell viability in response to misfolded protein stress. *Cell* **115**, 727–738 (2003).
46. Fuentes-Prior, P. & Salvesen, G. S. The protein structures that shape caspase activity, specificity, activation and inhibition. *Biochem. J.* **384**, 201–232 (2004).
47. Baliga, B. C. et al. Role of prodomain in importin-mediated nuclear localization and activation of caspase-2. *J. Biol. Chem.* **278**, 4899–4905 (2003).
48. Hofmann, K. & Falquet, L. A ubiquitin-interacting motif conserved in components of the proteasomal and lysosomal protein degradation systems. *Trends Biochem. Sci.* **26**, 347–350 (2001).
49. Evans, R. et al. Protein complex prediction with AlphaFold-Multimer. Preprint at *bioRxiv* https://doi.org/10.1101/2021.10.04.463034 (2022).
50. Husnjak, K. & Dikic, I. Ubiquitin-binding proteins: decoders of ubiquitin-mediated cellular functions. *Annu. Rev. Biochem.* **81**, 291–322 (2012).
51. Park, C.-W. & Ryu, K.-Y. Cellular ubiquitin pool dynamics and homeostasis. *BMB Rep.* **47**, 475–482 (2014).
52. Peng, H. et al. Ubiquitylation of p62/sequestosome1 activates its autophagy receptor function and controls selective autophagy upon ubiquitin stress. *Cell Res.* **27**, 657–674 (2017).

53. Schweizer, A., Briand, C. & Grütter, M. G. Crystal structure of caspase-2, apical initiator of the intrinsic apoptotic pathway. *J. Biol. Chem.* **278**, 42441–42447 (2003).
54. Hill, S. M., Hao, X., Liu, B. & Nystrom, T. Life-span extension by a metacaspase in the yeast *Saccharomyces cerevisiae*. *Science* **344**, 1389–1392 (2014).
55. Lee, R. E. C., Brunette, S., Puente, L. G. & Megeney, L. A. Metacaspase Yca1 is required for clearance of insoluble protein aggregates. *Proc. Natl Acad. Sci. USA* **107**, 13348–13353 (2010).
56. Wang, K. et al. Structural mechanism for GSDMD targeting by autoprocessed caspases in pyroptosis. *Cell* **180**, 941–955 (2020).
57. Dawar, S. et al. Caspase-2 protects against ferroptotic cell death. *Cell Death Dis.* **15**, 182 (2024).
58. Dorstyn, L. et al. Transcriptome profiling of caspase-2 deficient EμMyc and Th-MYCN mouse tumors identifies distinct putative roles for caspase-2 in neuronal differentiation and immune signaling. *Cell Death Dis.* **10**, 56 (2019).
59. Troy, C. M. & Ribe, E. M. Caspase-2: vestigial remnant or master regulator?. *Sci. Signal.* **1**, pe42 (2008).
60. Hou, X.-N. & Tang, C. The pros and cons ofubiquitination ontheformation of protein condensates. *Acta Biochim. Biophy. Sin.* **55**, 1084–1098 (2023).
61. Xu, D. et al. Modulating TRADD to restore cellular homeostasis and inhibit apoptosis. *Nature* **587**, 133–138 (2020).
62. Xu, Z.-X. et al. Caspase-2 promotes AMPA receptor internalization and cognitive flexibility via mTORC2–AKT–GSK3β signaling. *Nat. Commun.* **10**, 3622 (2019).

[1]State Key Laboratory of Medical Proteomics, National Center for Protein Sciences (Beijing), Beijing Institute of Lifeomics, Beijing, China. [2]School of Medicine, Tsinghua University, Beijing, China. [3]Department of Pathophysiology, School of Basic Medical Sciences, Anhui Medical University, Hefei, China. [4]Department of General Surgery, The First Medical Centre, Chinese PLA General Hospital, Beijing, China. [5]Department of Neurobiology, Beijing Institute of Basic Medical Sciences, Beijing, China. [6]Chinese Institute for Brain Research, Beijing, China. [7]CAS Key Laboratory of Pathogenic Microbiology and Immunology, Institute of Microbiology, Chinese Academy of Sciences, Beijing, China. [8]Savaid Medical School, University of Chinese Academy of Sciences, Beijing, China. [9]These authors contributed equally: Yingwei Ge, Lijie Zhou, Yesheng Fu. ✉e-mail: liucuihua@im.ac.cn; zhanglq@nic.bmi.ac.cn

Methods

Ethics statement

All experiments were performed in strict accordance with the 'Guide for the Care and Use of Laboratory Animals' and the 'Principles for the Utilization and Care of Vertebrate Animals', and were proved by the Institutional Animal Care and Use Committee at the Beijing Institute of Lifeomics (IACUC-20200705-42MBe).

Cell culture and treatment

HEK293T, HeLa and SH-SY5Y cells were obtained from the American Type Culture Collection. HEK293T and HeLa cells were cultured in DMEM medium (HyClone). SH-SY5Y cells were cultured in DMEM/F12 medium (Gibco). All media were supplemented with 10% fetal bovine serum, 100 units ml^{-1} penicillin and 0.1 mg ml^{-1} streptomycin. Cells were cultured in an incubator at 37 °C with 5% CO_2.

For the HS treatments, the cell dishes or plates were transferred from the 37 °C incubator to a pre-warmed 42 °C incubator at the indicated time points. After HS, the cells were moved back to the 37 °C incubator for recovery or harvesting. Bortezomib (Selleck, S1013) was mostly used at a concentration of 1 μM for the indicated time. For other drugs, cells were treated with 400 nM bafilomycin A1 (Selleck, S1413) and 1 μM VER155008 (Selleck, S7751) for 10 h. For the hypertonic treatment, the cell culture medium was replaced with fresh medium containing 0.2 M sucrose and treated for 20 min. For the oxidative stress treatment, 1 mM H_2O_2 (Sigma) was added to the medium and the treatment was performed for 30 min. For the E1-activating enzyme inhibitor treatment, cells were incubated with 2 μM TAK-243 (Selleck, S8341) for the indicated time during HS or BTZ treatment. For the etoposide (Beyotime, SC0173) treatment, the cells were treated with 10 μM etoposide for 24 h.

Isolation of primary cortical neurons

Culture dishes were precoated with poly-D-lysine (Sigma, P7280). Primary cortical neurons were isolated from mouse embryos on embryonic day 16.5. The cortex was dissected in ice-cold PBS using a stereo microscope, shredded using ophthalmic scissors and digested in Accutase (Yeasen, 40506ES60) solution for 10 min at 37 °C. The isolated cells were filtered with cell strainers and centrifuged. The primary cortical neurons were seeded in dishes containing DMEM/F12 medium supplemented with 10% fetal bovine serum, 10% horse serum (Gibco, 26050088), 2 mM GlutaMAX (Gibco, 35050061), 100 units ml^{-1} penicillin and 0.1 mg ml^{-1} streptomycin for 4–6 h. The primary cortical neurons were then cultured in Neurobasal Plus medium (Gibco, A3582901) supplemented with 2% B27 (Gibco, 1750404), 2 mM GlutaMAX, 100 units ml^{-1} penicillin and 0.1 mg ml^{-1} streptomycin in an incubator at 37 °C with 5% CO_2.

Antibodies

The following primary antibodies were used in this study at the indicated dilutions: anti-ubiquitin (clone P4D1; 1:1,000 for immunoblotting (IB); sc-8017) was purchased from Santa Cruz Biotechnology; anti-ubiquitin, Lys48-specific (clone Apu2; 1:2,000 for IB and 1:500 for immunofluorescence (IF); 05-1307) was purchased from Millipore; anti-G3BP (1:1,000 for IB and 1:250 for IF; ab181150), anti-PSMB4 (1:1,000 for IB; ab137087), anti-hnRNP U/p120 (1:5,000 for IB; ab180952), anti-BAG2 (1:1,000 for IB; ab79406), anti-MCM7/PRL (1:1,000 for IB; ab52489), anti-UHRF1 (1:5,000 for IB; ab213223), anti-TDP-43 (1:1,000 for IB; ab109535), anti-HSF1 (1:200 for IF; ab52757), anti-synaptophysin (1:200 for IF; ab16659), anti-NUP133 (1:1,000 for IB and 1:200 for IF; ab155990), anti-nesprin 2 (1:200 for IF; ab314872) and anti-mCherry (1:1,000 for IB; ab213511) were purchased from Abcam; anti-NONO (1:1,000 for IB; 90336S), anti-USP10 (1:200 for IF; catalogue number 8501), anti-PARP (1:1,000 for IB; 9542T), anti-FBL (1:2,000 for IB; catalogue number 2639), anti-HDAC6 (1:1,000 for IB and 1:200 for IF; 7558T), anti-TBK1 (1:1,000 for IB; catalogue number 3504), anti-phospho-TBK1 (1:1,000 for IB; catalogue number 5483), anti-caspase-3 (1:1,000 for IB; 14220T), anti-caspase-6 (1:1,000 for IB; 9762T), anti-caspase-7 (1:1,000 for IB; 12827T), anti-caspase-8 (1:1,000 for IB; 9746T), anti-caspase-9 (1:1,000 for IB; 9508T), anti-neurofilament-L/NF (1:400 for IF; 2837T) and anti-DYKDDDDK (1:5,000 for IB and 1:500 for IF; 14793S) were purchased from Cell Signaling Technology; anti-pTDP-43 (pS409/S410) (1:200 for IF; 66318-1-Ig), anti-GAPDH (1:2,000 for IB; 60004-1-Ig), anti-HSP40 (1:5,000 for IB; 13174-1-AP), anti-HSP70 (1:5,000 for IB; 10995-1-AP), anti-CDK1 (1:1,000 for IB; 19532-1-AP), anti-CASP2 (1:300 for IF; 10436-1-AP), anti-pTDP-43 (pS409/S410) (1:2,000 for IB; 22309-1-AP) and anti-RAIDD (1:1,000 for IB;10401-1-AP) were purchased from Proteintech; anti-multi-ubiquitin (clone FK2; clone FK2 has been reported to recognize K29-, K48- and K63-linked poly-ubiquitinated and mono-ubiquitinated proteins but not free ubiquitin; 1:2,000 for IB and 1:500 for IF; D058-3), anti-MYC (1:5,000 for IB; M192-3) and anti-HA (1:5,000 for IB and 1:500 for IF; M180-3) were purchased from MBL; anti-FLAG (clone M2; 1:5,000 for IB; F1804) was purchased from Sigma; anti-CASP2 (1:2,000 for IB; MA5-31999) was purchased from Invitrogen; anti-VCP/p97 (1:2,000 for IB; A2795), anti-USP5 (1:200 for IF; A4202), anti-USP48 (1:200 for IF; A5046), anti-choline acetyltransferase (1:800 for IF; A19031) and anti-HSP90 (1:2,000 for IB; A5006) were purchased from ABclonal; anti-α-tubulin (1:5,000 for IB; B1052) was purchased from Biodragon; anti-lamin B1 (1:2,000 for IB; P01L16) was purchased from Gene-Protein Link; and anti-HIS (1:5,000 for IB; TA-02) was purchased from ZSGB-BIO.

The following secondary antibodies were used in this study: horseradish peroxidase (HRP)-AffiniPure goat anti-mouse IgG (H+L) (1:10,000 for IB; 115-035-003) and HRP-AffiniPure goat anti-rabbit IgG (H+L) (1:10,000 for IB; 111-035-003) were purchased from Jackson; IPKine HRP, goat anti-mouse IgG LCS (A25012) was purchased from Abbkine; goat anti-mouse IgG (H+L) affinity purified, Alexa Fluor 488 (1:500 for IF; A32723), goat anti-rabbit IgG (H+L) affinity purified, Alexa Fluor 488 (1:500 for IF; A32731), goat anti-mouse IgG (H+L) affinity purified, Alexa Fluor 594 (1:500 for IF; A-11005), donkey anti-mouse IgG (H+L) affinity purified, Alexa Fluor 647 (1:500 for IF; A-31571) and goat anti-rabbit IgG (H+L) affinity purified, Alexa Fluor 594 (A-11012; 1:500 for IF) were purchased from Invitrogen.

Preparation of cell fractions and lysates

To isolate the three fractions of the cells (Fig. 1a), HEK293T, HeLa or SH-SY5Y cells were harvested by centrifugation and lysed with SI buffer (50 mM HEPES, 10 mM NaCl, 5 mM $MgCl_2$, 5 mM EDTA and 1% NP-40, pH 7.4) containing protease inhibitor cocktail (MCE, HY-K0010). Following centrifugation of the cell lysates for 4 min at 2,000*g* and 4 °C, the supernatants were collected as the Soluble I fraction and the insoluble fraction was washed three times with SI buffer. The insoluble components were lysed with RIPA buffer (50 mM Tris, 200 mM NaCl, 5 mM EDTA, 0.5% sodium deoxycholate and 1% Triton X-100 plus protease inhibitor cocktail, pH 7.4), followed by sonication. The lysates were centrifuged for 15 min at 20,000*g* and 4 °C, and the supernatant was collected as the Soluble II fraction. After centrifugation, the final insoluble fraction was washed three times with RIPA buffer and then collected as the Pellet fraction.

To collect whole-cell lysates, cells were lysed with RIPA buffer containing protease inhibitors, followed by sonication. The lysates were centrifuged for 10 min at 15,000*g* and 4 °C, and the supernatants were collected.

Gel electrophoresis and staining

Samples were run on SDS–PAGE gels and proteins were separated via electrophoresis. Next, the gels were washed with double-distilled water to remove the electrophoresis buffer and stained with Coomassie brilliant blue R250. After staining, the gels were washed with a destaining solution (50% methanol, 10% acetic acid and 40% double-distilled water) until the protein bands in the gels were clear.

Protein analysis by immunoblotting

Samples were acquired and mixed with 5×SDS loading buffer (250 mM Tris, 500 mM dithiothreitol, 10% SDS, 0.5% bromophenol blue and 50% glycerol, pH 6.8). The Pellet fraction was dissolved in 1×Urea loading buffer (5×SDS loading buffer diluted 1/5 to 1× with 8 M urea). The samples were boiled for 8 min and electrophoresis was performed via SDS–PAGE. After the proteins were transferred to nitrocellulose membranes, the membranes were blocked with 5% non-fat milk in TBST (TBS with 0.1% Tween-20) and incubated overnight with the appropriate primary antibody at 4 °C and the indicated dilution. To visualize mono-ubiquitin, the gel was transferred to a polyvinylidene difluoride membrane. Next, the membranes were washed and probed with HRP-conjugated secondary antibody at a dilution of 1:10,000 and exposed to X-ray film in the darkroom.

Label-free quantitative proteomics of the Pellet fractions

Sample preparation. As shown in Fig. 1a, HeLa cells were treated with HS (42 °C, 2 h) and BTZ (1 μM, 8 h). These cells were harvested immediately following treatment; untreated HeLa cells were used as the control. The cells were sequentially lysed with SI buffer and RIPA buffer. The Pellet fraction was resuspended in 8 M Urea lysis buffer. After the addition of SDS loading buffer, the samples were boiled and separated by SDS–PAGE. In-gel trypsin digestion of samples was performed according to the standard protocol[63]. The desalting peptides digested from the gel were dissolved in 5% formic acid and then analysed by LC–MS/MS.

LC–MS/MS. For the HPLC separation, 0.5 μg of peptide mixture resolved in buffer A (0.1% formic acid) was loaded onto a 2 cm self-packed trap column (100 μm inner diameter; ReproSil-Pur C18-AQ, 3 μm, Dr. Maisch) using buffer A and separated on a column with a 150 μm inner diameter and a length of 12 cm (ReproSil-Pur C18-AQ, 1.9 μm, Dr. Maisch) over a 90 min gradient at a flow rate of 600 nl min^{-1} as follows: 0–7 min, 7–12% buffer B (0.1% formic acid in 80% acetonitrile); 7–67 min,12–30% buffer B; 7–83 min, 30–42% buffer B; 83–85 min, 42–95% buffer B and 85–90 min, 95% buffer B.

For the MS, peptides separated by liquid phase chromatography were ionized by a nanoESI source and then passed to a Q-Exactive HF X (Thermo Fisher Scientific) tandem mass spectrometer for detection in data-dependent acquisition mode. The main parameters were set as follows: voltage of the ion source, 2.2 kV; capillary at 320 °C; MS1 scanning range, 350–1,400 m/z with a resolution of 120,000; and MS2 starting m/z set to 120 with a resolution of 15,000. The ion-screening parameters for the MS2 fragmentation were: 2+ to 6+ (charge) and the top 25 parent ions. The automatic gain control was fixed to: MS2, 5×10^4; and MS1, 3×10^6. The higher-energy collisional dissociation was set at 27% for ion fragmentation, and the fragmented ions were spotted in Orbitrap. The dynamic exclusion time was fixed to 15 s.

Data analysis. Quantitation analysis of the raw data was performed using MaxQuant 2.1.4 based on the UniProt *Homo sapiens* database (version 2021.03). The digestion type was selected as trypsin/P and the maximum missed cleavages was set to two. The Match Between Runs (MBR) algorithm was enabled to improve data reproducibility. The protein group output file was used to perform quantitative analysis. The intensity values were used as the relative quantitative values of protein abundance. The missing values were replaced with the minimum value detected in the same sample, and the FC between the BTZ or HS groups and control groups was calculated. An unpaired Student's t-test was used to calculate the P values between groups.

The criteria of BTZ specifically enriched pellet protein were: (1) Con.1-3_Peptide ≤ 1 and BTZ.1-3_Peptide ≥ 4; (2) FC > 5 and $P < 0.01$. The criteria of HS specifically enriched pellet protein were: (1) Con.1-3_Peptide ≤ 1 and HS.1-3_Peptide ≥ 2; (2) FC > 4.5 and $P < 0.01$. The Kyoto Encyclopedia of Genes and Genomes enrichment analysis was performed using the R package clusterProfiler[64].

Plasmids

Mammalian expression vectors. The human spleen complementary DNA library was used as the clone resource to amplify most of the cDNA sequences in this work. Phanta max master mix (Vazyme, P515) was used as the DNA polymerase to amplify the cDNA and mutant sequences. Human *CASP1*, *CASP4* and CASP5 in pCS2-3×FLAG vector were gifts from F. Shao (National Institute of Biological Sciences, Beijing). Human *CASP2*, *CASP3*, *CASP6*, *CASP7*, *CASP8* and *CASP9* were inserted into the pCS2-3×FLAG vector. The *CASP2* mutants and other point mutant sequences were amplified using the reverse PCR method and restructured with homemade Gibson assembly mix[65]. The *mGFP* sequence was reconstructed from pEGFP-C1 with A207K mutant and fused with CASP2-CA-FL and truncation. CASP2-CA-FL, CASP2-CA-ΔCARD, CASP2-CARD-WT and the CARD-3A and -3E mutant sequences were fused with mEGFP and subcloned into the pCDH-CMV vector. The lentivirus expression vectors 3×FLAG–CASP2-C320A and 3×FLAG–CASP2-L439A were cloned into the pCDH-CMV vector. Human *PSMB2* was cloned into the pmCherry-N1 vector. The *Ubc9* yeast sequence was synthesised with a Y68L mutation[31] (Genscript). The *mCherry* sequence was fused with the *Ubc9* sequence and subcloned into the pcDNA3.1-Myc-HIS vector. Luciferase cDNA was purchased from Addgene (catalogue number 90170) and reconstructed into pEGFP-N1 and pCDH-CMV vectors. Human *TDP-43* and *VHL*-L159P mutant sequences were inserted into pcDNA3.1-Myc-HIS. The DUB mammalian expression vectors and HA-tagged ubiquitin (HA–RPS27A) were resources of our laboratory[66]. To acquire the mCherry–ubiquitin expression vector, the human RPS27A sequence was fused with the *mCherry* sequence and cloned into pCDH-CMV vectors. The sequences of the 5DE and 5DA mutants of ubiquitin were synthesised and subcloned into the same vector of HA-tagged ubiquitin.

Prokaryotic expression vectors. The human *UBA1*, *UBE2R1*, *UBE2L3*, *AREL1* and *UBE3C* sequences were amplified from the human spleen cDNA library. *UBA1* was cloned into the pET28a vector with an amino (N)-terminal 6×His tag, and human *UBE2R1* and *UBE2L3* were cloned into the pGEX-6P-1 vector. The sequences of *AREL-HECT* and *UBE3C-HECT* were amplified according to the instructions[67] and cloned into pGEX-6P-1. The GST-NleL expression vector was a gift from R. Hu (Shanghai Institute of Biochemistry and Cell Biology, Chinese Academy of Sciences, Shanghai). The GFP–8Ub expression vector was a gift from L. Yu (Tsinghua University, Beijing). The GFP–monoUb vector was cloned by fusing the *mGFP* sequence with single ubiquitin sequence into the pET28a vector. A *MBP* cDNA sequence was synthesised and cloned into the pETDuet-1 vector with an N-terminal 6×His tag. CASP2-CA-FL, CASP2-CA-ΔCARD and the CASP2 CARD domain were cloned into pETDuet-1 and fused with a 6×His-MBP tag. The CARD-3A (F102A, L105A and T109A) and CARD-3E (F102E, A105E and L106E) mutants were restructured using Gibson assembly. The CASP2 catalytic core domain and the C320A mutant were cloned into pET21a fused with a C-terminal 6×His tag. The yeast *MCA1* sequence was amplified from yeast BY4741 strain cDNA and cloned into pET28a. MCA1-catalysis core domain (amino acid residues 87–432) and the C276A mutant were amplified and cloned into the same vector. The 4×*TUBE* sequence was synthesised as quadruple UBA domain (amino acid residues 535–589) of human *Ubiquilin-1* (ref. 68) and inserted into pET28a fused with a 6×His and Halo tag.

Cell transfection and lentivirus packaging

Transient transfection of plasmids was performed using Lipofectamine 2000 (Invitrogen, catalogue number 11668019) or homemade polyethylenimine according to the manufacturer's instructions. Packaging of lentivirus was conducted in HEK293T cells using the second-generation

system. The transfer plasmid, packaging plasmid (pSPAX2; Addgene, catalogue number 12260) and envelope plasmid (pMD2.G; Addgene, catalogue number 12259) were co-transfected into cells at a ratio of 4:3:1 using polyethylenimine. The supernatants were collected 24 and 48 h after transfection and filtered through a 0.22 μm filter.

Generation of stable cell lines

To generate HEK293T cells stably expressing mGFP–CASP2-CA, the packed lentiviruses were added to the supernatant to infect the cells. After infection, puromycin (InvivoGen, ant-pr) was added into the medium at a concentration of 2 μg ml^{-1}. The viable cells were further sorted by cytometry (BD FACSAria SORP) to ensure uniform fluorescence intensity. HEK293T cells stably expressing mGFP–CASP2-CARD, mGFP–CASP2-ΔCARD, mGFP–CASP2-CARD-3A, mGFP–CASP2-CARD-3E, 3×FLAG–CASP2-L439A and 3×FLAG–CASP2-C320A were generated using the same procedure.

To generate control and *CASP2*-KO cells, human *CASP2* genomic RNA oligonucleotides (5′-ATCGTGGCACTCCTCTCGCA-3′) were synthesised and inserted into the pSpCas9(BB)-2A-GFP vector (Addgene, catalogue number 48138). The control and validated single guide RNA vectors were transfected into HEK293T cells. Two days after transfection, the GFP^{+} cells were sorted as single cells by cytometry (BD FACSAria SORP). After cultivation for nearly two weeks, the colony-formed cells were picked out for further validation through immunoblotting.

Live-cell imaging

An Andor BC43 Benchtop Confocal Microscope (Oxford Instruments) equipped with a stage-top incubator to maintain the temperature and CO_2 concentration was used for the live-cell imaging. HEK293T cells stably expressing mGFP–CASP2 were plated on a polymer-coverslip-bottom 35 mm μ-dish (ibidi, 81156). The cells were treated with 1 μM BTZ for 60 min before imaging or HS (42 °C) during imaging. Images were captured using a ×60 oil objective and a 488 nm laser. The representative images were analysed by ImarisViewer 9.8.0 (Oxford Instruments).

Immunofluorescence microscopy of cells

Immunostaining and fluorescence images were acquired using a NIKON A1R confocal microscope (NIS-Elements Viewer 5.21) and a ×60 1.4 numerical aperture (NA) oil objective. For immunofluorescence assays, cells were seeded on a polymer-coverslip-bottom 35 mm μ-dish. After 48 h of cultivation and treatment, the cells were rinsed with PBS and fixed with 4% paraformaldehyde (PFA) in PBS for 15 min, permeabilized in 0.25% Triton X-100 in PBS for 20 min and blocked in 2% BSA in PBS for 30 min. The cells were treated with antigen-retrieval buffer (Beyotime, P0090) for 5 min (for CASP2 and pTDP-43 immunostaining) before permeabilization. Primary antibodies were diluted in a blocking buffer plus 0.1% Triton X-100. The cells were incubated overnight at 4 °C in primary antibody at the indicated dilution. The next day, the cells were rinsed three times with PBST (PBS supplemented with 0.05% Tween-20). After removing the PBST buffer from the dishes, the cells were incubated in Alexa Fluor-conjugated secondary antibodies (1:500 in PBST) for 1 h and 1 μg ml^{-1} DAPI (Cell Signaling Technology, catalogue number 4083) in PBST for 10 min at room temperature. The cells were rinsed four times and observed using confocal microscopy. Cells transfected with fluorescent protein-fused expression vectors were cultured for 48 h, rinsed with PBS and fixed with 4% PFA in PBS for 15 min. The cells were incubated in 1 μg ml^{-1} DAPI in PBST for 10 min at room temperature and observed using confocal microscopy.

Images were analysed using ImageJ (National Institutes of Health) for all co-localization analyses. A straight line across the different marker proteins of condensates was drawn and recorded as the region of interest. The fluorescence intensities of the region of interest in each channel were quantified using the plot profile tool in ImageJ.

Fluorescence recovery after photobleaching

A laser intensity of 100% at 488 nm was used to bleach GFP–CASP2-containing puncta in HEK293T cells. Post-bleaching images were captured at the indicated time points. The images were captured using a Zeiss LSM880 confocal microscope (ZEN 3.6) with a ×63 1.4 NA oil objective.

In vitro phase-separation assay

Recombinant MBP, MBP–CASP2-FL, MBP–CASP2-CARD and MBP–CASP2-ΔCARD proteins were labelled with fluorescent dye Cy3 (Yeasen, 40777ES03). The Cy3-labelled protein, and GFP–8Ub and GFP–monoUb proteins were incubated in 20 mM HEPES (pH 7.5), 150 mM NaCl and 5% dextran. The mixture was incubated at room temperature for 15 min before observation. The mixtures were plated on confocal dishes and images were captured using a NIKON A1R confocal microscope with a ×60 1.4 NA oil objective.

Cell-colony formation

Control and *CASP2*-KO HEK293T cells were seeded in six-well plates at a density of 300 cells per well. The non-treated group was cultured at 37 °C and the HS group was treated with two rounds of HS (42 °C, 2 h)—that is, HS on the first and third day of cultivation. After two weeks, colonies in all the plates were fixed with 4% PFA in PBS for 15 min and stained with 0.05% crystal violet for 25 min. The colonies were washed with double-distilled water and colony images were acquired using a Canon camera. Quantification of the colony number was performed using ImageJ. Results are represented as the mean ± s.e.m. of three technical repeats.

Cell counting kit-8 assay

Control and *CASP2*-KO HEK293T cells were seeded on 96-well plates at a density of 3,000 cells per well. The cells were treated with different concentration gradients of BTZ for 36 h. Cell proliferation was measured according to the manufacturer instructions for the Enhanced cell counting kit-8 (Beyotime, C0041).

Cell death assay

Cell death was analysed by propidium iodide staining, a ToxiLight non-destructive cytotoxicity bioassay kit (Lonza, LT07-217) for measuring the plasma membrane integrity or the release of the enzyme AK from damaged cells[69].

Propidium iodide staining. Control and *CASP2*-KO cells treated with BTZ were incubated with propidium iodide for 10 min at 37 °C. Each sample required four fields of cells to be captured with the fluorescence microscope. Quantification of total cells and propidium iodide staining-positive cell numbers were performed by ImageJ.

AK assay. The cell culture medium was replaced with serum-free medium 12 h before detection. The supernatants of control and *CASP2*-KO cells treated with BTZ were collected, added to a luminescence-compatible 96-well plate and mixed with the AK assay buffer. Luminescence intensity was read using Veritas Microplate Luminometer (Turner Biosystems).

Immunoprecipitation

To detect ubiquitination of proteins, the HA–Ub vector and expression vectors of the proteins to be tested were co-transfected into HEK293T cells. Two days after transfection, the cells were harvested and lysed in RIPA buffer supplemented with 0.2% SDS. After sonication, the lysis reaction was centrifuged for 10 min at 15,000*g*. The supernatants were transferred to a new tube. Leaving 10% of lysate as the immunoprecipitation input sample, the remanent lysates were incubated with the indicated antibodies and Protein A/G agarose beads (Santa Cruz Biotechnology, sc-2003) at 4 °C. After overnight

incubation, the protein–antibody beads mixtures were separated through centrifugation at 1,000*g* for 3 min and washed four times with RIPA buffer. The samples were mixed with 2×loading buffe and then boiled for immunoblotting.

HIS pull-down assay

HEK293T cells were transfected with mCherry–Ubc9ts-Myc-6×His or TDP-43-Myc-6×His vectors for 48 h before being treated with HS (42 °C) for 2 h or HS followed by recovery (Rec, 37 °C) for 1 and 3 h. Next, cells were rinsed and harvested using PBS. After discarding the Soluble I fraction, the remanent components were washed three times with SI buffer. Next, HIS pull-down buffer (50 mM Tris, 300 mM NaCl, 8 M urea and 25 mM imidazole, pH 7.4) was added to lyse these remanent components (Soluble II and Pellet fractions) with sonication on ice. Following centrifugation at 15,000*g* for 10 min, the supernatants were collected and incubated with 6×His-tag purification resin (Beyotime, P2233) for 3 h at 4 °C. The remanent mixtures were washed four times using HIS pull-down buffer, and 2×loading buffer containing urea was added to the mixtures. Further analysis was performed via immunoblotting.

Gel filtration chromatography

Chromatography was performed on an ÄKTA pure system (Cytiva). Non-treated and HS-treated HEK293T cells were harvested and the Soluble II fraction was prepared. A 500 µl volume of the Soluble II fraction (8 mg ml^{-1}) was loaded onto a Superdex 200 increase 10/300 column (Cytiva, catalogue number 28990944). The column was pre-equilibrated with PBS buffer and a flow rate of 0.5 ml min^{-1} was used. Fraction collection started when the Soluble II sample was injected into the column and each sample was fractionated as 500 µl fractions. After gel filtration, 15 µl aliquots of each fraction were analysed via immunoblotting.

IP–MS analysis

Sample preparation. As shown in Fig. 5b, HEK293T cells transfected with FLAG vector and FLAG–CASP2-C320A were pretreated with HS for 2 h and lysed following the cell fraction procedure to isolate Soluble I and Soluble II fractions. The Soluble II fraction was loaded onto a Superdex 200 increase 10/300 column to separate the fractions containing CASP2 (fractions 16, 17 and 18). These fractions were incubated with 2 µg FLAG M2 antibodies at 4 °C for 2 h, followed by the addition of Protein A/G agarose beads for another 4 h. The Soluble I fraction was incubated with antibodies and beads as the same procedures. After incubation for 4 h, all samples were centrifuged at 1,000*g* for 3 min and washed four times with RIPA buffer. Next, 2×loading buffer was added to the remanent mixtures and the samples were boiled to release the proteins. The samples were then separated through SDS–PAGE electrophoresis and in-gel trypsin digestion was performed to release the peptides. All samples were prepared as three repeats.

LC–MS/MS. The peptides were resolved in 0.1% formic acid and analysed using an ultra-performance LC–MS/MS platform. Liquid chromatography separation was performed on an EASY-nLC 1200 system (Thermo Fisher Scientific) with an in-house packed capillary column (75 µm inner diameter × 20 cm) with 1.9 µm C18 reverse-phase fused-silica (Michrom Bioresources). Peptides were separated at 60 °C. The sample was eluted with a 90 min nonlinear gradient ramped from 7 to 45% mobile phase B (phase A, 0.1% formic acid in water; phase B, 0.08% formic acid in 80% acetonitrile) at a flow rate of 0.3 µl min^{-1}. Eluted peptides were analysed using an Orbitrap Exploris 480 mass spectrometer (Thermo Fisher Scientific). The MS data acquisition was performed in data-dependent acquisition mode with full MS resolution set to 60,000 at 200 *m*/*z*, and the automatic gain control target was 300% with an injection time of 50 ms. The mass range was set to 350–1,500. The automatic-gain-control target values for fragment spectra was 75% with a resolution of 15,000 and injection times of 22 ms, and the cycle time was set to 1.3 s. The intensity threshold was kept at 2×10^4. The isolation width was set to 1.6 *m*/*z*, the normalized collision energy to 27%, the dynamic exclusion time to 45 s, the FAIMS compensation voltage was set to −45 V and −65 V and default settings were used for the remaining parameters.

Analysis and validation of potential interactors from IP–MS

Raw format data from the Orbitrap Exploris 480 mass spectrometer were converted to MzXML format using the FAIMS MzXML Generator. Quantitation analysis was performed using MaxQuant 2.1.4 based on the UniProt *H. sapiens* database (version 2021.12.07). The digestion type was selected as trypsin/P and maximum missed cleavages were set to two. The intensity-based absolute quantitation (iBAQ) values were used as the relative quantitative values of protein abundance. The potential interactors of CASP2 in Soluble I and Soluble II fractions were filtered with the FC and *P* value. The filtration criteria were $\log_2$FC > 1.5 and $P < 0.05$. Proteins that identified only one peptide in all groups (column F) were excluded from the result.

Protein expression and purification

Prokaryotic expression of proteins was performed using *Escherichia coli* BL21 (DE3) cultured in LB medium with the appropriate antibiotics. Briefly, transformed BL21 (DE3) cells were cultured in a shaker at constant temperature (37 °C). When the optical density of the culture solution reached 0.8 at 600 nm, 0.4 mM isopropyl β-D-1-thiogalactopyranoside was added and the temperature was adjusted to 20 °C to start protein expression. After a suitable cultivation time, the bacteria were harvested through centrifugation.

For the purification of 6×His-tagged proteins, cells were resuspended in HIS binding buffer (50 mM Tris, 300 mM NaCl, 25 mM imidazole and 0.05% Tween-20, pH 7.8) plus lysozyme. The bacterial cell lysates were sonicated and centrifugated to obtain clear cell lysates. The 6×His-tagged proteins were affinity purified using a HisTrap HP (Cytiva) or gravity column according to the purification scale. The HIS-tagged proteins were gradient eluted using HIS binding buffer and HIS elution buffer (50 mM Tris, 300 mM NaCl and 500 mM imidazole, pH 7.5).

For the purification of GST-tagged and MBP-tagged proteins, cells were resuspended in GST/MBP binding buffer (50 mM Tris, 300 mM NaCl, 0.05% Tween-20 and 5 mM EDTA, pH 7.8) plus lysozyme. The clear cell lysates were loaded on a GSTrap FF (Cytiva) or MBPsep Dextrin 6FF (Yeasen) column for affinity purification. GST-tagged proteins were eluted in GST elution buffer (50 mM Tris, 300 mM NaCl and 10 mM reduced glutathione, pH 7.8) and MBP-tagged proteins were eluted in MBP elution buffer (50 mM Tris, 300 mM NaCl and 10 mM maltose, pH 7.8).

The purity of elution proteins was confirmed via SDS–PAGE and Coomassie brilliant blue staining, and further purification was performed using an ÄKTA pure (Cytiva) system equipped with a Superdex 200 increase 10/300 (Cytiva) or Capto HiRes Q (Cytiva) column. All proteins were concentrated using an Amicon ultrafiltration centrifugal tube (Millipore) and stored in HEPES protein buffer (50 mM HEPES and 150 mM NaCl, pH 7.5) plus 10% glycerol.

In vitro assembly of poly-ubiquitin chains

Untagged free ubiquitin and HA-tagged ubiquitin proteins were purchased from R&D Systems. The in vitro ubiquitin chain assembly reactions were modified from a previously published protocol[62]. The free monoUb proteins used in the in vitro assembly were mixed with untagged monoUb and HA-tagged monoUb at a ratio of 9:1. The reaction was assembled in a buffer containing 50 mM Tris (pH 7.5), 10 mM ATP, 10 mM $MgCl_2$ and 1 mM dithiothreitol. To assemble Lys48-poly-ubiquitin chains, the reaction was started with the addition of 200 nM E1 (UBA1), 20 µM E2 (Lys48: UBE2R) and 50 µM ubiquitin. NleL, UBE3C and AREL1 were respectively used as E3, and UBE2L3 was

used as E2 to assemble the mixed poly-ubiquitin chains (NleL, 20 μM, Lys6/Lys48 chains; UBE3C, 30 μM, Lys48/Lys29/Lys11 chains; AREL, 30 μM, Lys33/Lys11/Lys48 chains; UBE2L3, 10 μM). Generally, the reactions were incubated at 37 °C for 2 h.

MBP pull-down assay

MBP and MBP-CARD proteins were expressed in *E. coli* BL21 (DE3) cells, and the proteins were purified and stored at −80 °C. The cell lysates were obtained from RIPA-lysed HEK293T cells. The in vitro assembly ubiquitin chains were obtained from the reaction mentioned above. Whole-cell lysates (500 μg) or 50 μl in vitro assembly ubiquitin chains were incubated with 20 μg MBP or MBP-CARD proteins. The HS treatment was carried out in a water bath at 42 °C for 20 min. All samples were incubated at room temperature for another 30 min. The pull-down assays were performed by adding 10 μl MBP-binding resin (Yeasen, 20515ES08) and incubating the samples for 2 h at 4 °C. The MBP-binding resin and conjugates were centrifuged at 500*g* for 3 min and washed four times with MBP-PD buffer (50 mM Tris, 200 mM NaCl, 5 mM EDTA and 0.05% Tween-20, pH 7.5). The ubiquitin-binding capacity was monitored using immunoblots.

In vitro cleavage assay

The reaction was assembled in a buffer containing 25 mM HEPES (pH 7.5), 150 mM NaCl, 0.01% Tween-20, 10% sucrose and 10 mM dithiothreitol. Cells with HA-tagged ubiquitin chains were lysed in SDC buffer (50 mM HEPES and 1% sodium deoxycholate, pH 7.5) with sonication and the lysates were subsequently boiled for 3 min to denature the native proteins. Next, the buffer of boiled lysates was replaced with 0.5×reaction buffer using ultrafiltration (Amicon, 30 kDa). CASP2 or MCA1-catalysis core protein was mixed with the 10 μM lysate. To monitor the reaction with time, 20 μg μl^{-1} lysate and 10 μM enzyme were mixed and equal amounts of samples were collected at the indicated time points by adding 4×LDC buffer (Genscript) to terminate the reaction. The CASP2 and MCA1 reactions were incubated at 37 °C or 30 °C, respectively. Ubiquitinated TDP-43 was purified from HS-treated HEK293T cells transiently expressing TDP-43–Myc-6×His. The cells were lysed in HIS pull-down buffer and samples were purified using HisTrap HP agarose. The reaction was performed on beads-cleavage as the indicated groups. The cleavage results were visualized by immunoblotting.

The activity of CASP2 proteins was measured using chromogenic substrate: 250 μM Ac-Val-Asp-Gln-Gln-Asp-pNA (Beyotime, P9705) or Ac-Val-Asp-Val-Ala-Asp-pNA (Santa Cruz Biotechnology, sc-311279) was incubated with 5 μM CASP2 protein in 20 μl reaction buffer. The reaction was assembled in 384-well plates (Cellvis, P384-1.5H-N) for 2 h at 37 °C. The raw values of absorbance at 405 nm were determined using a μDrop system (Thermo Fisher Scientific).

Yeast strain construction

The *Saccharomyces cerevisiae* BY4741-Δ*mca1* strain was constructed using homologous recombination methods. Briefly, the KanMX sequence was amplified from the pFA6-kanMX4 plasmid using one-step PCR. The sequence contained the homologous complementary of the *mca1* open reading frame (NC_001147.6). Purified PCR products and salmon sperm DNA were transformed into BY4741 cells using the lithium acetate transformation method. The cells were cultured for 48 h at 30 °C on an YPDA broth plate containing 200 μg G418. Single colonies were picked from the plate and cultured in YPD medium with G418 in a shaker at constant temperature (30 °C). The replaced KanMX cassette was verified by PCR.

The *mca1-FL* and *mca1*-Δ*Pro* sequences were amplified and fused with the *mGFP* sequence at the N terminus. The fused sequences were subcloned into the pESC-HIS vector. To construct the stably expressing GFP–MCA1-FL and GFP–MCA1-ΔPro yeast strains, BY4741 cells were transformed with the plasmids and subsequently cultured in SC-HIS-Glucose plates. After cultivation for 48–72 h, single colonies were picked and cultured in SC-HIS-Glucose medium.

Preparation of Soluble and Pellet fractions in yeast cells

Wild-type BY4741 cells were cultured in YPD medium and Δ*mca1* cells were cultured in YPD medium plus G418 at 30 °C in a shaker at constant temperature. For stress treatments, the cells were HS treated (38 °C, 1 h), followed by harvesting or recovery for 30 and 60 min. The cells were lysed with glass beads in yeast lysis buffer (100 mM HEPES, 300 mM NaCl and 1% Triton X-100, pH 7.5) containing protease inhibitors. The cell lysates were centrifuged at 2,000*g* for 5 min to separate the cell debris. The soluble fractions were transferred to a new tube and centrifuged at 16,000*g* for 15 min to isolate the Soluble and Pellet fractions, to which 5×loading buffer and 1×Urea loading buffer, respectively, were added. The samples were boiled for 8 min and analysed via immunoblotting.

Immunofluorescence in yeast cells

The mca1-FL–GFP and *mca1*-Δ*Pro–GFP* strains were cultured in SC-HIS-Glucose medium. After 2 h of cell starvation in SC-HIS medium without a carbon source, galactose and raffinose were added to induce protein expression. After cultivation for 12 h, the cells were treated with HS (38 °C, 2 h) or BTZ (2 μM, 12 h). Following stress treatment, the cells were harvested with PBS and fixed using 4% PFA in PBS for 1 h. The samples were washed with PBS and mounted with PBS containing DAPI on glass slides. Yeast images were captured using a GE DeltaVision microscope.

Protein sequence alignments

The protein sequences were obtained from UniProt in FASTA format. The sequence alignment was performed using Jalview software with MUSCLE methods. The raw alignment results were exported and modified in Adobe Illustrator.

Structure prediction and analysis

The CASP2 full-length protein structure was downloaded from the AlphaFold Protein Structure Database[70] (AF-P42575-F1). The protein structure prediction and protein interaction model were calculated using the AlphaFold2 online platform ColabFold v1.5.2 with AlphaFold2-multimer[71]. The predicted results were acquired as five top-ranked models. All of the results were reviewed and the representative structure models were visualized and captured using PyMOL.

Preparation of Halo-TUBE and TUBE-captured ubiquitinated protein analysis

Sample preparation. 6×His-Halo-TUBE was expressed in BL21 (DE3) and purified using a HisTrap HP column (Cytiva). The eluted proteins were concentrated to 12.5 μg μl^{-1} and stored frozen in single-dose tubes. Before incubating with cellular lysates, the 6×His-Halo-TUBE protein was pre-incubated with HaloLink resin (Promega) in RIPA buffer at a ratio of 250 μg:50 μl. Control and *CASP2*-KO HEK293T cells were treated following the diagram in Fig. 2a. After discarding the Soluble I fraction, the Soluble II fraction was lysed in RIPA buffer plus protease inhibitor. The insoluble Pellet fraction was further lysed in RIPA buffer containing 8 M urea (pH 7.5) and diluted to 2 M urea by adding RIPA buffer. Next, the Soluble II and Pellet fractions from the same sample were mixed and centrifuged at 20,000*g* for 15 min to isolate the final insoluble material. The supernatants of each sample were incubated overnight with the pre-loaded TUBE-HaloLink resin. The resins were washed three times in RIPA buffer through centrifugation at 1,000*g* for 3 min. The resins were washed a further two times with RIPA buffer containing 300 mM NaCl and 2 M urea to reduce non-specific protein binding. The remaining proteins were released from the resin via boiling in loading buffer. The TUBE-captured samples were loaded onto an SDS–PAGE gel, and further in-gel digestion was performed using the abovementioned method.

LC–MS/MS. The peptides of TUBE-captured ubiquitinated proteins were analysed using EASY-nLC 1200 (Thermo Fisher Scientific) and Orbitrap Exploris 480 (Thermo Fisher Scientific) mass spectrometer following the methods described in the 'IP–MS analysis' section.

Data analysis. Raw format data obtained from the Orbitrap Exploris 480 mass spectrometer were converted to MzXML format using the FAIMS MzXML Generator. Quantitation analysis was performed using MaxQuant 2.1.4 based on the UniProt *H. sapiens* database (version 2021.12.07). The iBAQ values were used to relatively quantify the ubiquitination level of the identified proteins. The ratio was calculated by dividing the intensity at recovery 2 h by the average intensity of the HS control (ratio = $iBAQ_{R2h}$ / $iBAQ_{Con}$). The filter criteria were set as follows (Supplementary Table 2):

(1) $P < 0.05$ for the comparison of the control and KO ratios and both ratios were <1.2.
(2) To filter out the different proteins, the filter criteria used were: KO ratio / control ratio > 1.5 and $P < 0.01$, and $P < 0.05$ for the comparison of HS and R2h KO samples.

Mice

All mice had the same genetic background (C57BL/6J) and were housed in specific pathogen-free conditions. *Casp2*$^{-/-}$ mice were generated by Gempharmatech Co., Ltd using clustered regularly interspaced short palindromic repeats (CRISPR)–CRISPR associated protein 9 (guide RNA sequence 5′-GTTGAAAATGATCTTAGGAC-3′ or 5′-CTGCTTACGTGTGACTGTAC-3′). The mouse behaviour experiments were performed on approximately equal numbers of male and female mice. Ten- to 14-month-old *Casp2*$^{+/+}$ and *Casp2*$^{-/-}$ mice were used in the rotarod, grip-strength, CatWalk gait and hindlimb-clasping tests as well as electromyographic recording and NMJ staining. For immunofluorescence staining of brains and spinal cord, 12–16-month-old *Casp2*$^{+/+}$ and *Casp2*$^{-/-}$ mice were used. Two-month-old *Casp2*$^{+/+}$ and *Casp2*$^{-/-}$ mice were used for the AAV injection study.

AAV injections. AAV-PhP.eB–GFP or AAV-PhP.eB–GFP–TDP-43 (GENECHEM Biotech) was i.c.v. injected into the brains of wild-type or *Casp2*$^{-/-}$ C57BL/6J mice on postnatal day 1. Following the previously published guidance[72], the neonatal mice were anaesthetized by placing them on an ice plate for 1–3 min. The injection location was determined to be two-fifths of the distance from the lambda midline of the head of the mouse to each eye, and the needle was slowly inserted at an oblique angle of 45° and a depth of 3 mm; both ventricles were injected. The injection volume was 1.8×10^{10} vector genomes for each ventricle. After the injection, the mouse was returned to the home cage after recovering body temperature.

Rotarod test. The rotarod apparatus (Ugo Basile) was used to assess motor function and coordination in mice. The mice were trained three times at the same time for three consecutive days before the tests. The rotarod apparatus was accelerated from 4 rpm to 40 rpm over a period of 5 min. Latency to fall was recorded when either of the following occurred: the mouse fell from the bar or the mouse rotated continuously around the bar. Each mouse was tested three times to obtain three stable data points and data are shown as the average of all three tests.

Grip-strength test. A grip-strength meter (Maze Engineers) was used to test the strength of the forelimb and forelimb–hindlimb grip of mice. The forelimbs or forelimbs–hindlimbs of the mouse were placed on the grip-strength meter, the tail of the mouse was pulled away from the horizontal bar and the peak value read by the grip-strength meter was recorded. The experiment was performed at least three experiments to obtain three stable data points. Data are shown as the average of all three tests.

CatWalk gait test. The CatWalk (Noldus Information Technology B.V.) was used to analyse the gait parameters of mice. CatWalk XT Version 10.6 was used to record and analyse each paw print and the gait parameters of the mice. The relevant gait parameters were recorded for each mouse that successfully ran out of the test area. At least three test data points were obtained for each mouse. Data are shown as the average of all three tests.

Hindlimb-clasping test. The hindlimb-clasping test was performed according to standard criteria (Extended Data Fig. 4a). The score of each mouse was evaluated with a grade of 0–3 according to their hindlimb position. The mouse was lifted by its tail away from the surrounding objects, the hindlimb position was observed for 10 s and the mouse was assigned a score: 0, both hindlimbs were kept away from the abdomen and the toes were separated for 50% of the observation time; 1, a single hindlimb was retracted or both hindlimbs were partially retracted without touching the abdomen for 50% of the observation time; 2, both hindlimbs were partially retracted by touching the abdomen for 50% of the observation time; 3, both hindlimbs were clenched and completely retracted by touching the abdomen for 50% of the observation time.

Electromyographic recording. Mice were anaesthetized with an intraperitoneal injection of pentobarbital sodium (70 mg kg^{-1}). The mice were then mounted into a stereotaxic frame and the left hindlimb was shaved. To record the resting electromyographic value, a pair of gold-plated stainless steel needle electrodes (Shike Biotechnology (Beijing) Co., LTD) was placed into the gastrocnemius muscle (distance between recording electrodes, 0.25 cm). A reference electrode was placed subcutaneously on the contralateral side of the recording. The electrodes were connected to a three-lead Shielded Bio Amp Cable (ADInstruments) and the resting electromyographic with amplified signal was recorded using a Bio Amp amplifier (ADInstruments). To record myogenic motor-evoked potentials, the mice were mounted into a stereotaxic frame and the scalp over motor cortex was cut open to expose the skull. A pair of gold-plated stainless steel needle electrodes was surgically implanted into the right motor cortex (distance between recording electrodes, 0.2 cm) using coordinates (from bregma anteroposterior, +1.15–1.2 mm; mediolateral, +1.75 mm and dorsoventral, +0.6–1.0 mm) according to a Mouse Brain Atlas. Motor-evoked potentials were elicited by electrical stimulation with a pulse duration of 0.5 ms at 5 mA using an isolated stimulator Iso-flex. Myogenic motor-evoked potentials were recorded with similar methods to that used for the resting electromyographic. The recorded signals were sampled at 20 kHz, digitalized and stored using the PowerLab 8/35 data-acquisition system LabChart (ADInstruments) in PC for subsequent analysis using the Igor Pro software (WaveMetrics).

Preparation of mouse brain tissue lysates. Mouse brain tissues were lysed with steel beads in RIPA buffer plus protease inhibitor cocktail. The lysates were centrifuged at 2,000*g* for 5 min to discard tissue debris and the supernatant was centrifuged at 20,000*g* for 15 min to harvest Soluble and Pellet fractions. The Pellet fraction was dissolved in 1× Urea loading buffer. The analysis was performed using immunoblotting.

Immunofluorescence in mouse tissue. Frozen slides of brain and spinal cord samples were warmed to room temperature, permeabilized in 0.5% Triton X-100 in PBS for 25 min and blocked in goat serum in PBS for 30 min. The slides were incubated overnight at 4 °C with the appropriate primary antibodies at the indicated dilution, after which they were rinsed four times with PBST and incubated in Alexa Fluor-conjugated secondary antibodies (diluted 1:500 in PBST) for 1 h. Next, the slides were rinsed five times with PBST and mounted with DAPI (Invitrogen, 2273678). Images of the slides were captured

using a NIKON A1R confocal microscope with a ×60 1.4 NA oil objective. Quantification of Lys48-Ub puncta was performed using ImageJ. The properties of the Lys48-Ub puncta were quantified using the analyse particles tool in ImageJ. To exclude the abnormal puncta, the Lys48-Ub puncta sizes and numbers were quantified according to the following criteria: (1) the size of Lys48-Ub puncta was >1.5 μm^2 and (2) the circularity of Lys48-Ub puncta was >0.2. For NMJ staining, tibialis anterior mouse muscles were fixed overnight at 4 °C with 4% PFA in PBS, rinsed with 0.1 M glycine in PBS for 30 min, permeabilized in 1% Triton X-100 in PBS for 30 min, placed in antigen-retrieval buffer for 7 min and blocked in 2% BSA plus 0.5% Triton X-100 and goat serum for 30 min. The muscles were incubated overnight at 4 °C in primary antibody and rinsed three times with PBS for 10 min. The muscles were incubated in α-bungarotoxin–Cy3 (Botium, B00018) and Alexa Fluor-conjugated secondary antibodies for 2–4 h at room temperature, and rinsed three times with PBS for 30 min. The samples were then mounted with VECTASHIELD mounting medium. *Z* serial images were captured using a NIKON A1R confocal microscope with a 20× 0.75 NA objective and shown in maximum intensity projection.

Statistical analyses

Samples or animals were randomly allocated to the experimental groups. No statistical methods were used to pre-determine sample sizes but our sample sizes are similar to those reported in previous publications[69,73]. Data distribution was assumed to be normal but this was not formally tested. In the in vitro study, investigators were not blinded during data collection because the readouts were quantitative and not susceptible to the subjective judgement of investigators. However, in the in vivo study, the mice experiments and statistical analyses were conducted by independent researchers in a blinded manner. No mice or data points were excluded from the analysis.

An unpaired two-tailed Student's *t*-test was used to compare two independent groups with a normal distribution. A paired two-tailed Student's *t*-test was used to compare two paired groups with a normal distribution. If the two independent groups were not normally distributed, the Mann–Whitney *U*-test was used for comparison. A one-way ANOVA was used to compare three or more independent groups. A two-way ANOVA was used to compare the differences between two or more independent groups with two different factors. Most statistical data analyses were performed using GraphPad Prism 9.4.1; the Mann–Whitney *U*-test was performed using Rstudio (2022.02.3, R version 4.2.0). All the statistical data are available in Source data.

Reporting summary

Further information on research design is available in the Nature Portfolio Reporting Summary linked to this article.

Data availability

All data are available in the main text or the source data. The databases utilized in this study include UniProt (https://www.uniprot.org), BioGRID (https://thebiogrid.org) and PhaSePred (http://predict.phasep.pro/). The MS proteomics data have been deposited to the ProteomeXchange Consortium via the iProX partner repository with the dataset identifier PXD041964. All other data supporting the findings of this study are available from the corresponding author on reasonable request. Source data are provided with this paper.

References

63. Shevchenko, A., Tomas, H., Havli, J., Olsen, J. V. & Mann, M. In-gel digestion for mass spectrometric characterization of proteins and proteomes. *Nat. Protoc.* **1**, 2856–2860 (2006).
64. Wu, T. et al. clusterProfiler 4.0: a universal enrichment tool for interpreting omics data. *Innovation* **2**, 100141 (2021).
65. Gibson, D. G. et al. Enzymatic assembly of DNA molecules up to several hundred kilobases. *Nat. Methods* **6**, 343–345 (2009).
66. Yuan, L. et al. Deubiquitylase OTUD3 regulates PTEN stability and suppresses tumorigenesis. *Nat. Cell Biol.* **17**, 1169–1181 (2015).
67. Michel, M. A., Komander, D. & Elliott, P. R. Enzymatic assembly of ubiquitin chains. *Methods Mol. Biol.* **1844**, 73–84 (2018).
68. Hjerpe, R. et al. Efficient protection and isolation of ubiquitylated proteins using tandem ubiquitin-binding entities. *EMBO Rep.* **10**, 1250–1258 (2009).
69. Zhang, T. et al. Prolonged hypoxia alleviates prolyl hydroxylation-mediated suppression of RIPK1 to promote necroptosis and inflammation. *Nat. Cell Biol.* **25**, 950–962 (2023).
70. Varadi, M. et al. AlphaFold Protein Structure Database: massively expanding the structural coverage of protein-sequence space with high-accuracy models. *Nucleic Acids Res.* **50**, D439–D444 (2022).
71. Mirdita, M. et al. ColabFold: making protein folding accessible to all. *Nat. Methods* **19**, 679–682 (2022).
72. Kim, J.-Y., Grunke, S. D., Levites, Y., Golde, T. E. & Jankowsky, J. L. Intracerebroventricular viral injection of the neonatal mouse brain for persistent and widespread neuronal transduction. *J. Vis. Exp.* https://doi.org/10.3791/51863 (2014)
73. Xie, M. et al. TREM2 interacts with TDP-43 and mediates microglial neuroprotection against TDP-43-related neurodegeneration. *Nat. Neurosci.* **25**, 26–38 (2022).

Acknowledgements

We thank F. Shao (National Institute of Biological Sciences, Beijing) for providing the CASP1, -4 and -5 expression vectors. We thank R. Hu (Shanghai Institute of Biochemistry and Cell Biology, Chinese Academy of Sciences, Shanghai) for providing the NleL expression vector. We thank L. Yu (Tsinghua University, Beijing) for providing the GFP–8Ub expression vector. We thank P. Li (Tsinghua University, Beijing) and C. Liu (Shanghai Institute of Organic Chemistry, Chinese Academy of Sciences, Shanghai) for their constructive instruction on the research. We thank Y. Li and W. Shen (Beijing Institute of Basic Medical Sciences, Beijing) for their help in the guidance on the primary cortex neuron culture and NMJ staining. We thank Y. Guan (Chinese PLA General Hospital, Beijing) for his assistance in the CatWalk gait test. We thank the Imaging Facility (C. Zhang and J. Chen), the Flow Cytometry Facility (C. Han, Y. Hao and Y. Wang), the Animal Facility (C. Qiu), the Translational Medicine Facility (J. Jiang, S. Zhang and X. Liu) and the Mass Spectrum Facility (S. Chen and S. Wang) of the National Center for Protein Sciences in Beijing (NCPSB) for their assistance. This work was supported by the National Key Research and Development Program of China (grant numbers 2021YFA1300200 to L. Zhang and 2022YFC2302900 to C.H.L.), the National Natural Science Foundation of China (grant number 82330069 to C.H.L.), the key project from the State Key Laboratory of Proteomics (grant number SKLP-K202001 and SKLP-X202401 to L. Zhang) and the Young Elite Scientists Sponsorship Program by CAST (grant number YESS20220049 to Y.F.).

Author contributions

The project was conceived by L. Zhang, C.H.L. and Y.G. Most of the experiments and data analysis were performed by Y.G. and L. Zhou with help from Y.F., L.H., Y.C. and D.L. The MS analysis was performed with help from Y.X., Yangjun Zhang and W.Y. The fluorescence imaging analysis was performed with help from S.Y. The resources of the experiment were provided by H.D., Z.P., Yong Zhang, B.W., X.Z. and C.-P.C. The mouse behaviour experiments and electromyographic recordings were performed with help from J.Y. and H.W. Funding was acquired by L. Zhang, C.H.L. and Y.F. The original manuscript was written by Y.G. and L. Zhou. The reviewing and editing of the manuscript were performed by L. Zhang, C.H.L. and Y.F.

Competing interests
The authors declare no competing interests.

Additional information
Extended data is available for this paper at https://doi.org/10.1038/s41556-024-01522-8.

Supplementary information The online version contains supplementary material available at https://doi.org/10.1038/s41556-024-01522-8.

Correspondence and requests for materials should be addressed to Cui Hua Liu or Lingqiang Zhang.

Peer review information *Nature Cell Biology* thanks Benedikt Kessler, Ji-Young Youn and the other, anonymous, reviewer(s) for their contribution to the peer review of this work.

https://doi.org/10.1038/s41556-024-01522-8

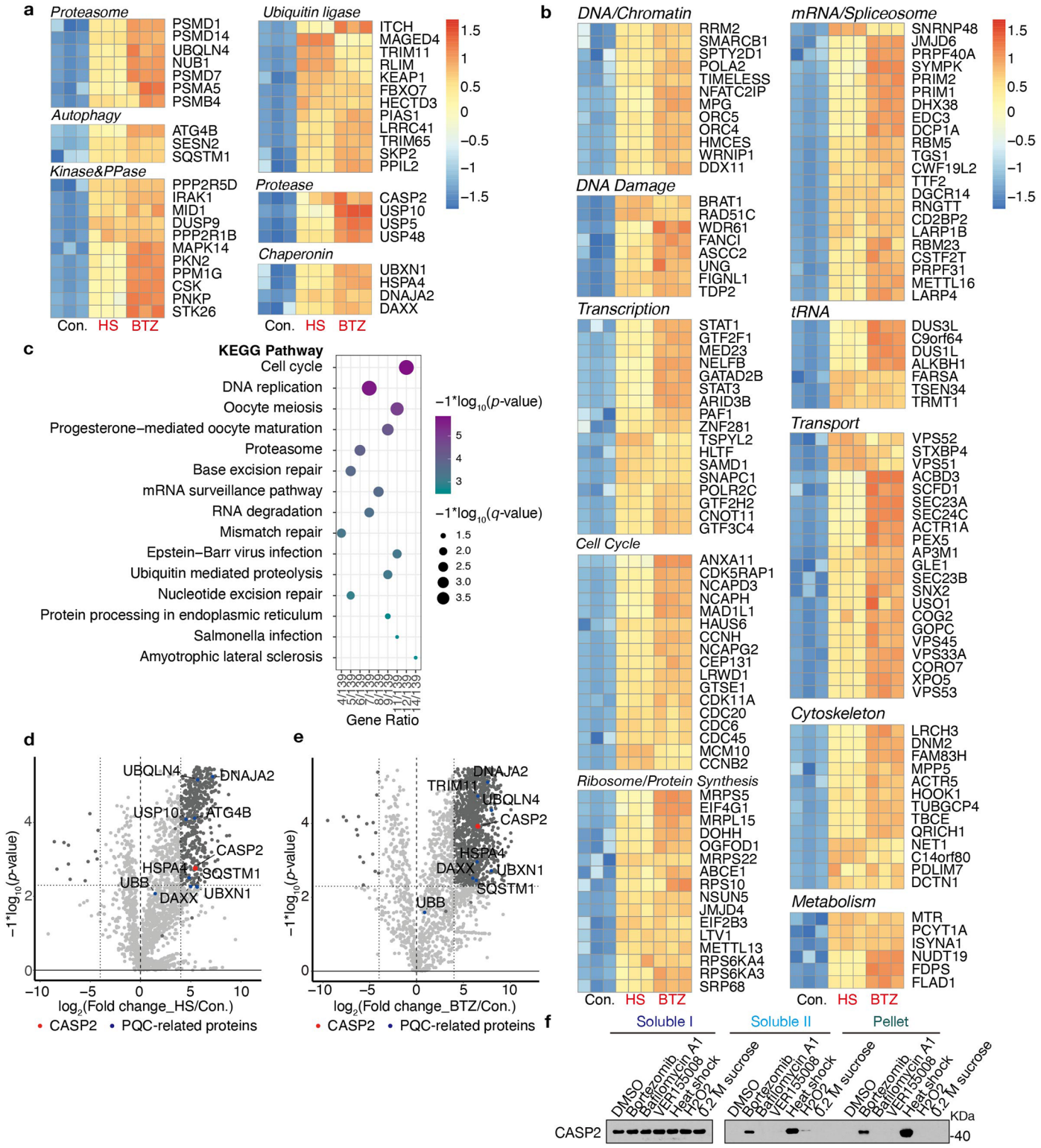

Extended Data Fig. 1 | Identification of CASP2 as a potential regulator accumulated in the *Pellet* fraction upon proteome stress. a,**b**, Heatmap showing the relative abundance of the overlapping proteins identified in HS- and BTZ-treated *Pellet* fraction. The proteins are grouped according to their function. The potential regulatory proteins involved in the ubiquitin-proteasome system, autophagy, chaperonin, and other factors are shown in (**a**). The proteins involved in the diverse biological pathways which are sensitive to proteome stress are shown in (**b**). **c**, Bubble chart showing the enriched KEGG pathways for the overlapping proteins identified in HS- and BTZ-treated *Pellet* fraction. **d**,**e**, Volcano plot showing changes in total protein abundance for HS versus control samples (**d**) and total protein abundance for BTZ versus control samples (**e**). **f**, Immunoblot analysis of CASP2 in fractions of HeLa cells exposed to different stress. The data was produced using the same sample in Fig. 1b. Data are representative of three independent experiments.

https://doi.org/10.1038/s41556-024-01522-8

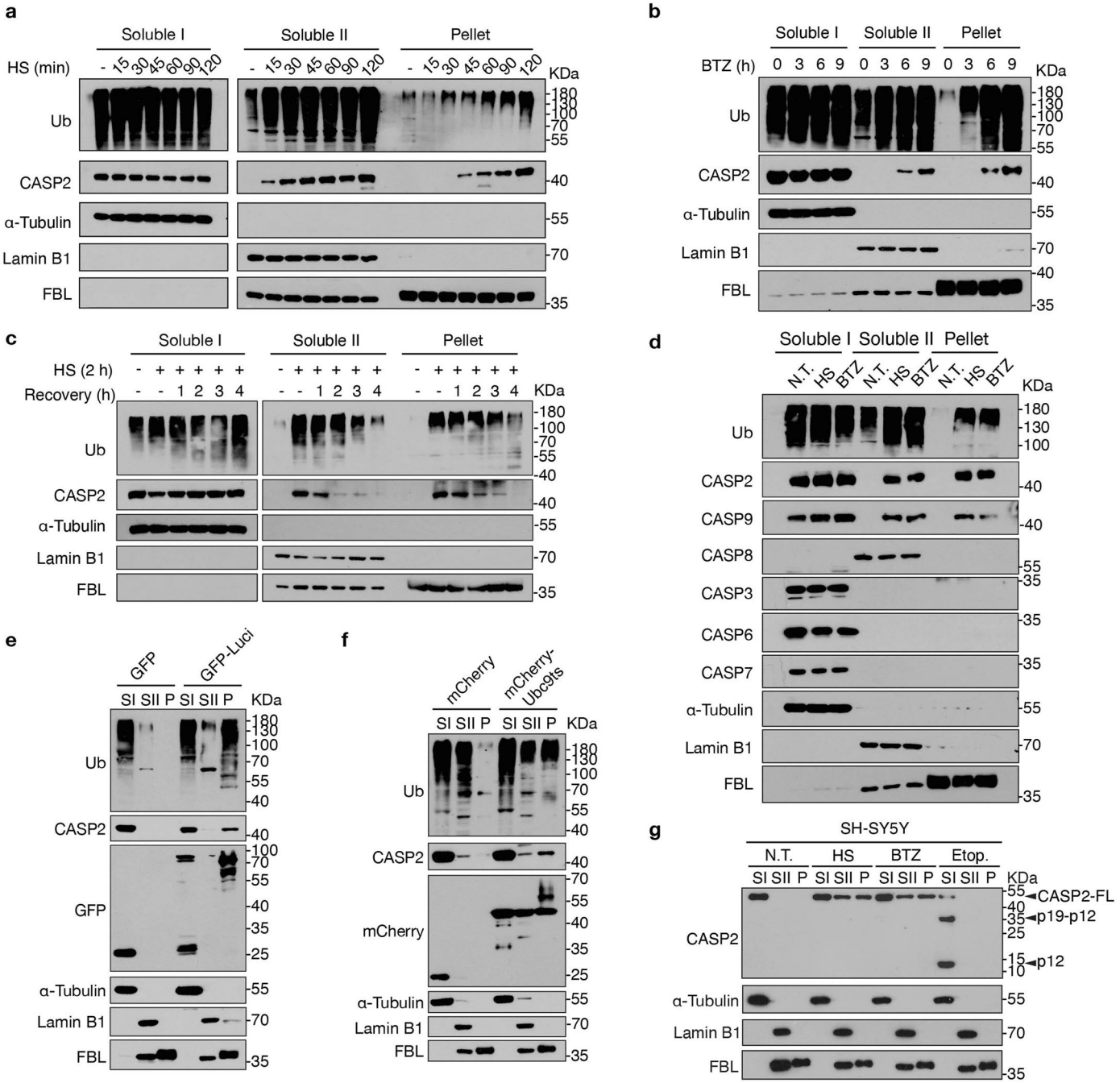

Extended Data Fig. 2 | Dynamic accumulation of CASP2 in the *Soluble II* and *Pellet* fractions. a, HEK293T cells were exposed to 42 °C HS treatment at the indicated time points. Immunoblot analysis was performed to detect the poly-ubiquitin and CASP2 in the isolated fractions. **b**, HEK293T cells were treated with 1 μM BTZ at the indicated time points. Immunoblot analysis was performed to detect the poly-ubiquitin and CASP2 in the isolated fractions. **c**, After being pre-treated with 42 °C HS for 2 hours, HEK293T cells were harvested at the indicated recovery time points. Immunoblot analysis was performed to detect the poly-ubiquitin and CASP2 in the isolated fractions. **d**, Immunoblot analysis of the caspases distribution in the isolated fractions in HEK293T cells exposed to HS (42 °C, 2 hours) and BTZ (1 μM, 10 hours). **e**, HEK293T cells were transfected with GFP-vector and GFP-luciferase (Luci) respectively. Immunoblot analysis was performed to detect the poly-ubiquitin and CASP2 in the isolated fractions. **f**, HEK293T cells were transfected with mCherry-vector and mCherry–Ubc9ts respectively. Immunoblot analysis was performed to detect the poly-ubiquitin and CASP2 in the isolated three fractions. **g**, SH-SY5Y cells were treated with HS, BTZ and Etoposide (Etop.). Immunoblot analysis was performed to detect the CASP2. Data are representative of three independent experiments.

https://doi.org/10.1038/s41556-024-01522-8

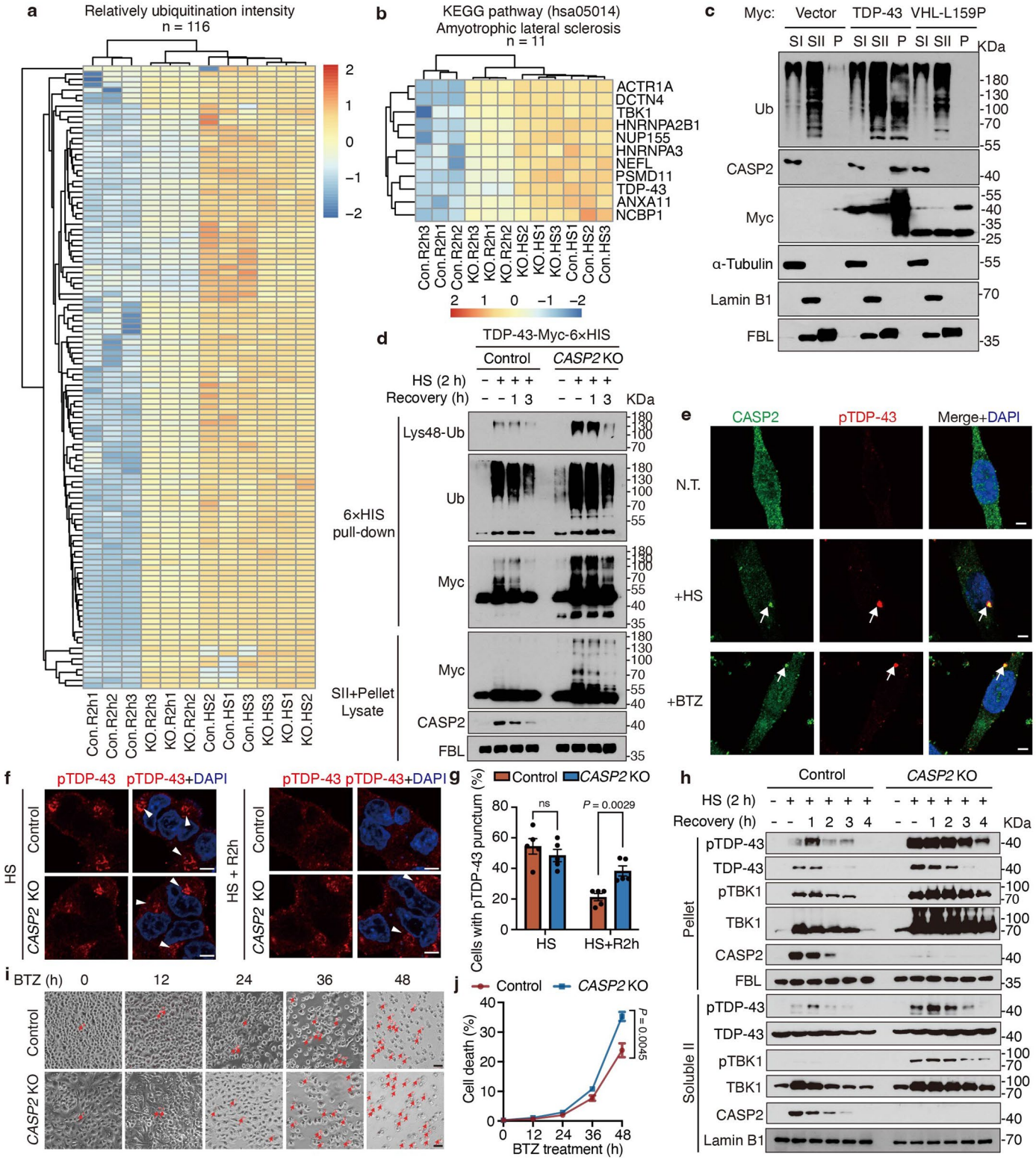

Extended Data Fig. 3 | See next page for caption.

https://doi.org/10.1038/s41556-024-01522-8

Extended Data Fig. 3 | *CASP2*-KO cells show a decreased turnover of ubiquitinated conjugates after heat shock. a, Heatmap showing the relative values of the 116 significant proteins of the 12 samples. **b**, Heatmap showing the ubiquitination fold change (FC) of the 11 ALS-associated proteins enriched in the KEGG pathways. **c**, Immunoblot analysis was performed to detect the poly-ubiquitin and CASP2 in the isolated fractions of HEK293T. **d**, Immunoblot analysis of TDP-43 ubiquitination in HIS pull-down buffer. HEK293T cells were transfected with Myc-6×HIS-tagged TDP-43, and the cells were then treated with HS (42 °C, 2 hours), followed by recovery for the indicated time points. **e**, Representative immunofluorescent staining of CASP2 and pTDP-43 in SH-SY5Y cells after being treated with HS (42 °C, 2 hours) or BTZ (1 μM, 8 hours). Scale bars, 5 μm. **f**,**g**, Control and *CASP2*-KO HEK293T cells were treated with HS and followed recovery for 2 hours (HS + R2h). Representative immunofluorescent staining of pTDP-43 in these cells was shown in (**f**), and the arrowhead indicates the accumulated pTDP-43 puncta. The percent of cells containing the pTDP-43 punctum is shown in (**g**). Scale bars, 5 μm. n = 5 independent replicates per group, two-tailed unpaired *t*-test. $P > 0.05$, ns. **h**, Immunoblot analysis of the TDP-43 and TBK1 in *Soluble II* and *Pellet* fractions of control and CASP2 KO HEK293T cells exposed to HS (42 °C, 2 hours) and recovery (37 °C) at the indicated time points. **i**,**j**, Propidium iodide (PI) staining (**i**) of the control and *CASP2*-KO HEK293T cells treated 1 μM BTZ for the indicated time points to analyse cell death. Quantification of the cell death is shown in (**j**). n = 4 independent replicates per group, two-way ANOVA test. All data are shown as mean ± SEM. Data are representative of three independent experiments.

https://doi.org/10.1038/s41556-024-01522-8

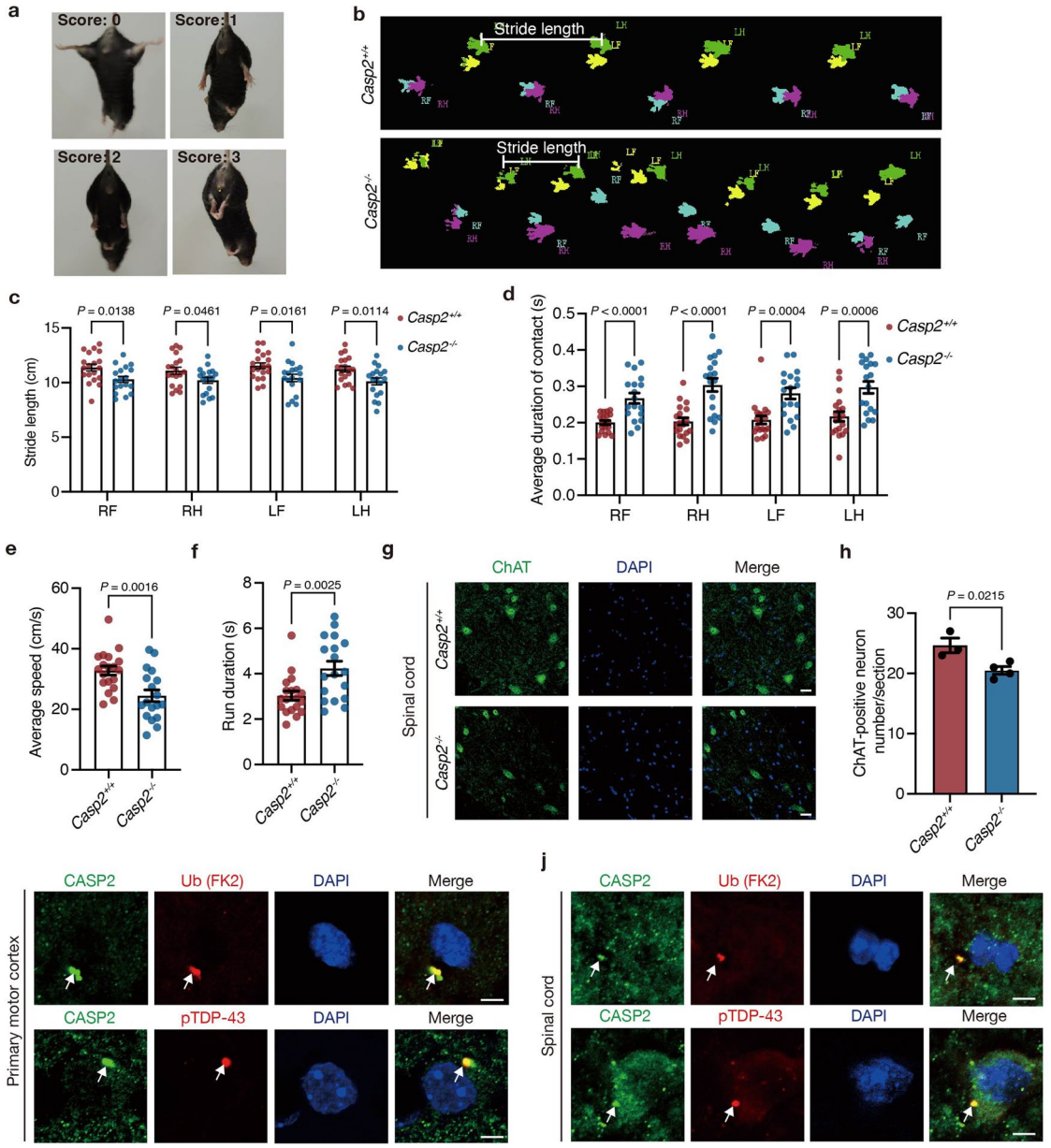

Extended Data Fig. 4 | Casp2-KO mice display motor deficits. a, The scoring criteria for the hindlimb-clasping test. Corresponding to Fig. 3a. **b**, Footprints of *Casp2*$^{+/+}$ and *Casp2*$^{-/-}$ mice of 10–14 months old. Left forelimb (LF), left hindlimb (LH), right forelimb (RF), right hindlimb (RH). **c**–**f**, Stride length (**c**), average contact duration (**d**), average speed (**e**) and run duration (**f**) of *Casp2*$^{+/+}$ and *Casp2*$^{-/-}$ mice of 10–14 months old. n = 19 and 18 mice respectively, two-tailed unpaired *t*-test for (**c**–**f**). **g**,**h**, Representative immunofluorescent staining images (**g**) and quantification (**h**) of ChAT-positive motor neurons in the ventral horn in the lumbar spinal cord of *Casp2*$^{+/+}$ and *Casp2*$^{-/-}$ mice of 12–16 months old. n = 3 and 4 mice respectively, two-tailed unpaired *t*-test. Scale bars, 25 μm. **i**,**j**, Representative immunofluorescent staining images of colocalization of CASP2 with poly-ubiquitin (FK2) or pTDP-43 in the primary motor cortex (**i**) and spinal cord (**j**) of *Casp2*$^{+/+}$ of 12–16 months old. Scale bars, 5 μm. All data are shown as mean ± SEM. Data are representative of three independent experiments.

https://doi.org/10.1038/s41556-024-01522-8

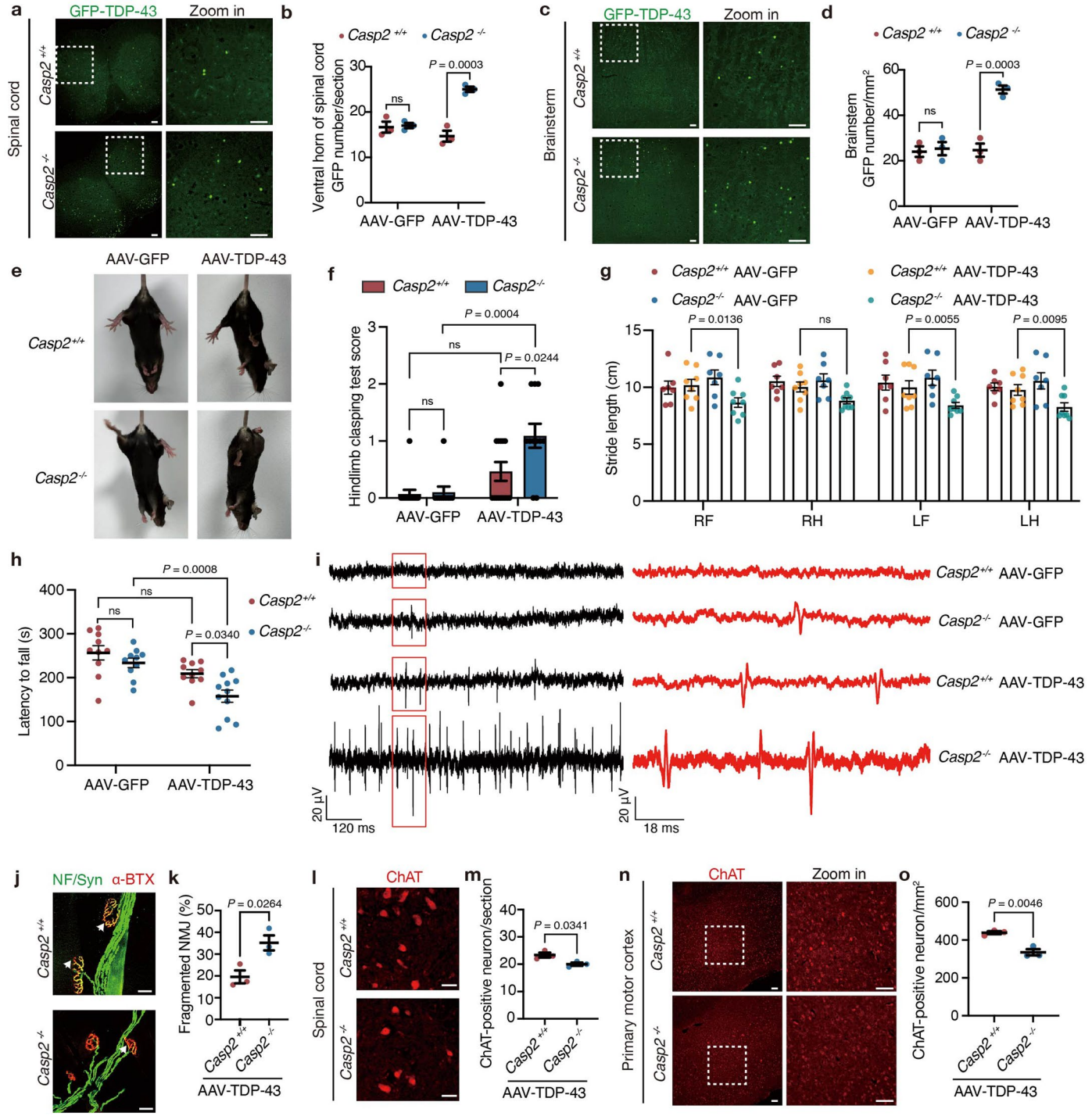

Extended Data Fig. 5 | AAV–TDP-43 overexpression aggravates motor deficits in Casp2-KO mice. a–**d**, Representative images (**a**,**c**) and quantification (**b**,**d**) of AAV-PhP.eB-GFP-TDP-43 in the spinal cord (**a**,**b**) and brainstem (**c**,**d**) of *Casp2*$^{+/+}$ and *Casp2*$^{-/-}$ mice. Scale bar, 100 μm. n = 3 mice per group, two-way ANOVA with Tukey's multiple comparisons test. **e**,**f**, Representative images (**e**) and quantification (**f**) of hindlimb-clasping phenotype in *Casp2*$^{+/+}$ and *Casp2*$^{-/-}$ AAV-injected mice. n = 14 (*Casp2*$^{+/+}$ AAV–GFP), 10 (*Casp2*$^{-/-}$ AAV–GFP), 15 (*Casp2*$^{+/+}$ AAV–GFP-TDP-43) and 11 (*Casp2*$^{-/-}$ AAV–GFP-TDP-43) mice, two-way ANOVA with Šídák's multiple comparisons test. **g**, Stride length of *Casp2*$^{+/+}$ and *Casp2*$^{-/-}$ AAV injected mice. n = 7 (*Casp2*$^{+/+}$ AAV–GFP), 7 (*Casp2*$^{-/-}$ AAV–GFP), 8 (*Casp2*$^{+/+}$ AAV–GFP-TDP-43) and 8 (*Casp2*$^{-/-}$ AAV–GFP-TDP-43) mice, two-way ANOVA with Tukey's multiple comparisons test. **h**, Rotarod test of *Casp2*$^{+/+}$ and *Casp2*$^{-/-}$ AAV injected mice. n = 10 (*Casp2*$^{+/+}$ AAV–GFP), 10 (*Casp2*$^{-/-}$ AAV–GFP), 10 (*Casp2*$^{+/+}$ AAV–GFP-TDP-43) and 11 (*Casp2*$^{-/-}$ AAV–GFP-TDP-43) mice, two-way ANOVA with Tukey's multiple comparisons test. **i**, Resting electromyographic of gastrocnemius muscle in *Casp2*$^{+/+}$ and *Casp2*$^{-/-}$ AAV injected mice. **j**,**k**, Representative images (**j**) and quantification (**k**) of NMJs in the tibialis anterior muscles of *Casp2*$^{+/+}$ and *Casp2*$^{-/-}$ AAV–GFP-TDP-43-injected mice. The arrowhead indicates the denervated or partially innervated endplate. n = 3 mice per group, two-tailed unpaired *t*-test. Scale bars, 25 μm. **l**,**m**, Representative immunofluorescent staining images (**l**) and quantification (**m**) of ChAT-positive motor neurons in the ventral horn in the lumbar spinal cord of *Casp2*$^{+/+}$ and *Casp2*$^{-/-}$ AAV–GFP-TDP-43-injected mice. n = 3 mice per group, two-tailed unpaired *t*-test. Scale bars, 50 μm. **n**,**o**, Representative immunofluorescent staining images (**n**) and quantification (**o**) of ChAT-positive motor neurons in the primary motor cortex of *Casp2*$^{+/+}$ and *Casp2*$^{-/-}$ AAV–TDP-43-injected mice. n = 3 mice per group, two-tailed unpaired *t*-test. Scale bars, 100 μm. All data are shown as mean ± SEM; $P > 0.05$, ns. Data are representative of three independent experiments.

https://doi.org/10.1038/s41556-024-01522-8

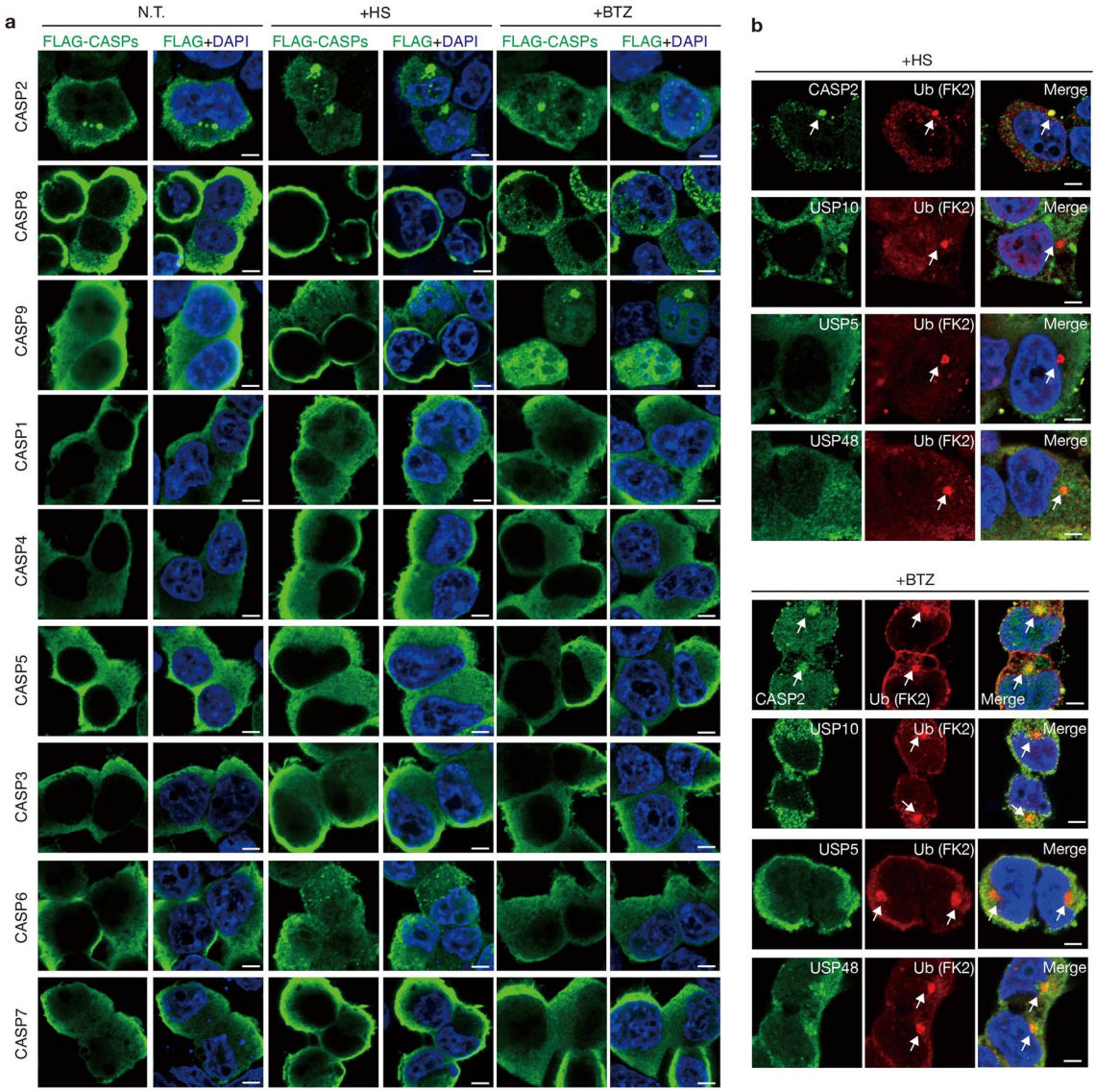

Extended Data Fig. 6 | CASP2 forms a condensate upon proteome stress. **a**, Representative immunofluorescent staining of the indicated caspases in HEK293T cells transfected with FLAG-tagged caspases with or without HS (42 °C, 2 hours) or BTZ (1 μM, 8 hours) treatment. Scale bars, 5 μm. **b**, Representative immunofluorescent staining of the indicated CASP2 and DUBs with poly-ubiquitin (FK2) with HS (42 °C, 2 hours) or BTZ (1 μM, 8 hours) treatment. The arrow indicates the ub-positive puncta. Scale bars, 5 μm. Data are representative of three independent experiments.

https://doi.org/10.1038/s41556-024-01522-8

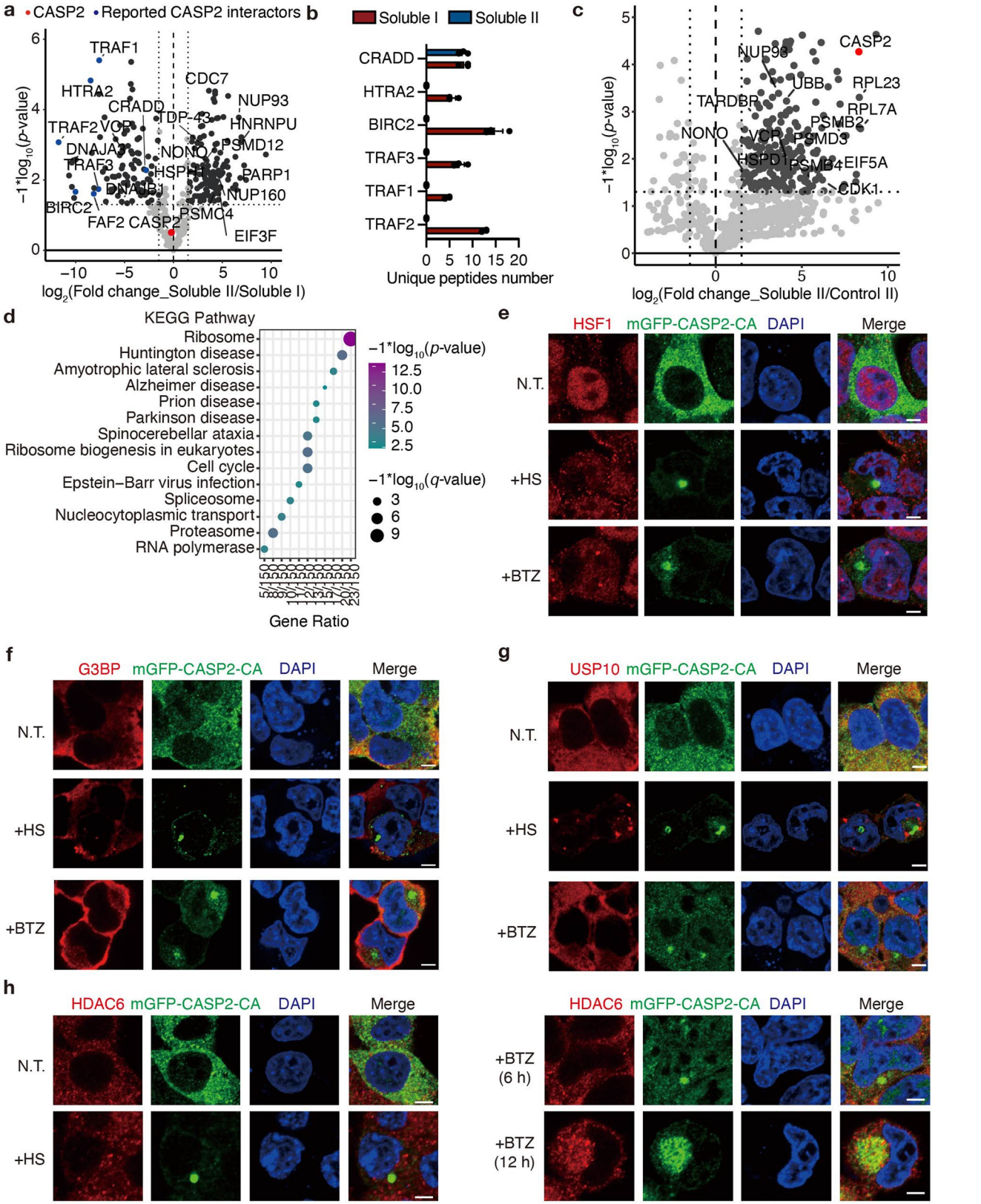

Extended Data Fig. 7 | CASP2 is integrated into a biomolecular condensate. **a**, Volcano plot indicating the potential interactors of CASP2 in *Soluble II* fraction compared to that in *Soluble I* fraction. The *X*-axis represents the ratio between *Soluble II* and *Soluble I*. **b**, Bar plot indicating the identified peptides number of previously reported interactors of CASP2 in *Soluble I* and *Soluble II* fractions. n = 3 independent replicates per group. Data are shown as mean ± SEM. **c**, Volcano plot indicating the interactors of CASP2 in *Soluble II* fraction. **d**, Bubble chart showing the enriched KEGG pathways for identified interactors of CASP2 in *Soluble II* fraction. **e**–**h**, Representative immunofluorescent staining of HSF1 (**e**), G3BP (**f**), USP10 (**g**), and HDAC6 (**h**) in HEK293T cells stably expressing mGFP–CASP2-CA after being treated with HS (42 °C, 2 hours) or 1 μM BTZ treatment. Scale bars, 5 μm. Data are representative of three independent experiments.

https://doi.org/10.1038/s41556-024-01522-8

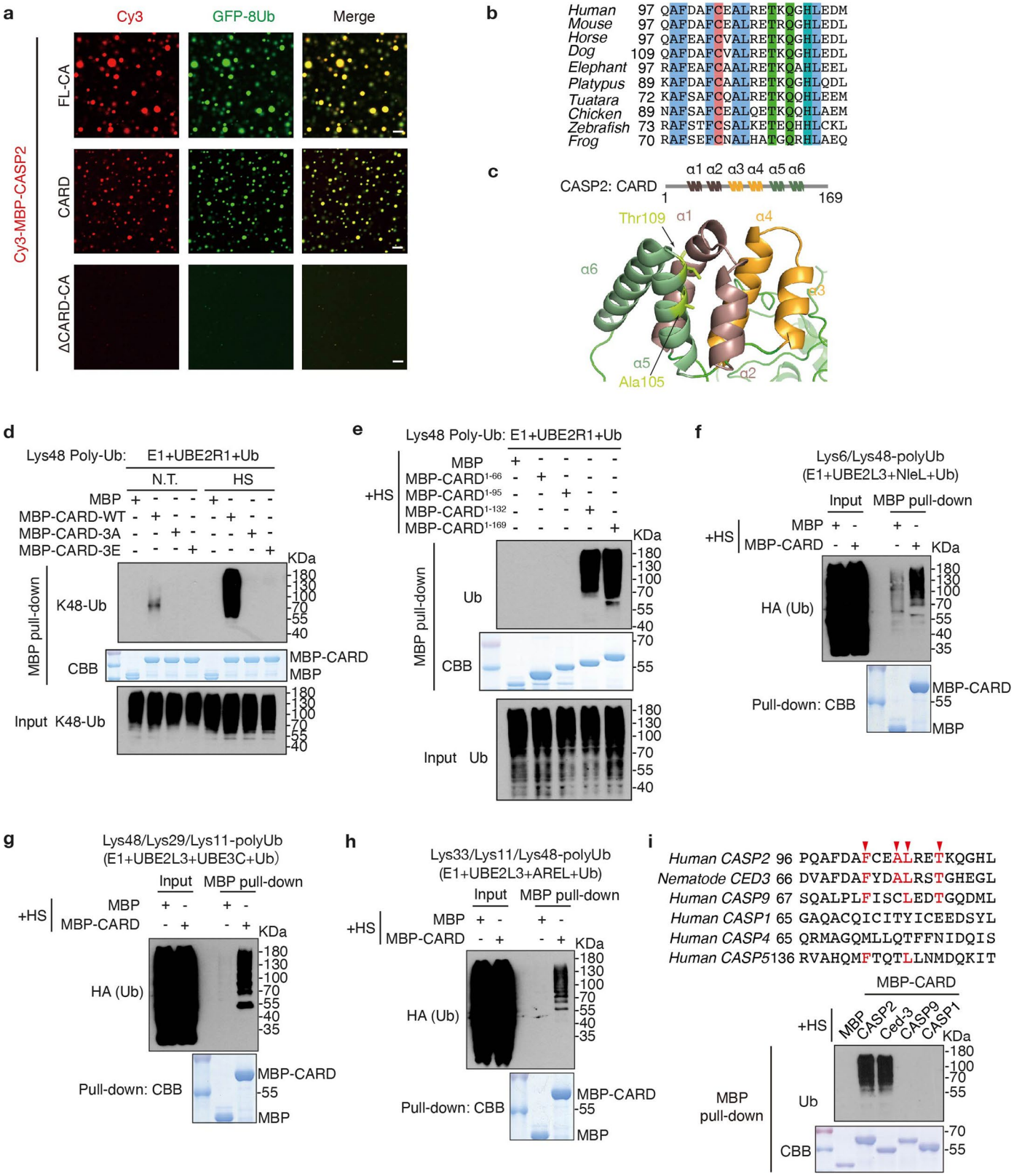

Extended Data Fig. 8 | See next page for caption.

https://doi.org/10.1038/s41556-024-01522-8

Extended Data Fig. 8 | CASP2 harbours a UIML region for binding the poly-ubiquitin chains. a, Representative images of phase separation by mixing GFP-8Ub proteins (20 μM) with MBP–CASP2-FL-CA, CARD and ΔCARD-CA proteins labelled Cy3 (20 μM). Scale bars, 5 μm. **b**, Alignment of UIML region sequences of CASP2 across species by Jalview. **c**, The structure model of CASP2 CARD domain predicted by AlphaFold2. **d**,**e**, MBP pull-down assay followed by immunoblotting and CBB staining to monitor the ubiquitin-binding capacity of MBP–CASP2-CARD mutants (**d**) and truncations (**e**). The ubiquitin chains were assembled *in vitro*. **f**–**h**, MBP pull-down assay followed by immunoblotting and CBB staining for monitoring the binding between HS-treated MBP–CASP2-CARD and the *in vitro* assembly ubiquitin chains. The ubiquitin chains were assembled using different E2 or E2/E3. The ubiquitin proteins used in (**c**–**g**) are a mixture of no-tagged ubiquitin and HA-tagged ubiquitin at a ratio of 9:1. **i**, Alignment of CARD domain sequences of CASP2, CED-3, caspase-1/4/5/9. MBP pull-down assay followed by immunoblotting and CBB staining for monitoring the binding between the HS-treated CARD domain and the cell lysate. Data are representative of three independent experiments.

https://doi.org/10.1038/s41556-024-01522-8

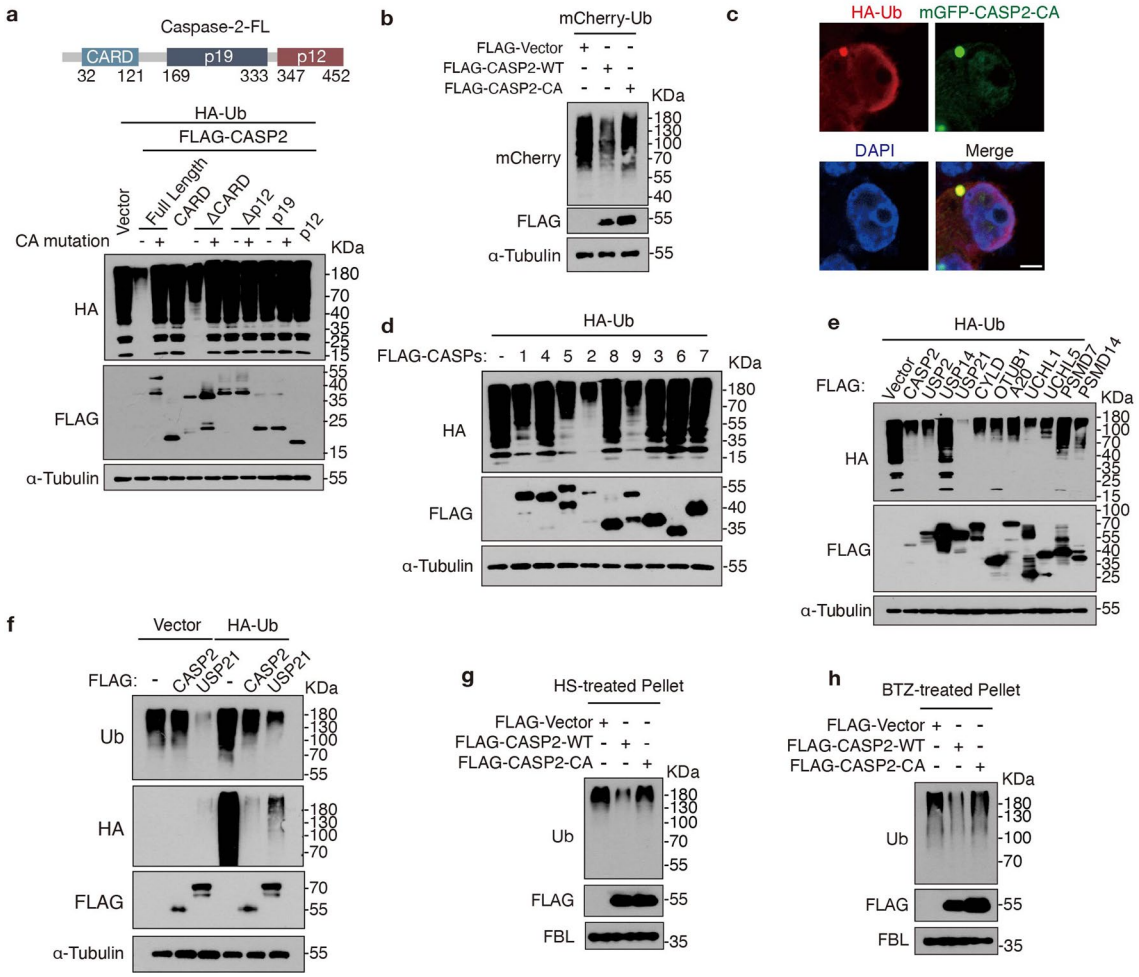

Extended Data Fig. 9 | CASP2 decreases the overloaded ubiquitin chains. **a**, Immunoblot analysis of the protein ubiquitination in HEK293T cells transfected with CASP2-WT, mutants, and truncations. CA mutant represents the C320A mutant. **b**, Immunoblot analysis of mCherry-tagged ubiquitin in HEK293T cells transfected with FLAG-tagged CASP2 or its CA mutant. **c**, Representative immunofluorescent staining images of HA-tagged ubiquitin in HEK293T cells stably expressing mGFP−CASP2-CA. Scale bars, 5 μm. **d**, Immunoblot analysis of HA-tagged ubiquitin expression with co-transfection of FLAG-tagged caspases in HEK293T cells. **e**, Immunoblot analysis of HA-tagged ubiquitin with co-transfection of FLAG-tagged deubiquitinases and CASP2 in HEK293T cells. **f**, Immunoblot analysis of ubiquitination in CASP2 (or USP21) expressed HEK293T cells transfected with or without HA-tagged ubiquitin. **g**,**h**, Immunoblot analysis of protein ubiquitination in the *Pellet* fraction of HEK293T cells transfected with CASP2 WT and CASP2 CA (C320A) after HS (**g**) and BTZ (**h**) treatment. Data are representative of three independent experiments.

https://doi.org/10.1038/s41556-024-01522-8

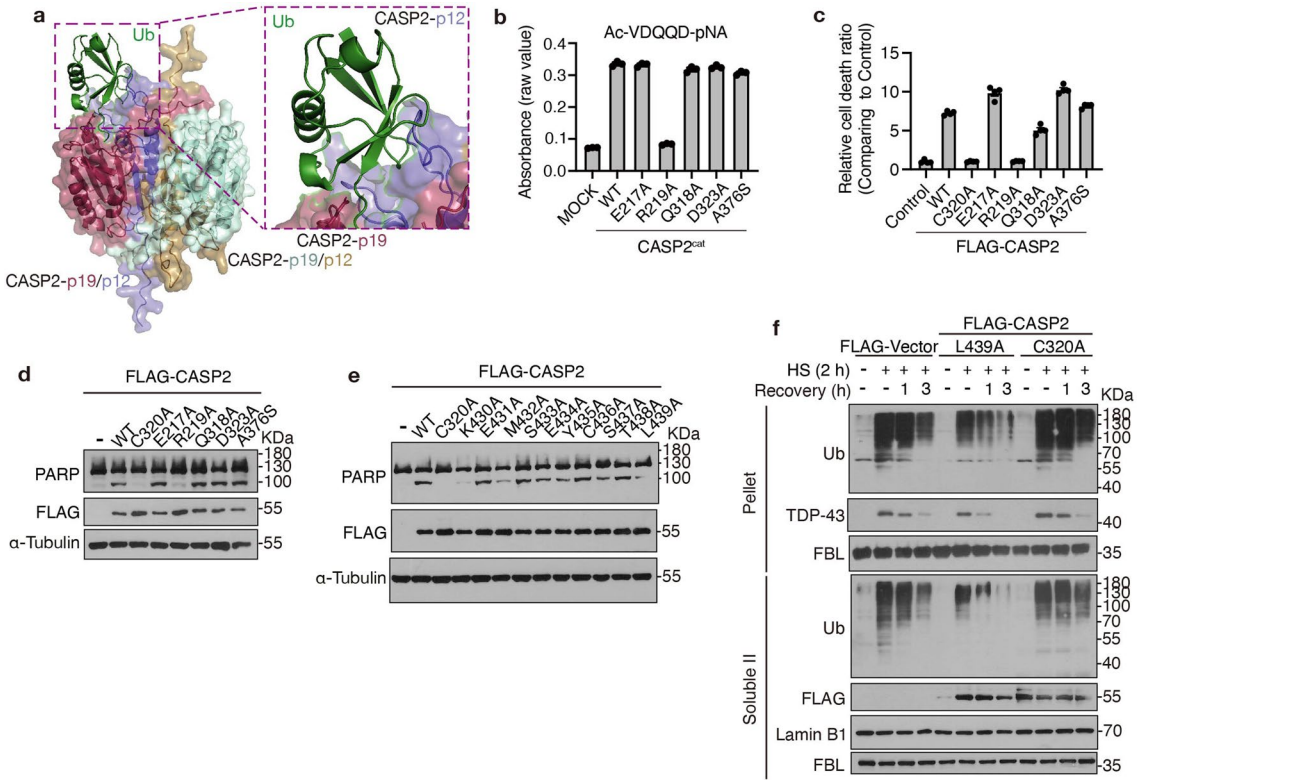

Extended Data Fig. 10 | CASP2 functions as both deubiquitinase and aspartic protease. a, The predicted structure of the heterologous CASP2 dimer (CASP2-p19/p12) recognizing the free ubiquitin. The structure models were predicted using AlphaFold2-multimer. The large (p19) and small (p12) subunits were labelled with distinct colours. **b**, Quantification of the activities of CASP2^{cat} WT and the indicated mutants towards the tetrapeptide substrate. Ac-VDQQD-pNA, a colorimetric substrate for CASP2, is used as an *in vitro* cleavage substrate. The absorbance was detected at 405 nm. n = 3 independent replicates per group. **c**, Cell death of HEK293T cells overexpressing the CASP2-WT and its mutants. The cell death ratio was evaluated by detecting the release of the adenylate kinase (AK) from damaged cells. n = 4 independent replicates per group. **d**,**e** Immunoblot analysis of the indicated proteins in HEK293T cells overexpressing CASP2-WT and its mutants. **f**, Immunoblot analysis of the indicated proteins in isolated fractions of the HEK293T cells stably expressing the CASP2 mutants. All data are shown as mean ± SEM. Data are representative of three independent experiments.

nature portfolio

Corresponding author(s): Lingqiang Zhang & Cui Hua Liu

Last updated by author(s): Jul 23, 2024

Reporting Summary

Nature Portfolio wishes to improve the reproducibility of the work that we publish. This form provides structure for consistency and transparency in reporting. For further information on Nature Portfolio policies, see our Editorial Policies and the Editorial Policy Checklist.

Statistics

For all statistical analyses, confirm that the following items are present in the figure legend, table legend, main text, or Methods section.

n/a	Confirmed
☐	☒ The exact sample size (*n*) for each experimental group/condition, given as a discrete number and unit of measurement
☐	☒ A statement on whether measurements were taken from distinct samples or whether the same sample was measured repeatedly
☐	☒ The statistical test(s) used AND whether they are one- or two-sided *Only common tests should be described solely by name; describe more complex techniques in the Methods section.*
☒	☐ A description of all covariates tested
☐	☒ A description of any assumptions or corrections, such as tests of normality and adjustment for multiple comparisons
☐	☒ A full description of the statistical parameters including central tendency (e.g. means) or other basic estimates (e.g. regression coefficient) AND variation (e.g. standard deviation) or associated estimates of uncertainty (e.g. confidence intervals)
☐	☒ For null hypothesis testing, the test statistic (e.g. *F*, *t*, *r*) with confidence intervals, effect sizes, degrees of freedom and *P* value noted *Give P values as exact values whenever suitable.*
☒	☐ For Bayesian analysis, information on the choice of priors and Markov chain Monte Carlo settings
☒	☐ For hierarchical and complex designs, identification of the appropriate level for tests and full reporting of outcomes
☒	☐ Estimates of effect sizes (e.g. Cohen's *d*, Pearson's *r*), indicating how they were calculated

Our web collection on statistics for biologists contains articles on many of the points above.

Software and code

Policy information about availability of computer code

Data collection	1. Mass spectrometry data was collected by Q-Exactive HF X or Orbitrap Exploris 480 mass spectrometer (Thermo Fisher Scientific) processed with MaxQuant 2.1.4 (version 2021.12.07). 2. Fluorescence images were collected by Nikon A1R confocal microscope with the NIS-Elements Viewer 5.21, Zessi LSM880 confocal microscope with the ZEN 3.6, and Andor BC43 benchtop confocal microscope with the ImarisViewer 9.8.0. 3. The absorbance was read via µDrop (Thermo Fisher Scientific). 4. The luminescence intensity was read via Veritas Microplate Luminometer (Turner Biosystems).
Data analysis	1. Fluorescence images were analyzed using ImageJ 1.53k (National Institutes of Health). 2. The data analysis and graphs were generated with GraphPad Prism 9.4.1 and Rstudio (2022.02.3, R version 4.2.0). 3. The sequence alignment was performed using Jalview (Version 2.11.2.0 (2.11.2.0)) with MUSCLE methods. 4. The protein structure prediction and protein interaction model were calculated using AlphaFold2 online platform ColabFold v1.5.2 with AlphaFold2-multimer. 5. Protein quantification and data normalization relied on the raw intensity or iBAQ in MaxQuant 2.1.4 (version 2021.12.07). 6. The protein structure simulations were performed using Pymol v2.54 (https://pymol.org/2). 7. The KEGG enrichment analysis was performed using the R package clusterProfiler.

For manuscripts utilizing custom algorithms or software that are central to the research but not yet described in published literature, software must be made available to editors and reviewers. We strongly encourage code deposition in a community repository (e.g. GitHub). See the Nature Portfolio guidelines for submitting code & software for further information.

Data

Policy information about availability of data

All manuscripts must include a data availability statement. This statement should provide the following information, where applicable:

- Accession codes, unique identifiers, or web links for publicly available datasets
- A description of any restrictions on data availability
- For clinical datasets or third party data, please ensure that the statement adheres to our policy

The databases utilized in this study include UniProt (https://www.uniprot.org), BioGRID (https://thebiogrid.org) and PhaSePred (http://predict.phasep.pro/). All data are available in the main text or the source data. The mass spectrometry proteomics data have been deposited to the ProteomeXchange Consortium via the iProX partner repository with the dataset identifier PXD041964. Source data are provided with this study. All other data supporting the findings of this study are available from the corresponding author on reasonable request.

Research involving human participants, their data, or biological material

Policy information about studies with human participants or human data. See also policy information about sex, gender (identity/presentation), and sexual orientation and race, ethnicity and racism.

Reporting on sex and gender	None
Reporting on race, ethnicity, or other socially relevant groupings	None
Population characteristics	None
Recruitment	None
Ethics oversight	None

Note that full information on the approval of the study protocol must also be provided in the manuscript.

Field-specific reporting

Please select the one below that is the best fit for your research. If you are not sure, read the appropriate sections before making your selection.

☒ Life sciences ☐ Behavioural & social sciences ☐ Ecological, evolutionary & environmental sciences

For a reference copy of the document with all sections, see nature.com/documents/nr-reporting-summary-flat.pdf

Life sciences study design

All studies must disclose on these points even when the disclosure is negative.

Sample size	No statistical methods were used to pre-determine sample sizes but our sample sizes are similar to those reported in previous publications (e.g. Zhang et al., Nat. Cell Biol., 2023; Xie et al., Nat. Neurosci., 2022).
Data exclusions	No data were excluded from analysis.
Replication	Independent biological replicates are described in the corresponding figure legend and all attempts were successful.
Randomization	Samples or animals were allocated randomly into experimental groups.
Blinding	In the in vitro study, investigators were not blinded to the samples during data collection because the readouts were quantitative and not susceptible to the subjective judgment of investigators. In the in vivo study, mice experiments and statistical analysis were conducted by independent researchers in a blinded fashion.

Reporting for specific materials, systems and methods

We require information from authors about some types of materials, experimental systems and methods used in many studies. Here, indicate whether each material, system or method listed is relevant to your study. If you are not sure if a list item applies to your research, read the appropriate section before selecting a response.

Materials & experimental systems

n/a	Involved in the study
☐	☒ Antibodies
☐	☒ Eukaryotic cell lines
☒	☐ Palaeontology and archaeology
☐	☒ Animals and other organisms
☒	☐ Clinical data
☒	☐ Dual use research of concern
☒	☐ Plants

Methods

n/a	Involved in the study
☒	☐ ChIP-seq
☒	☐ Flow cytometry
☒	☐ MRI-based neuroimaging

Antibodies

Antibodies used

The following primary antibodies were used in this study: Anti-Ubiquitin (clone P4D1; Cat# sc-8017; 1:1,000 for IB) was purchased from Santa Cruz Biotechnology. Anti-Ubiquitin, Lys48-Specific (clone Apu2; Cat# 05-1307; 1:2,000 for IB; 1:500 for IF) was purchased from Millipore. Anti-G3BP (Cat# ab181150; 1:1,000 for IB; 1:250 for IF), anti-PSMB4 (Cat# ab137087; 1:1,000 for IB), anti-hnRNP U/p120 (Cat# ab180952; 1:5,000 for IB), anti-BAG2 (Cat# ab79406; 1:1,000 for IB), anti-MCM7/PRL (Cat# ab52489; 1:1,000 for IB), anti-UHRF1 (Cat# ab213223; 1:5,000 for IB), anti-TDP-43 (Cat# ab109535; 1:1,000 for IB), anti-HSF1 (Cat# ab52757; 1:200 for IF), anti-Synaptophysin/SYN (Cat# ab16659; 1:200 for IF), anti-NUP133 (Cat# ab155990; 1:1,000 for IB; 1:200 for IF), anti-Nesprin 2 (Cat# ab314872; 1:200 for IF) and anti-mCherry (Cat# ab213511; 1:1,000 for IB) were purchased from Abcam. Anti-NONO (Cat# 90336S; 1:1,000 for IB), anti-USP10 (Cat# 8501; 1:200 for IF), anti-PARP (Cat# 9542T; 1:1,000 for IB), anti-Fibrillarin (FBL, Cat# 2639; 1:2,000 for IB), anti-HDAC6 (Cat# 7558T; 1:1,000 for IB; 1:200 for IF), anti-TBK1 (Cat# 3504; 1:1,000 for IB), anti-phospho-TBK1 (Cat# 5483; 1:1,000 for IB), anti-Caspase-3 (Cat# 14220T; 1:1,000 for IB), anti-Caspase-6 (Cat# 9762T; 1:1,000 for IB), anti-Caspase-7 (Cat# 12827T; 1:1,000 for IB), anti-Caspase-8 (Cat# 9746T; 1:1,000 for IB), anti-Caspase-9 (Cat# 9508T; 1:1,000 for IB), anti-Neurofilament-L/NF (Cat# 2837T; 1:400 for IF) and anti-DYKDDDDK (Cat# 14793S; 1:5,000 for IB; 1:500 for IF) were purchased from Cell Signaling Technology. Anti-pTDP-43 (pS409/S410) (Cat# 66318-1-Ig; 1:200 for IF), anti-GAPDH (Cat# 60004-1-Ig; 1:2,000 for IB;), anti-HSP40 (Cat# 13174-1-AP; 1:5,000 for IB), anti-HSP70 (Cat# 10995-1-AP; 1:5,000 for IB), anti-CDK1 (Cat# 19532-1-AP; 1:1,000 for IB), anti-Caspase-2 (Cat# 10436-1-AP; 1:300 for IF), anti-pTDP-43 (pS409/S410) (Cat# 22309-1-AP; 1:2,000 for IB) and anti-RAIDD (Cat# 10401-1-AP; 1:1,000 for IB) were purchased from Proteintech. Anti-Multi-ubiquitin (clone FK2; Cat# D058-3; Clone FK2 has been reported to recognize K29-, K48-, K63-linked poly-ubiquitinated and mono ubiquitinated proteins but not free ubiquitin; 1:2,000 for IB; 1:500 for IF), anti-MYC (Cat# M192-3; 1:5,000 for IB) and anti-HA (Cat# M180-3; 1:5,000 for IB; 1:500 for IF) were purchased from MBL. Anti-FLAG ® (clone M2; Cat# F1804; 1:5,000 for IB) was purchased from Sigma. Anti-Caspase-2 (Cat# MA5-31999; 1:2,000 for IB) was purchased from Invitrogen. Anti-VCP/p97 (Cat# A2795; 1:2,000 for IB), anti-USP5 (Cat# A4202; 1:200 for IF), anti-USP48 (Cat# A5046; 1:200 for IF), anti-ChAT (Cat# A19031; 1:800 for IF), and anti-HSP90 (Cat# A5006; 1:2,000 for IB) were purchased from ABclonal. Anti-α-Tubulin (Cat# B1052; 1:5,000 for IB) was purchased from Biodragon. Anti-Lamin B1(Cat# P01L16; 1:2,000 for IB) was purchased from Gene-Protein Link. Anti-HIS (Cat# TA-02; 1:5,000 for IB) was purchased from ZSGB-BIO.
The following secondary antibodies were used in this study: HRP-AffiniPure goat anti-mouse IgG (H+L) (Cat# 115-035-003; 1:10,000 for IB) and HRP-AffiniPure goat anti-rabbit IgG (H+L) (Cat# 111-035-003; 1:10,000 for IB) were purchased from Jackson. IPKine™ HRP, goat anti-mouse IgG LCS (Cat# A25012), was purchased from Abbkine. Goat anti-mouse IgG (H+ L) affinity purified, Alexa Fluor™ 488 (Cat# A32723; 1:500 for IF), Goat anti-rabbit IgG (H+L) affinity purified, Alexa Fluor™ 488 (Cat# A32731; 1:500 for IF), Goat anti-mouse IgG (H+L) affinity purified, Alexa Fluor™ 594 (Cat# A-11005; 1:500 for IF), Donkey anti-mouse IgG (H+ L) affinity purified, Alexa Fluor™ 647 (Cat# A-31571; 1:500 for IF) and Goat anti-rabbit IgG (H+L) affinity purified, Alexa Fluor™ 594 (Cat# A-11012; 1:500 for IF) were purchased from Invitrogen.

Validation

All the antibodies used in this study have been validated as reported in manufacture's website:
Anti-GAPDH antibody, Cat# sc-365062, https://www.scbt.com/p/gapdh-antibody-g-9?requestFrom=search;
Anti-Ubiquitin (clone P4D1) antibody, Cat# sc-8017, https://www.scbt.com/p/ubiquitin-antibody-p4d1;
Anti-Ubiquitin, Lys48-Specific (clone Apu2) antibody, Cat# 05-1307, https://www.sigmaaldrich.cn/CN/zh/product/mm/051307;
Anti-G3BP antibody, Cat# ab181150, https://www.abcam.cn/products/primary-antibodies/g3bp-antibody-epr13986b-ab181150.html;
Anti-PSMB4 antibody, Cat# ab137087, https://www.abcam.cn/products/primary-antibodies/psmb4-antibody-epr9397-ab137087.html
Anti-hnRNP U/p120 antibody, Cat# ab180952, https://www.abcam.cn/products/primary-antibodies/hnrnp-up120-antibody-epr122782b-ab180952.html;
Anti-BAG2 antibody, Cat# ab79406, https://www.abcam.cn/products/primary-antibodies/bag2-antibody-epr3567-ab79406.html;
Anti-MCM7/PRL antibody, Cat# ab52489, https://www.abcam.cn/products/primary-antibodies/mcm7prl-antibody-ep1974y-ab52489.html;
Anti-UHRF1 antibody, Cat# ab213223, https://www.abcam.cn/products/primary-antibodies/uhrf1-antibody-epr18803-11-ab213223.html;
Anti-TDP43 antibody, Cat# ab109535, https://www.abcam.cn/products/primary-antibodies/tdp43-antibody-epr5810-ab109535.html;
Anti-HSF1 antibody, Cat# ab52757, https://www.abcam.cn/products/primary-antibodies/hsf1-antibody-ep1710y-chip-grade-ab52757.html;
Anti-Synaptophysin/SYN antibody, Cat# ab16659, https://www.abcam.cn/products/primary-antibodies/synaptophysin-antibody-sp11-ab16659.html;
Anti-NUP133 antibody, Cat# ab155990, https://www.abcam.cn/products/primary-antibodies/nup133-antibody-epr10808b-ab155990.html;
Anti-Nesprin 2 antibody, Cat# ab314872, https://www.abcam.cn/products/primary-antibodies/nesprin-2-antibody-epr28137-54-ab314872.html;
Anti-mCherry antibody, Cat# ab213511, https://www.abcam.cn/products/primary-antibodies/mcherry-antibody-epr20579-ab213511.html;
Anti-NONO antibody, Cat# 90336S, https://www.cellsignal.cn/products/primary-antibodies/nono-antibody/90336;

Anti-USP10 antibody, Cat# 8501, https://www.cellsignal.cn/products/primary-antibodies/usp10-d7a5-rabbit-mab/8501;
Anti-PARP antibody, Cat# 9542T, https://www.cellsignal.cn/products/primary-antibodies/parp-antibody/9542;
Anti-Fibrillarin FBL antibody, Cat# 2639, https://www.cellsignal.cn/products/primary-antibodies/fibrillarin-c13c3-rabbit-mab/2639;
Anti-HDAC6 antibody, Cat# 7558T, https://www.cellsignal.cn/products/primary-antibodies/hdac6-d2e5-rabbit-mab/7558;
Anti-TBK1 antibody, Cat# 3504, https://www.cellsignal.cn/products/primary-antibodies/tbk1-nak-d1b4-rabbit-mab/3504;
Anti-phospho-TBK1 antibody, Cat# 5483, https://www.cellsignal.cn/products/primary-antibodies/phospho-tbk1-nak-ser172-d52c2-xp-rabbit-mab/5483;
Anti-Caspase-3 antibody, Cat# 14220T, https://www.cellsignal.cn/products/primary-antibodies/caspase-3-d3r6y-rabbit-mab/14220;
Anti-Caspase-6 antibody, Cat# 9762T, https://www.cellsignal.cn/products/primary-antibodies/caspase-6-antibody/9762;
Anti-Caspase-7 antibody, Cat# 12827T, https://www.cellsignal.cn/products/primary-antibodies/caspase-7-d2q3l-rabbit-mab/12827;
Anti-Caspase-8 antibody, Cat# 9746T, https://www.cellsignal.cn/products/primary-antibodies/caspase-8-1c12-mouse-mab/9746;
Anti-Caspase-9 antibody, Cat# 9508T, https://www.cellsignal.cn/products/primary-antibodies/caspase-9-c9-mouse-mab/9508;
Anti-Neurofilament-L/NF antibody, Cat# 2837T, https://www.cellsignal.cn/products/primary-antibodies/neurofilament-l-c28e10-rabbit-mab/2837;
Anti-DYKDDDDK antibody, Cat# 14793S, https://www.cellsignal.cn/products/primary-antibodies/dykddddk-tag-d6w5b-rabbit-mab-binds-to-same-epitope-as-sigma-aldrich-anti-flag-m2-antibody/14793;
Anti-pTDP-43 (pS409/S410), antibody, Cat# 66318-1-Ig, https://www.ptgcn.com/products/phospho-409-410--TDP43-Antibody-66318-1-Ig.htm;
Anti-GAPDH antibody, Cat# 60004-1-Ig, https://www.ptgcn.com/products/GAPDH-Antibody-60004-1-Ig.htm;
Anti-HSP40 antibody, Cat# 13174-1-AP, https://www.ptgcn.com/products/DNAJB1-Antibody-13174-1-AP.htm#product-information;
Anti-HSP70 antibody, Cat# 10995-1-AP, https://www.ptgcn.com/products/HSPA1A-Antibody-10995-1-AP.htm;
Anti-CDK1 antibody, Cat# 19532-1-AP, https://www.ptgcn.com/products/CDC2-Specific-Antibody-19532-1-AP.htm;
Anti-Caspase2 antibody, Cat# 10436-1-AP, https://www.ptgcn.com/products/CASP2-Antibody-10436-1-AP.htm;
Anti-pTDP-43 (pS409/S410) antibody, Cat# 22309-1-AP, https://www.ptgcn.com/products/phospho-409-410--TDP43-Antibody-22309-1-AP.htm;
Anti-RAIDD antibody, Cat# 10401-1-AP, https://www.ptgcn.com/products/CRADD-Antibody-10401-1-AP.htm;
Anti-Multi-ubiquitin (clone FK2) antibody, Cat# D058-3, https://www.mbl-chinawide.cn/search012?keyword=D058-3;
Anti-MYC antibody, Cat# M192-3, https://www.mbl-chinawide.cn/search012?keyword=%20M192-3;
Anti-HA antibody, Cat# M180-3, https://www.mbl-chinawide.cn/search012?keyword=M180-3
Anti-FLAG ® (clone M2) antibody, Cat# F1804, https://www.sigmaaldrich.cn/CN/zh/product/sigma/f1804;
Anti-Caspase-2 antibody, Cat# MA5-31999, https://www.thermofisher.cn/cn/zh/antibody/product/Caspase-2-Antibody-clone-SR44-01-Recombinant-Monoclonal/MA5-31999;
Anti-VCP/p97 antibody, Cat# A2795, https://abclonal.com.cn/catalog/A2795;
Anti-USP5 antibody, Cat# A4202, https://abclonal.com.cn/catalog/A4202;
Anti-USP48 antibody, Cat# A5046, https://abclonal.com.cn/catalog/A5046;
Anti-ChAT antibody, Cat# A19031, https://abclonal.com.cn/catalog/A19031;
Anti-HSP90 antibody, Cat# A5006, https://abclonal.com.cn/catalog/A5006;
Anti-α-Tubulin antibody, Cat# B1052, https://www.biodragon.cn/cn/goods/goodsView?GoodsId=12552;
Anti-Lamin B1 antibody, Cat# P01L16, http://www.gplink.com.cn/biofriendship/cgi/product_detail.php?product_id=205&product_number=P01L16
Anti-HIS antibody, Cat# TA-02, http://www.zsbio.com/product/TA-02;
HRP-AffiniPure goat anti-mouse IgG (H+L) antibody, Cat# 115-035-003, https://www.jacksonimmuno.com/catalog/products/115-035-003;
HRP-AffiniPure goat anti-rabbit IgG (H+L) antibody, Cat# 111-035-003, https://www.jacksonimmuno.com/catalog/products/111-035-003;
IPKine™ HRP, goat anti-mouse IgG LCS antibody, Cat# A25012, https://www.abbkine.cn/w/product/detail/A25012/CN/s;
Goat anti-mouse IgG (H+ L) affinity purified, Alexa Fluor™ 488 antibody, Cat# A32723, https://www.thermofisher.cn/cn/zh/antibody/product/Goat-anti-Mouse-IgG-H-L-Highly-Cross-Adsorbed-Secondary-Antibody-Polyclonal/A32723;
Goat anti-rabbit IgG (H+L) affinity purified, Alexa Fluor™ 488 antibody, Cat# A32731, https://www.thermofisher.cn/cn/zh/antibody/product/Goat-anti-Rabbit-IgG-H-L-Highly-Cross-Adsorbed-Secondary-Antibody-Polyclonal/A32731;
Goat anti-mouse IgG (H+L) affinity purified, Alexa Fluor™ 594 antibody, Cat# A-11005, https://www.thermofisher.cn/cn/zh/antibody/product/Goat-anti-Mouse-IgG-H-L-Cross-Adsorbed-Secondary-Antibody-Polyclonal/A-11005;
Donkey anti-mouse IgG (H+ L) affinity purified, Alexa Fluor™ 647 antibody, Cat# A-31571, https://www.thermofisher.cn/cn/zh/antibody/product/Donkey-anti-Mouse-IgG-H-L-Highly-Cross-Adsorbed-Secondary-Antibody-Polyclonal/A-31571
Goat anti-rabbit IgG (H+L) affinity purified, Alexa Fluor™ 594 antibody, Cat# A-11012, https://www.thermofisher.cn/cn/zh/antibody/product/Goat-anti-Rabbit-IgG-H-L-Cross-Adsorbed-Secondary-Antibody-Polyclonal/A-11012

Eukaryotic cell lines

Policy information about cell lines and Sex and Gender in Research

Cell line source(s)	HEK293T (Cat# CRL-11268), HeLa (Cat# CCL-2) and SH-SY5Y (Cat# CRL-2266) cells were obtained from ATCC.
Authentication	Cells are authenticated by STR profiling.
Mycoplasma contamination	All cells tested negative for mycoplasma contamination.
Commonly misidentified lines (See ICLAC register)	No cell lines adopted in this study is listed in the database of commonly misidentified cell lines maintained by ICLAC.

Animals and other research organisms

Policy information about studies involving animals; ARRIVE guidelines recommended for reporting animal research, and Sex and Gender in Research

Laboratory animals	All mice had the same genetic background (C57BL/6J) and were housed under specific pathogen-free (SPF) conditions in individually ventilated cages (12 h light-dark cycle, 50% relative humidity, between 25 and 27 °C). Casp2-/- mice were generated by Gempharmatech Co., Ltd using CRISPR-Cas9 (gRNA sequence 5′-3′: GTTGAAAATGATCTTAGGAC or CTGCTTACGTGTGACTGTAC). Casp2 +/+ and Casp2-/- mice of 10-14 months old were used in the rotarod test, grip strength test, CatWalk gait test, hindlimb clasping test, electromyographic recording and neuromuscular junctions (NMJ) staining. Casp2+/+ and Casp2-/- mice of 12-16 months old were used in immunofluorescence in brains and spinal cord. AAV-PhP.eB-GFP/GFP-TDP-43 (GENECHEM Biotech) was injected intracerebroventricularly (i.c.v.) into C57BL/6J wild type or Casp2-/- neonatal mouse brain on P1 (postnatal day 1). 2-month-old Casp2 +/+ and Casp2 -/- AAV injected mice were used in this study.
Wild animals	No wild animals were used in this study.
Reporting on sex	Female and male mice were both used in this study.
Field-collected samples	No field collected samples were used in the study.
Ethics oversight	The Institutional Animal Care and Use Committee of the Beijing Institute of Lifeomics is responsible for ethical compliance approval of all animal protocols (IACUC-20200705–42MBe).

Note that full information on the approval of the study protocol must also be provided in the manuscript.

Plants

Seed stocks	None
Novel plant genotypes	None
Authentication	None